

Deconstructing Hard Surface Cleaning Formulations

Naomi Sarah Brown

Department of Chemistry
Faculty of Science
The University of Sheffield

A thesis submitted in partial fulfilment of the requirements for the degree of Doctor of Philosophy

February 2019

Declaration

The work described in this thesis was carried out at the University of Sheffield under the supervision of Prof. Anthony J. Ryan, OBE between October 2015 and March 2020 and has not been submitted, either wholly or in part, for this or any other degree. All work is the original work of the author except where acknowledged.

Naomi Brown February 2019 Department of Chemistry University of Sheffield

Acknowledgements

Firstly, I would like to thank my supervisor, Prof. Tony Ryan OBE, for giving me the opportunity to pursue a PhD. In addition, his enduring enthusiasm, vast knowledge and supportive advice has been invaluable. In addition, I would like thank Mike for everything he did to support this project, including: the many hours of constructive discussions over telecon, all the technical instruction regarding QCM-D, his hospitality on every lab visit and his valuable comments on this thesis.

I would like to that the ESPRC for providing the funding for this work through the Centre for Doctoral Training in Polymers, Soft Matter and Colloids.

The Bayesian Optimisation studies were performed in collaboration with Prof. Neil Lawrence, Dr. Javier Gonzalez and Dr. Alan Saul, in the Department for Computer Science. Many thanks to both Javier and Alan for doing all the computational work required and your patience in explaining the process to me.

I would like to thank Andrew Morse for showing me how to use the Surface Tensiometer, Rob Hanson training me on the DSC and TGA and Dan Toolan for helping me to run Bar Microscopy experiments. A huge thank you to Darren Robinson in the Light Microscopy Facility for your assistance in Confocal Microscopy, Simon Thorpe for running the GC-MS and LC-MS. A huge thank you to Tom Neal and Sasha Mykhaylyk for all the SAXS training and assistance. I would also like to thank the many other members of the SMALL Lab for your assistance, especially James Jennings for your help running the TAG film experiments and your insightful comments on my thesis. I am very grateful to my longest serving lab mate, Sarah Wilson, for graciously sharing your lab space and showing me how to use/find many pieces of lab equipment. In addition, I'd like to thank all my colleagues in the RyMyk group for their support, as well as, the enjoyable pub trips and the ski trip.

I cannot ignore the fact that there were some low points in the process of getting here and so I would like to thank each and every person that provided support in those times. Thanks to the everyone in the Spain group and Armes group who "adopted" me at various points, so I never felt like a lone PhD student. Thanks to every friend that got me through it, especially Rheanna, Kat, Dom, Cate, Paul and Olly. The last couple of years would not have been the same without Reb. Thanks for telling me I could do it, providing distractions when you could tell I needed a break, offering to look over chapters of my thesis, and your astute observations about baking trays!

Throughout my PhD, I've been so lucky to have be part of an incredibly supportive community of Swing dancers. On days when I've been close to quitting, a great dance or a lovely chat has really lifted my spirits. I'll always be thankful to Kanika for getting me obsessed, as well as, being a great friend.

Finally, that brings me to a very special group of people that I would not be here without, my family. Thanks to you all for showing an interest in my research (whether or not you understand it). Thank you to my grandparents for their support throughout my education. Thank you, Emily, for being the world's best sister, travel buddy and friend. Finally, a special thank you to my mum and dad for always being there for me and encouraging me to never give up, you are both an inspiration.

Abstract

The development of hard surface cleaning formulation typically involves the combination of design of experiment approaches, intuition held by formulators, and some guiding principles. The aim of this thesis was to apply a machine learning methodology to optimise cleaning formulations, as it could be faster and more efficient. Bayesian Optimisation is a method to rapidly globally optimise parameters with regard to a number of multiple inputs by designing sequential experiments. Initially, the optimal binary and ternary mixtures with respect to the minimum in surface tension were identified for the surfactants lauramine oxide (LO), benzalkonium chloride (BC) and decyl glucoside (DG) with a reduced number of required experiments compared to the use of a compared to use of a factorial or matrix method. In the optimised binary mixture of LO, a zwitterionic surfactant, and BC, a cationic surfactant, the concentration of surfactants was lower than their individual CMCs, 70% of its CMC for 70 and 18.8% of its CMC for BC. In addition, the surface tension of the solution was 29.89 ± 0.07 mN m⁻¹ which was lower than either surfactant's minimum, 33.49 mN m⁻¹ for LO and 35.17 mN m⁻¹. Multiple ternary mixtures were identified around an optimum surface tension of 28.04 ± 0.20 mN m⁻¹ which was lower than both the surfactants alone and the optimised binary mixtures. Subsequently, Bayesian Optimisation was applied to the optimisation of a ternary surfactant mixture with respect to its cleaning efficacy. A repeatable method to measure the removal of a triacylglyceride (TAG) film (soil) was developed for this purpose. A ternary surfactant mixture was optimised from a starting solution achieving 55% removal, to a final solution of LO at 1636 times the CMC, DG at 1.5 times the CMC at pH 11, which removed 95.73 ± 2.36 %, within 40 experiments. Due to the inherent black-box nature of Bayesian Optimisation, there is a lack of ability to provide insight into the mechanism of soil removal by the surfactant system. Hence, a study was performed to attempt to understand the mechanisms by which the triacyl glyceride soil is removed from hard surfaces, by the surfactants LO, BC and DG. It was found that BC was much poorer at soil removal that LO and DG, comparison of the critical micelle concentrations of DG and LO with the relationship between concentration and soil removal showed correlation between the onset of soil removal and the formation of micelles suggesting surfactant micelles are required for the removal of soil and high pH causes soil removal due to saponification of the surfactant.

Table of Contents

De	clarat	ion	2
Αc	knowl	edgements	3
ΑŁ	stract	-	4
Δŀ	brevio	rtions	7
		oduction	
		Cleaning Science	
	1.1.1		
	1.1.2		
	1.1.3		
	1.1.4		
	1.1.5	Biocide	
	1.1.6	Additives	
	1.2	Surfactants and detergents	12
	1.2.1	Thermodynamics of surfactant adsorption	. 13
	1.2.2	Hydrophobic Effect	. 13
	1.2.3		
	1.2.4		
		Soils	
		Soil Removal	
	1.4.1		
	1.4.2		
	1.4.3		
	1.4.4	8	
		Formulation Optimisation	
	1.5.1	-	
		Aims	
		References	
		ials and methods	
		Surfactants	
		Analytical Techniques	
		Solids Content	-
		Mass Spectrometry	
		Surface Tensiometry	
		Differential Scanning Calorimetry (DSC)	
		Scattering Techniques	
		Microscopy	
	2.2.7 2.3	Film removal test	
		Film Preparation	
		Film removal measurement	
		Area change measurement	
		Machine Learning	
		Bayesian Optimisation	
		Optimisation Process	
		References	
3.		sical Chemistry of Surfactant Structures	
	-	Introduction	
		Surfactant Characterisation	
		Critical micelle concentration determination	
		Micelle Size and Shape Characterisation	
		DLS	
		SAXS	

	3.3.3	Comparison of DLS and SAXS	79
	3.5	Characterisation of micelles in binary mixtures	80
	3.6	Conclusions	82
	3.7	References	83
4	Bay	esian Optimisation with respect to Surface Tension	. 85
	4.1	Introduction	
	4.2	Design Loop	
	4.3	Bayesian Optimisation of LO and BC	
	4.4	Bayesian Optimisation of LO and DG	
	4.5	Bayesian Optimisation of a Binary Mixture Conclusions	
	4.6	Bayesian Optimisation of a Ternary Mixture	
	4.7	Conclusions	
	4.8	References	
_	_	isation of soil removal	
Э.	5.1	Soil removal tests used in academic and industrial research	
	5.2	Alternative Soil Removal Test	
	_		
	5.3	Soil removal test development	
		Stirring Rate	
		Measuring Film Area for Soil Removal	
		Altering Film Components	
		Control Experiment	
		Summary of final method	
	5.4	Bayesian Optimisation with respect to soil removal	
	5.5	Conclusions	
	5.6	References	
6.	Mech	anism of Soil Removal	
٠.	6.1	Microscopy Investigation of Removal	
	6.2	Analysis of the model soil	
	6.3	Comparison of Surface Tension and Soil Removal	
	6.4	Oil in Micelles	
	6.5	QCM-D	
		Spin coating TAG on a QCM-D Sensor	
		Kinetics of surfactant-aided TAG film removal	
	6.6	Conclusions	
	6.7	References	
7	_	sions	
•	CUILLIU	JIVIIJ	$\tau \sigma \sigma$

Abbreviations

AE alcohol ethoxylate

$$HO \left[\begin{array}{c} \\ \\ \\ \\ \\ \\ \\ \end{array} \right] \left[(CH_2)_n CH_3 \right]$$

 $\begin{array}{ll} \mathsf{A} & \quad \mathsf{activity} \ \mathsf{co-efficient} \\ \alpha & \quad \mathsf{droplet} \ \mathsf{radius} \\ \alpha_p & \quad \mathsf{contact} \ \mathsf{radius} \end{array}$

BC alkyldimethyl benzylalkonium chloride

CB cocamidopropyl betaine

CMC critical micelle concentration
D translational diffusion co-efficient
DDAO N,N-Dimethyldodecylamine-N-oxide

 $\begin{array}{ll} D_i & \text{diameter of particle i} \\ DOE & \text{design-of-experiment} \\ D_z & \text{z-average diameter} \\ DG & \text{decyl glucoside} \\ \end{array}$

H OH OH
$$_{\rm OH}$$
 $_{\rm OH}$ $_{\rm CH_2)_nCH_3}$

DLS dynamic light scattering

DSC differential scanning calorimetry EDTA ethylene diamine tetra acetate

EI electron ionisation ESI electrospray ionisation

F resultant force

 F_{max} major radius of De Nouy ring

 $\begin{array}{ll} \text{fps} & \text{frames per second} \\ F_r & \text{ring correction factor} \\ \gamma & \text{surface tension} \end{array}$

 γ_{ow} oil-water interfacial tension γ_{so} surface-oil interfacial tension γ_{ws} water-surface interfacial tension Γ exponential decay constant

GC-MS gas chromatography mass spectrometry

GPs Gaussian processes

HLB hydrophilic-lipophilic balance

I(q) scattering intensity

k Boltzmann constant

 λ wavelength of incident radiation

 $\dot{\lambda}$ critical shear rate

LC-MS liquid chromatography – mass spectroscopy

LCSM laser scanning confocal microscopy

LO lauramine oxide

$$\begin{array}{c} CH_3 \\ \downarrow_{\bigoplus} \\ CH_3(CH_2)_n \\ N \longrightarrow O^{\scriptsize \bigcirc} \\ CH_3 \end{array}$$

LSCM laser scanning confocal microsopy

M+ molecular ion peak

Mr molar mass

OFAT one-factor-at-a-time

P(q) form factor

 ϕ_{lin} ratio of linseed oil to the total vegetable oil content

QCM quartz crystal microbalance

q scattering vector

QCM-D quartz crystal microbalance and dissonance

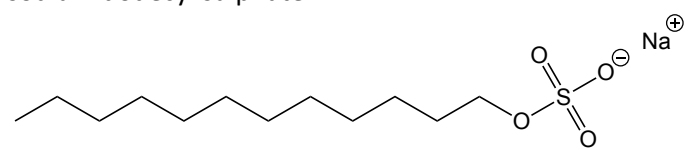
R_c core radius

 R_{min} minor axis of the ellipse R_{maj} major axis of the ellipse

R_s shell radius

RSM response surface methodologies

 $\begin{array}{ll} \rho_c & \text{electron density of core} \\ \rho_s & \text{electron density of shell} \\ \rho_{sol} & \text{electron density of solvent} \\ \text{SAXS} & \text{small angle x-ray scattering} \\ \text{SDS} & \text{sodium dodecyl sulphate} \end{array}$



SLD scattering length density

 S_i scattered intensity from the particle i

S(q) structure factor TAG triacyl glyceride

Tg glass transition temperature

 θ contact angle

 $\begin{array}{ll} \theta_a & \text{advancing contact angle} \\ \theta_r & \text{receding contact angle} \\ V_c & \text{volume of the core} \\ \text{VEN} & \text{valence electron number} \\ V_{\mathcal{S}} & \text{volume of the shell} \end{array}$

w/w% weight percentage concentrationx mole fraction of surfactant in the bulky mole fraction of surfactant in the micelle

1. Introduction

Cleaning formulations are complex mixtures of surfactants, solvents, fragrances and other additives which must be optimised, with regards to factors such as: efficacy of cleaning, speed of soil removal and cost, to develop highly effective cleaning products. Currently, much of formulation is empirical; using experimental testing guided by general principles. Theoretical chemistry cannot extend to full formulations because the current models for predicting the properties of surfactant mixtures only extends to 3 constituents (without taking into account the soil which dictates the performance of the formulation). Is there an alternative method by which a formulation could be optimised? In order to answer this question, the aims of this research are two-fold: to determine whether a cleaning formulation can be optimised more efficiently through the use of advanced applied statistics and to examine the role of the surfactant in the mechanism of cleaning a soiled surface.

1.1 Cleaning Science

The cleaning and maintenance products industry is large and growing; the European sector alone was estimated to be worth over 35 billion euros in 2017. Cleaning of surfaces in the home and workplace is extremely important in reducing the spread of illness from infection, mould or food poisoning. However, there has been little study of hard surface cleaning relative to the numerous examples of research in the development of laundry and personal care products. ^{2–5}

1.1.1 Formulation form and function

A hard surface cleaner performs multiple roles; however, its primary task is the removal of soil from a surface.^{6,7} A soil is an unwanted deposit that includes: food remains (sugars, proteins, starches, fats), solid particulates (rust, soot), grease and soap scum. One way to achieve cleaning is by removing the soil and homogenising the oil and grease into tiny water-dispersible particles in order to keep the soil in suspension and prevent re-deposition on the surface. Another way, for example, is to detach the soil from the surface without the need to break it up into small particles, by dissolving it in water or another solvent. In order to achieve the desired goal of complete soil removal, there are a number of other properties required by the cleaning formulation. Firstly, the solution must have good wetting properties to get the maximum contact of detergent with the substrate. Another important property is rinsing because the detergent solution and soil should drain from the surface without leaving behind any residues. In addition to these properties, a detergent for a specific end-use will have extra requirements to its function.⁴ For example, in a

hospital, the cleaner will be tailored to prevent the spread of sickness and infection caused by microorganisms on surfaces, in contrast, kitchen surface cleansers target the removal of the unsightly, insoluble materials formed from the baking of foodstuff (with some cleaners having antibacterial properties to ensure surfaces are safe for food preparation). As cleaners have different functions, each formulation will contain different components in variable ratios. In general, the base formulation will contain: one or more surfactants, a chelator, a solvent, and a biocide.

1.1.2 Surfactants

A cleaning solution relies on the surfactants to aid soil removal. Surfactants reduce the surface tension of the cleaning solution to aid its spread over the soil, *i.e.* improving wetting. Surfactants also reduce the interfacial tension between surface and soil, which aids the removal of solid soils. In addition, surfactants aid in emulsification and/or solubilization of soils, and help to prevent redeposition.^{8–10} The chemistry and method of action of surfactants in formulations will be discussed in detail later (section 1.2).

1.1.3 Sequestering and Chelating Agents

Sequestering and chelating agents are ligands which provide a binding site for the removal of unwanted metal ions in solution by formation of a complex. 11 Chelating agents are used to counteract problems caused by the magnesium and calcium ions in hard water. These divalent cations hinder cleaning activity by interacting with any anionic components of surfactant mixtures and decrease the surfactant activity. Additionally, under alkaline conditions in the presence of anionic surfactants, these cations can cause the formation of insoluble precipitates that lead to unsightly cloudy films on hard surfaces, also known as 'soap scum'. 12 This is one reason to use nonionic surfactants, such as straight-chain or branched alcohol ethoxylates or alkyl polyglycosides, as they are not hindered by these ions. Good chelating agents have multiple binding sites for the metal ions and so tend to be multivalent, for example, ethylene diamine tetra acetate (EDTA). 13 Previously, phosphates were commonly used, but due to negative environmental impacts, such as eutrophication, have been discontinued in favour of other chelating agents, *e.g.* sodium citrate, zeolites, hydroxyethyl ethylene diamine and amino tri(methylene phosphonic) acid. 7,14

1.1.4 Solvent

Solvents are used to create a homogeneous product by solubilisation of the components and enhance cleaning ability by aiding the softening of soils for easier removal and providing a medium for dispersal of the soil to prevent re-deposition. The most common solvent in hard surface cleaners is water which can form up to 98% of the final formulation.⁴ Co-solvents, such as water-soluble glycol ethers, can be beneficial additions to aqueous formulations. They help to dissolve greasy soils by lowering the interfacial tension, increasing the uptake of hydrophobic soils into water, and have a lower rate of evaporation from the surface which minimises streaking.¹⁵

1.1.5 Biocide

Biocides or antimicrobial agents are used in cleaner formulations to reduce surface microbial concentrations and disrupt the growth of mould and mildew on surfaces. The most commonly used chemical antimicrobial agents are quaternary ammonium compounds, alcohols (which are also solvents) and peroxy compounds, *e.g.*, bleach.¹⁶ The method of antimicrobial action differs for each agent. Quaternary ammonium compounds are cationic surfactants and their positively charged headgroups bind irreversibly to the negatively charged surfaces of the bacteria, disrupting the cell membrane, denaturing proteins and affecting the metabolic reactions, leading to death.¹⁷ Alcohols cause proteins within the cells of the microorganisms to coagulate so that the cell membranes loose structure and collapse. Peroxy compounds are oxidizing agents, which form hydroxyl radicals in the presence of air, which react with the cell components causing cell collapse.¹⁸ Preservatives are a specific class of biocides added to liquid formulations to increase the shelf-life of the product by inhibiting microbial growth. Antimicrobial compounds are added in concentrations low enough to protect the product from contamination.¹⁹

1.1.6 Additives

A number of additives can be included in cleaning formulations to enhance the consumer experience, such as rheology modifiers, dyes and fragrances. The purpose of a rheology modifiers is to alter the flow behaviour of the final formulation, by changing its viscosity. Dyes are used to give colour to the final formulation which gives the consumer an indication of the brand or odour of each product. Fragrances are added to give the cleaner a pleasant smell or mask an unpleasant odour. These can be complex mixtures of chemicals derived from synthetic or natural sources, such as D-

limonene found in citrus oils.²⁰ Fragrances are often classed as trade secrets and therefore the components are not disclosed.

1.2 Surfactants and detergents

Surfactant originates from "SURFace ACTive AgeNT" which describes the preference of a surfactant molecule to align at interfaces.²¹ In this section, surfactants will be discussed with respect to a water-based rather than an oil based system. A surfactant molecule contains a hydrophilic head group and a hydrophobic tail, forming an amphiphilic molecule. The head group is polar, and may be charged, which makes it soluble in water. The tail group tends to be made up of linear or branched hydrocarbon chains, which are insoluble in water, and tend to be soluble in oil, so can also be described as lipophilic.

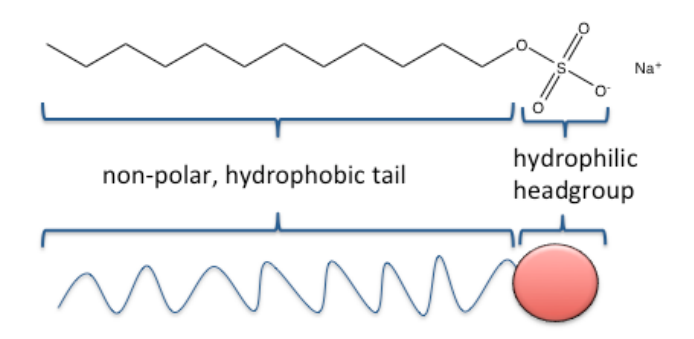


Figure 1.1: Structure of an example surfactant, sodium dodecyl sulfate (above), and a simplified diagram of surfactant molecule (below)

The type of head group can be used to classify different types of surfactants. Anionic surfactants have negatively charged head groups and cationic surfactants have positively charged head groups. Non-ionic surfactants have polar functional groups without dissociating ions, such as glucosides, polyhydroxy units or polyethylene oxide chains.

One advantage of non-ionic surfactants is the ability to tailor their behaviour by varying the hydrophilic-lipophilic balance (HLB). HLB is an empirical measure which can be calculated by either the relative sizes (using Griffin's method²²) or effectiveness (using Davies' method²³) of the hydrophilic and lipophilic regions in a molecule, and can easily be tuned by changing the ratios of the alkoxy and hydrocarbon chain lengths.^{24,25} A balance between the two sections allows the surfactant to align at different interfaces. If the HLB is very low, the lipophilic group dominates, and the surfactant molecule will be solubilised in oil and these surfactants tend to be used in formation

of water-in-oil emulsions. For good detergents, the hydrophilic group dominates so the HLB tends to be larger.²⁵

1.2.1 Thermodynamics of surfactant adsorption

Non-polar oils and water are immiscible due to the unfavourable Gibbs' free energy of mixing.²⁶ For spontaneous mixing to occur there must be a decrease in the Gibbs' free energy:

$\Delta G = \Delta H - T \Delta S$

where ΔH is the change in enthalpy, T is the temperature and ΔS is the change in entropy. The mixing of two liquids is favoured by an increase in entropy. However, in the case of a non-polar oil and water, there is a positive free energy, as a consequence of the highly negative entropic contribution from the structuring of water molecules around oil molecules. The tendency of non-polar oils to aggregate in water is called the hydrophobic effect.²⁷

1.2.2 Hydrophobic Effect

The hydrophobic effect is the spontaneous process of removing hydrophobic parts of molecules from contact with water.²⁷ The water molecules hydrogen bond around non-polar molecules to form an ordered structure called a clathrate cage. The hydrophobic effect is due to the favourable, negative Gibbs' free energy, achieved by a negative change in entropy upon forming this cage of water molecules surrounding the non-polar molecule.²⁸ There is entropy lost in breaking the hydrogen bonds initially, however the extra hydrogen bonds formed with neighbouring water molecules compensate.²⁹ The Gibbs' free energy to solvate a large number of well-spaced, small hydrophobic species can be higher than to solvate a larger cluster.³⁰ Therefore, there is effectively attraction of non-polar molecules in water and this is what drives the formation of micelles. By positioning the hydrophobic tails of the surfactants near each other, the system forms aggregates, called micelles.³¹

1.2.3 Micellisation

Micelle formation aids cleaning efficiency as some of the micelles can solubilise oily soil whilst others replenish the concentration of surfactant monomer in the bulk when surfactant is adsorbed at the oil-water interface.³² The formation of micelles is driven by the hydrophobic effect. Micelles are aggregates of surfactant molecules where the polar heads are orientated outwards, in contact with

water, and non-polar tails are sequestered into the core, away from the water, to minimise unfavourable interactions. When a surfactant is at a low concentration in water, the surfactant molecules distribute themselves between the gas/water interface and the bulk solution. As more surfactant is added, the interface becomes saturated with surfactant molecules, at which point, it becomes thermodynamically favourable to form micelles, in order to reduce the contact of the hydrophobic surfactant tails with water.³³

The thermal equilibrium in a surfactant solution is shown in figure 1.3. Surfactant molecules of the same species exchange positions from monomer in solution, the air-water interface and in micellar aggregates.^{34,35}

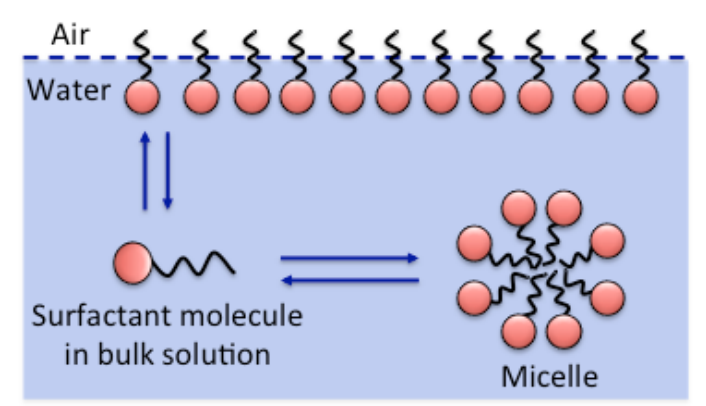


Figure 1.3 The possible locations of a surfactant molecule in a surfactant solution

The orientation of surfactant molecules at the interface between air and water causes a reduction in the surface tension of the solution. Surface tension is the cohesive force between liquid molecules caused by the difference in the forces acting on a molecule in the bulk and on the surface. The bulk molecules have similar neighbouring atoms in all directions so the attractive forces in action are equal in all directions, shown schematically in figure 1.4. In contrast, the surface molecules cohere strongly to the molecules directly associated with them which causes additional energy at the surface. In liquids, the surface tension is equivalent to the surface energy (which is also applied to solids). Surface energy is the energy required to form a surface. Surface tension, along with surface energy, drive wetting and adhesion behaviour. Water, and other polar species, have a "higher" surface tensions (e.g. γ (H₂O) \sim 72 mN m⁻¹) than non-polar species (e.g γ (C₈H₁₈) \sim 21 mN m⁻¹) due the greater interaction forces within the liquid.

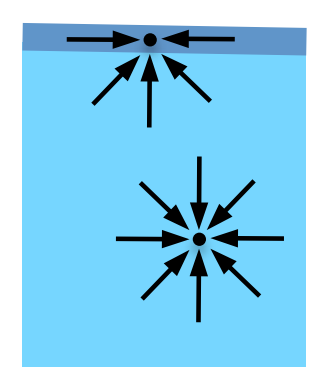


Figure 1.4 The forces, black arrows, on water molecules, black circle, in the bulk vs. on the surface, which cause surface tension.

Surface tension gives rise to an energy cost in creation of additional surface, arising from the imbalance of forces of intermolecular forces on the surface molecules verses those in the bulk, therefore, the liquid of interest will try to minimize its surface area. Figure 1.5 illustrates the decrease of surface tension as a function of surfactant concentration, caused by the alignment of surfactant molecules at the interface until saturation. The critical micelle concentration (CMC) is the concentration of surfactant at which micelles form. Below the CMC, as more surfactant is added, more surfactant molecules orientate at the oil-water interface leading to a surface tension reduction. Above the CMC, the interface is saturated with surfactant, and the surface tension plateaus as micelle formation occurs.^{21,36}

In a 2015 review, the structure of surfactants and the relationship with surface tension was discussed in terms of the importance of hydrophobic tail group. By considering the differences in packing between hydrocarbon, silicone and fluorocarbon surfactants, it was identified that the key factor to a high reduction in surface tension is a high surface coverage at the CMC.

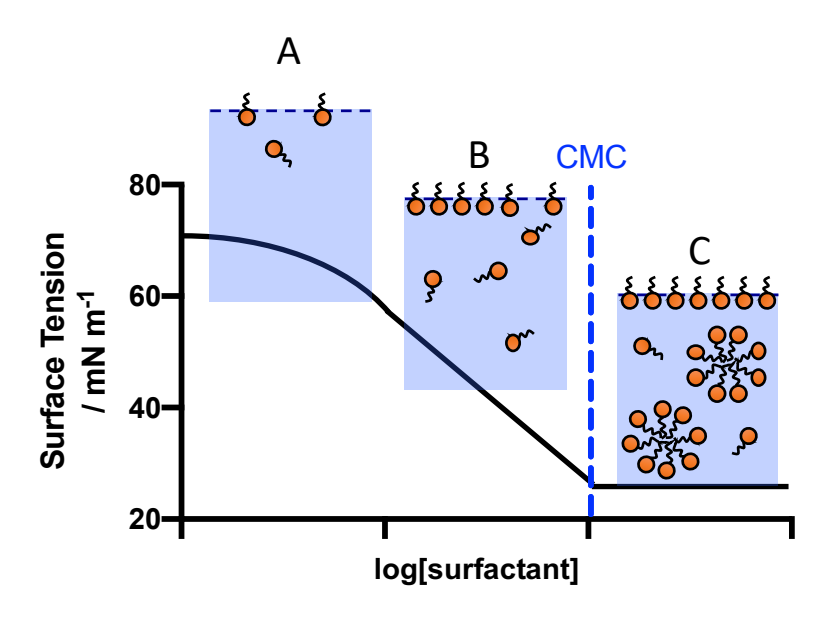


Figure 1.4: Change in surface tension with increasing surfactant concentration. The blue dotted line indicates the critical micelle concentration (CMC), the micelles are depicted as a red circle with a black "tail" and the solution is the area of light blue. A depicts the surfactant solution at high surface tension where concentration of surfactant is low, B depicts the surfactant solution when the surface tension decrease with addition of surfactant as the air-water interface is not yet saturated and C depicts the surfactant solution at concentrations above the CMC.

1.2.4 Mixed surfactant systems

In mixtures of surfactants, such as those with differing chain lengths or differing types of headgroup, it is possible for the CMC to be lower than that of either surfactant alone. This is an example of a synergistic effect, where the properties of the mixture are greater than that of either pure surfactant. These favourable effects are thought to be due to interaction between amphiphilic groups causing non-ideal mixing of surfactants at interfaces and in micellar aggregates.^{37,38} The opposite is also true; mixtures of surfactants can lead to properties inferior to those of either surfactant, *i.e.* higher CMC, so-called antagonistic effects. Surfactant synergism/antagonism has been observed to alter properties such as foaming, emulsification and dispersion.^{39–41}

The behaviour of a wide range of mixed surfactant systems has been studied.⁴¹ Due to the complexity of these systems, they have been difficult to model. In the 1960s, the determination of CMC's of mixtures of non-ionic/non-ionic and ionic/ionic surfactants was attempted by treating the mixed micelle as an ideal mixture of the pure surfactants.⁴² The relationship between the mole fraction of a surfactant component and the CMC for a binary surfactant mixture in an ideal system was determined to follow the relationship (A):

(A)
$$\frac{1}{cmc_{mix}} = \frac{x}{cmc_1} + \frac{1-x}{cmc_2}$$

where x is the mole fraction of surfactant 1 in the bulk. However, equation (A) was incorrect when predicting the surface tension for surfactants exhibiting non-ideal mixing of non-ionic headgroups in the monolayer at the air-water interface, e.g. n-octyl methyl sulphoxide and tetraethoxy-n-decanol. 43

The first non-ideal mixing model was proposed by Rubingh, and applied regular solution theory.⁴⁵ Regular solution theory states that for bulk liquid mixtures the enthalpy of mixing depends on the mixture composition whilst the entropy of mixing is ideal.⁴⁶ The deviations from the ideal conditions in real systems are accounted for in the following equation (B):

(B)
$$\frac{1}{cmc_{mix}} = \frac{x}{A_1 cmc_1} + \frac{1-x}{A_2 cmc_2}$$

where A_1 and A_2 are activity co-efficients.

$$A_1 = \exp\beta[1 - y_1]^2$$

$$A_2 = exp\beta[y_1]^2$$

 y_1 is the mole fraction of surfactant 1 in the micelle and β is an interaction parameter describing the deviations from ideal behaviour. The activity co-efficient describes the effect of each surfactant component in the micelle. Computational or experimental methods can be used to determine, by iteration, the value of β from the mixed CMC of a binary surfactant mixture and the mole fraction of the surfactant in the micelle. For attractive interactions, β is negative, and the CMC will be lower than expected. On the contrary, for repulsive interactions, β is positive and the CMC will be higher than expected. A large, negative β indicates a strong interaction and often leads to synergistic effects. The difference between equations (A) and (B) is a measure of synergism.

A study into the relationship between the synergistic effects of surfactant mixtures and oil removal from polyester fibres showed that certain ratios of a cationic-non-ionic surfactant mixtures were more effective at removing oily and particulate soils from cotton fibres than either surfactant individually. When a cationic surfactant is applied to an oily soiled fibre, the negatively charged fibre surface is neutralized, increasing hydrophobicity, which decreases wetting of the fibre inhibiting the removal of the soil. In contrast, when a mixed system of non-ionic and cationic surfactant is applied, there is enhanced adsorption of the non-ionic surfactant compared to a

solution containing only non-ionic surfactant. This is due to cationic surfactant adsorbing to the surface and neutralising the normally negative surface charge of the fibre (the charge on the surface will depend on the material of the surface being cleaned). By forming a neutrally charged surface, more non-ionic surfactant adsorbs, increasing the contact angle between the soil and the fibre, facilitating the removal of the soil.⁴⁸

The correlations between the physical properties of binary surfactant mixtures and properties applicable to cleaning have also been studied. Models were used to predict synergistic combinations of surfactants from the interaction parameter, β , for non-ionic/non-ionic, anionic/non-ionic, and anionic/cationic surfactant mixtures. These combinations showed synergism in regards to the following factors: CMC, surface tension, solubilising capacity, emulsifying ability, foaming ability, wetting time and cleaning performance.

The research by Rubingh and Rosen, to quantitatively investigate surfactant synergism by regular solution theory and non-ideal mixing, enabled the prediction of synergism, CMC and micelle composition for a binary mixture of surfactants, if the composition of the surfactants in solution and in the mixed micelle monolayer at the solution surface is known. ^{21,45,49–51} However, this is a simplified model and it has been shown that the model falls short in its representation of the CMC for some of the most commonly used surfactant mixtures. 52,53 Hines et al. were able to make predictions of the CMC for a ternary mixture of surfactants from composition.⁵⁴ However, this method requires large data sets that are not easily obtained: surface composition from neutron scattering experiments and interaction parameters derived from surface tension. Even though the prediction of synergism was successful, it proved difficult to predict the ratio of surfactants that would give the synergistic maxima of the properties listed previously. Hines concluded that no single physical parameter could be correlated with all the application parameters, due to competitive processes being involved and the complex cross terms in the thermodynamics of ternary mixtures. To conclude, it is difficult to predict the useful properties of surfactant mixtures due to the inability to obtain the parameters needed, the complexity of surfactant theory and the difficulties in describing a multi-component system.

1.3 Soils

In the context of cleaning and detergency, soils are a mixture of organic and inorganic matter. The inorganic component could be particles of: minerals, clays, metal, silicas, metal hydroxides. These particles tend to have a surface charge, which is pH-dependent due to adsorption of protons or hydroxyl ions. The organic components, *e.g.* oils, carbohydrates, or proteins, arise from living organisms in the nearby environment of the soil. The structures of these organic macromolecules tend to be ill-defined, due to degradation or rearrangement, and they can also have surface charge which affects surfactant interactions, *i.e.* electrostatic attraction or repulsion. In both cases, surfactant – soil interactions are determined by the soil components.

At this point, it is useful to consider the example of cleaning a dirty kitchen worktop, in which case, the soil would contain remnants of foodstuff. The removal of a soil occurs in three stages. First, the soil is separated from the substrate, the kitchen worktop in our example. There are three main mechanisms to facilitate this: emulsification, rolling up and solubilisation, which can occur alone, or in combination. Second, the soil needs to be dispersed into the solution applied to clean the surface, i.e. a kitchen cleaning spray or washing up liquid. Depending on the soil and solvent type, the dispersion could be achieved by emulsification of an oily soil within a surfactant micelle or solubilisation of the soil. For example, a water-insoluble fatty deposit would require emulsifying whereas a carbohydrate could be solubilised. Emulsification may require the introduction of a physical force by the use of a scrubbing tool, *e.g.* a scourer sponge or cloth. Third, there must be a system to prevent re-deposition of the soil, which can cause unattractive smearing of the soil. If the soil is not completely removed, repeated soiling and cleaning leading to the gradual growth of a residual soil that becomes increasingly difficult to remove.

1.4 Soil Removal

There are a number of possible mechanisms of soil removal due to the variety of soil types: water-soluble, oily, soil particulate and mixtures of solids and liquid, as well as "soft" and "hard" varieties in each type, *e.g.* cross-linked soils. The process can range from relatively simple, such as the solubilisation of water-soluble soils, to being extremely complex, particularly for oily soils. Much of the current literature on soil removal mechanisms include three processes that have been widely accepted to occur: 'roll-up', emulsification and solubilisation.²⁹

1.4.1 Rolling up

Roll up describes the detachment of an oil droplet from a surface caused by an increase in the contact angle between the soil and the substrate, θ , see figure 1.5.⁵⁶ Roll up can be aided by surfactants adsorbing at the soil-solution and surface-solution interfaces. When a liquid oily soil and aqueous surfactant form an interface there is competition between the interfacial tensions of the two media, leading to an oil displacement tension.⁵⁷ If the aqueous surfactant solution is more attracted to the surface of the substrate than that of the oily soil, the oily soil will be forced to contract and form spherical particles.

A formula based on Young's equation determines the conditions for oily soil roll up to occur.⁵⁸ Roll up occurs if the resultant force of the interfacial tensions, F, is positive:

$$F = \gamma_{so} - \gamma_{ws} + \gamma_{ow} cos\theta$$

where γ_{ws} is the water-surface interfacial tension, γ_{so} is the surface-oil interfacial tension, γ_{ow} is the oil-water interfacial tension and θ is the contact angle between the soil and the substrate.^{59,60}

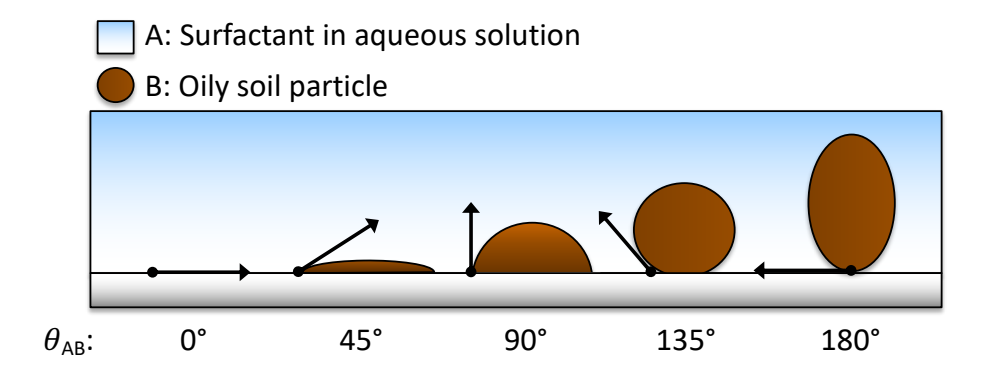


Figure 1.5: Schematic for the removal of a liquid oily soil by the rolling up process. θ_{AB} is the contact angle between the soil and the surface. θ_{AB} and the ease of soil removal increases from left to right which is time dependent.

If F = 0 when θ = 180°, theoretically there can be spontaneous detachment of the soil as the aqueous solution can displace the oily soil by forming a wedge under the oil. For roll-up to occur, F is positive with an increase in contact angle for 0 to 180°. As $cos\theta$ can be positive or negative, for F to be positive $\gamma_{so} - \gamma_{ws}$ is greater than γ_{ow} . Therefore, spontaneous roll-up is encouraged by a low interfacial tension between the oil and the solution and a low interfacial tension between the surface and the solution, *i.e.* a hydrophilic surface. Upon the addition of surfactant, γ_{ws} is decreased because the surfactant preferentially adsorbs at the oil-water interface. If, after the addition of

surfactant, F reaches 0 before θ reaches 180°, the oil droplet is partially detached and another mechanism is required to remove residues, for example, the application of mechanical force.

1.4.2 Emulsification

Emulsification is the removal of a liquid soil into the washing solution by deformation in droplets under shear. ¹⁰ For a soil particle attached to a flat surface, detachment occurs at a critical shear rate, $\dot{\lambda}$, described by:

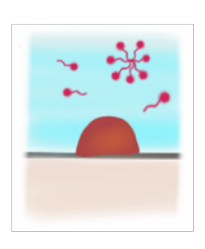
$$\dot{\lambda} = \frac{Y_{ow}\alpha_p(\cos\theta_r - \cos\theta_a)}{\eta a^2}$$

where α_p is the contact radius, θ_r is the receding contact angle, θ_a is the advancing contact angle, a is the radius of the droplet, and η is the viscosity, assuming that the advancing and receding contact angles are independent of the oil–water interfacial tension. 56,61

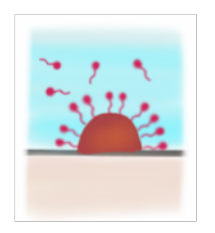
If only a small amount of surfactant is applied and the soil is strongly adhered to the surface, the oil-water interfacial tension is high and therefore, the critical shear rate is higher. The addition of surfactant decreases γ_{ow} and increases the surface area and radius of the oil droplet, both of which cause a decrease in critical shear rate.

1.4.3 Solubilisation

Solubilisation in surfactant solution has been suggested to occur alone and as a method to stabilise soil removed by other mechanisms, e.g. roll-up, and predominantly occurs when the surfactant concentration is large relative to the oil and above the CMC.⁶² During solubilisation, the soil is sequestered into the core of surfactant micelles present in the cleaning solution, figure 1.6. In the first step, surfactant adsorbs on a substrate, in the form of hemimicelles. The hemimicelles orientate around the oil before desorbing from the surface. Swollen micelles are reformed in the bulk solution with oil in the core, with the potential to break breaking down into smaller aggregates that are more thermodynamically stable.⁶³



Oil on a surface in a surfactant solution



Surfactant molecules orientate around the oil



Surfactant aggregates containing oil desorb

Figure 1.6: Schematic for the solubilisation mechanism of removal of an oil (dark brown) from a surface (beige) in the presence of surfactant (red).⁶⁴

1.4.4 Advances in understanding the soil removal mechanism

There have been multiple studies investigating the mechanism of removal for multiple soil types and most involve both surfactant activity and mechanical action. 8,64–66 In 1980, Shaewitz investigated the effect of fluid flow on the mechanism of solubilisation by using radiolabelled fatty acids applied to a rotating disk immersed in a cleaning solution. The rate of rotation of the disk was increased to increase the flow rate and the amount of solubilisation of palmitic acid in a 4 w/w% SDS solution was measured from the concentration of fatty acid in the cleaning bath with time.

The solubilisation of fatty acid in a surfactant solution was found to take 5 steps: 1) the surfactant aggregates diffuse to the soil surface, 2) the surfactant aggregates adsorb onto the solid surface, 3) the surfactant molecules mix with the adsorbed aggregate, 4) the aggregates containing both substrate and surfactant desorb and 5) the mixed aggregates diffuse away from the surface and into the bulk surfactant solution. From calculation of the rate constants for each step, the rate controlling steps were micelle desorption and diffusion (steps 4 and 5 as discussed above).

In an extensive review by Miller and Raney, the solubilisation-emulsification mechanisms involved in removing soil from fabric surfaces was shown to be faster and more complete than solubilisation into a micellar solution. The increased solubilisation was contributed to the solubilisation of the soil into an intermediate phase, *i.e.* a liquid crystal.¹⁰ In contrast, it was found that to detach the soil in one unit, significant wetting of the cleaning solution over the soil/solid surface is required, in addition to, a wicking-type movement using capillary forces, both of which depend on the interfacial tension and a density difference between the soil and the surface.^{32,67}

An in-depth study by Cox showcased three classes of soil removal methods: chemical (soil solvation and saponification), mechanical (abrasion) and detergency (surfactants). The importance of mechanical action was highlighted in a two-step mechanism. First, the surfactant and water penetrated the soil to soften and loosen it in a process called liquefaction. Second, the soil is removed from the surface by emulsification through agitation or mechanical abrasion. In addition, it was shown that if the product is used with mechanical action, the surfactants in the product should soften the soil and maximise penetration. Contrastingly, if the soil removal process is static, the surfactants should self-emulsify the soil, by creation of a microemulsion, and therefore, the HLB of the surfactant should be matched to the soil. Alternatively, to maximise both soil penetration and emulsification, blends of surfactants should be used.

Another similar study to Shaewitz into the kinetics of soil removal by analysing the loss of radiolabelled fatty acid films from rotating disks, identified a three step mechanism.⁶⁸ In the first step, fatty acid was solubilised into micellular aggregates. Next, part of the film was removed via shear. The third step was the previously described roll up. The surfactant structure was found to influence the cleaning mechanism; for surfactants effective at solubilization, the shear-driven emulsification process was shown not to occur. In addition, it was found that at concentrations above the CMC, more hydrophilic surfactants were more efficient due to their ability to partition into the film, encouraging liquefaction.

The mechanism of the removal of semi-solid oily soils has been studied, with the added difficulty arising from the possibility of liquid oil being trapped inside the crystalline solid fats. The removal of oily soils can follow a mechanism of incomplete roll-up where only part of the oil is detached from the surface and emulsified. However, for solid soils, roll-up may not occur. The surfactant needs to wet the soiled surface, followed by penetration to aid soil loosening and solubilisation-emulsification. ^{5,71}

In summary, soil removal is a complex process which varies significantly depending on soil type, shear applied, surfactant type and concentration, in addition to the type of surface (fabric vs hard surfaces, surface charge, hydrophobicity *etc.*). Therefore, to formulate an effective cleaning solution, both an understanding of the detergency mechanism and the synergistic behaviour of surfactant mixtures is important.

1.5 Formulation Optimisation

Optimisation is the improvement in the performance of a product, system or process to achieve the maximum possible advantage.⁷² The simplest type of optimisation (above trial-and-error) is a one-factor-at-a-time (OFAT) experiment where one variable is changed in each set of experiments.⁷³ This method remains widely used in cases where there are multiple factors, despite having a number of disadvantages. OFAT does not account for interactive effects between variables and does not describe the complete effect of each parameter in the final outcome.⁷³ In addition, a high number of experiments are required to examine all possible factors which can be wasteful of time and resources. To obtain the maximum amount of information from fewer experiments, an alternative method is to statistical design of experiments (DOE). In these, more than one variable is changed at a time so that the interactions between the variables can be calculated.

One of the most relevant multivariate statistical techniques for detergent formulation is Response Surface Methodologies (RSM). These are a collection of techniques based on fitting empirical models to experimental data.⁷⁴ Describing the trends in the data enables predictions of the values of each variable in the optimum situation, therefore, by using a sequence of experiments, multiple variables can be optimised simultaneously. Initially, an experimental design matrix must be chosen to efficiently select the experiments to be carried out within the boundary conditions set for each variable. If the data set is linear, first order models such as factorial designs can be used. For data that cannot be described by a linear function, quadratic response surfaces are used, and experimental designs are selected accordingly. The two most commonly used experimental design techniques in detergent optimisation are a full 3-level factorial design⁷⁵ or a Box-Behnken.⁷⁶

A full three-level factorial design involves each variable being measured at three levels. The number of experiments is therefore 3^k where k is the number of variables. As the number of experiments dramatically increases with the number of factors it is generally only used in the optimisation of two factors.

A Box-Behnken design utilises the three-level factorial design, however, a lower number of points are selected to more efficiently and economically obtain information about the relationship between multiple variables. The points selected are those on a hypersphere equidistant from the centre of the design space, with all variables measured at three equally spaced intervals. In this case, the number of experiments is $2k(k-1)+C_p$ where C_p is the number of central points. In comparison,

for optimisation of three variables, a full three factorial design requires 27 experiments whereas a Box-Behnken design requires 13.

Response surface methodologies have previously been used in the computer-aided design of disinfectant formulations. In 2010, a group based in Waterloo applied statistical methods to aid formulation design. 77,78 Historical data regarding a disinfectant formulation was augmented with new data, selected by a fractional factorial design (where only a necessary fraction of the experiments required for a full factorial design are selected), to improve the predictive capabilities of the final analysis. An empirical model was fitted, defining antimicrobial activity in terms of the formulation ingredients and pH, using multiple linear regression. An optimal formulation was predicted using an optimisation method called Levenberg- Marquardt and was shown to meet all the required performance criteria. The major success of this work was that no further fine-tuning experiments were required after the optimisation. In 2012, the methodology was extended to design a disinfectant formulation with a higher number of constraints.⁷⁹ The optimal formulation was compared to a successful product developed by 'trial-and-error methodology' and found to be: cheaper (nearly a quarter of the price), less toxic, less corrosive and more stable. This further reiterates the benefits of computer-aided design in formulation optimisation; prior data can be taken into account leading to a reduced number of experiments relative to trial and error methodology.

1.5.1 Optimisation using adaptive design

Difficulties arise in optimising a formulation using design of experiment methodologies when considering multiple variables due to the increased experimental costs as complexity increases. Current formulation development involves the combination of: design of experiment approaches, intuition held by formulators, and some guiding principles. Computational methods could be used to make predictions about the properties of the final formulations however these sometimes rely on detailed knowledge of the system of study from complex characterisation methods, *e.g.* neutron reflection and isotopic substitution. ^{52,53,80} In materials discovery, similar problems have been treated as black-box functions, where the relationship between the variables and output is unknown. A Bayesian optimisation is a machine learning based, experimental design algorithm for optimisation of black-box functions.

Machine learning is the use of computer algorithms to make predictions using data and a model. By finding and classifying the regularities in the data these machine learning methods can learn from

the data to infer plausible models, and subsequently make predictions about unobserved data. The benefits to using machine learning include the ability to handle a large number of parameters, large data sets and fast predictive analytics on timescales much faster than humans could ever achieve, through both thought and action.

Bayesian optimisation is a rapid method to globally optimise parameters with regard to a number of multiple inputs by designing sequential experiments.^{72,81} For example, if the aim is to maximise an output variable from a number of input variables, first you would collect a number of data points, *n*. To select the next measurement to be taken, a Bayesian regression function describing the relationship between the input and output variables is learnt from the *n* data points. The best candidate is chosen by balancing the goal of searching for mixtures with the highest values of the output variable (exploitation) with testing the design space where least experiments have been performed and therefore the uncertainty is greater (exploration). The data collected is added to the *n* data points previously recorded and the process is repeated to find the maximum in the output variable. The optimum is achieved in a minimum number of experiments which is preferable in cases where collecting data is expensive.

In Bayesian Optimisation, the black-box function is modelled by a stochastic Gaussian Process (GPs) which are a powerful technique for modelling and predicting numerical data. Although they are mathematically complex, the motivation behind their use is their quick computation, since they consist of entirely linear algebra.⁸² In addition, GPs are flexible meaning they can be used to model many different patterns, and few assumptions have to be made about the model initially. The GP mimics an experimenter; a mathematical model is built from experimental data acquired previously and then an "educated guess" is used to recommend the next experiment to perform. This process is repeated with each new piece of data collected; therefore the 'guess' becomes increasingly more accurate whilst the uncertainty about the "guess" decreases. Bayesian optimisation uses efficient global optimisation algorithms which give importance to areas close to the current minimum (in addition to exploring additional unexplored phase space) whereas the alternative, a grid search, gives equal importance to all points. Bayesian optimisation is an iterative experimental approach with data-driven models. The Bayesian method of experimental design has previously been adopted in the field of chemistry for the optimisation of materials, in a number of applications. Table 1.1 summarises the recent literature. As yet, there have been no studies of optimisation of surfactant mixtures.

Table 1.1: The of Bayesian Optimisation material science literature 2015-2018

Date	Parameter(s) Optimised	ion material science literature 2015-201 Input Parameters	Objective of Study	Reference
2015	Lattice thermal conductivity (minimum)	Chemical structure and composition	Identify thermoelectric materials with high conversion efficiency.	[⁸³]
2016	Maximizing the elastic moduli in nanolaminate, ternary alloys: bulk, shear or Young's modulus	Orbital radii of M (metal), A (atomic element in separating layer, and X (carbide or nitride)-atoms	Selection of M ₂ AX compound with optimal elastic properties	[84]
2016	Thermal hysteresis	Waber–Cromer pseudopotential radii, Pauling electronegativity, metallic radius, valence electron number (VEN), Clementi's atomic radii and Pettifor chemical scale	Discovery of very low thermal hysteresis NiTi-based shape memory alloys	[⁸⁵]
2017	Length, width and quality of fibres	Process parameters: position, constriction angle, channel width, polymer flow and solvent flow	Find the optimal conditions for short polymer fibres synthesis using a microfluidic process	[⁸⁶]
2018	Total energy of candidate crystal structure	Function describing the crystal structure from interatomic distances and unit cell volume	Identify the most stable crystal structure	[87]
2018	Solar cell efficiency	Doping ratio of Mn ²⁺ ion in CMZTSSe	Development of solar cell materials for photovoltaics	[88]

1.6 Aims

Although much research has studied fabric cleaning formulations, there is relatively little literature in the area of hard surface cleaning. Machine learning has been used previously in the prediction of material properties from their composition, however no previous studies have applied machine learning in optimising hard surface cleaning formulations. One of the drawbacks to optimisation is that results are only useful to the system to which it is applied to because of the black-box nature. Therefore, to understand why the optimum mixture is selected by the machine learning algorithm further study is required to gain an insight into the mechanism.

Hence, there are two primary aims of this study:

- 1. To apply a machine learning methodology to optimise hard surface cleaning formulations.
- 2. To gain an understanding of the mechanism that underpins the surfactant-aided removal of an oily soil from a hard surface.

Figure 1.7 shows how the optimisation and characterisation sections of this project are linked and summarises the main topics. The topics covered in this thesis are:

- Initial characterisation of the surfactants commonly used in cleaning formulations,
 because they were commercial grade, so a greater understanding of the characteristics
 and composition of the mixture was required to aid later formulation (Chapter 3).
- The use of a machine learning technique to optimise surface tension: a parameter important to both the cleaning process and characterisation of surfactants (Chapter 4).
- The application of this machine learning technique to a cleaning test, developed for use in this thesis, to determine the optimal cleaning formulation from a surfactant mixture (Chapter 5).
- An investigation into how soil removal occurs, to understand why the "optimal solutions" are successful at soil removal (Chapter 6).

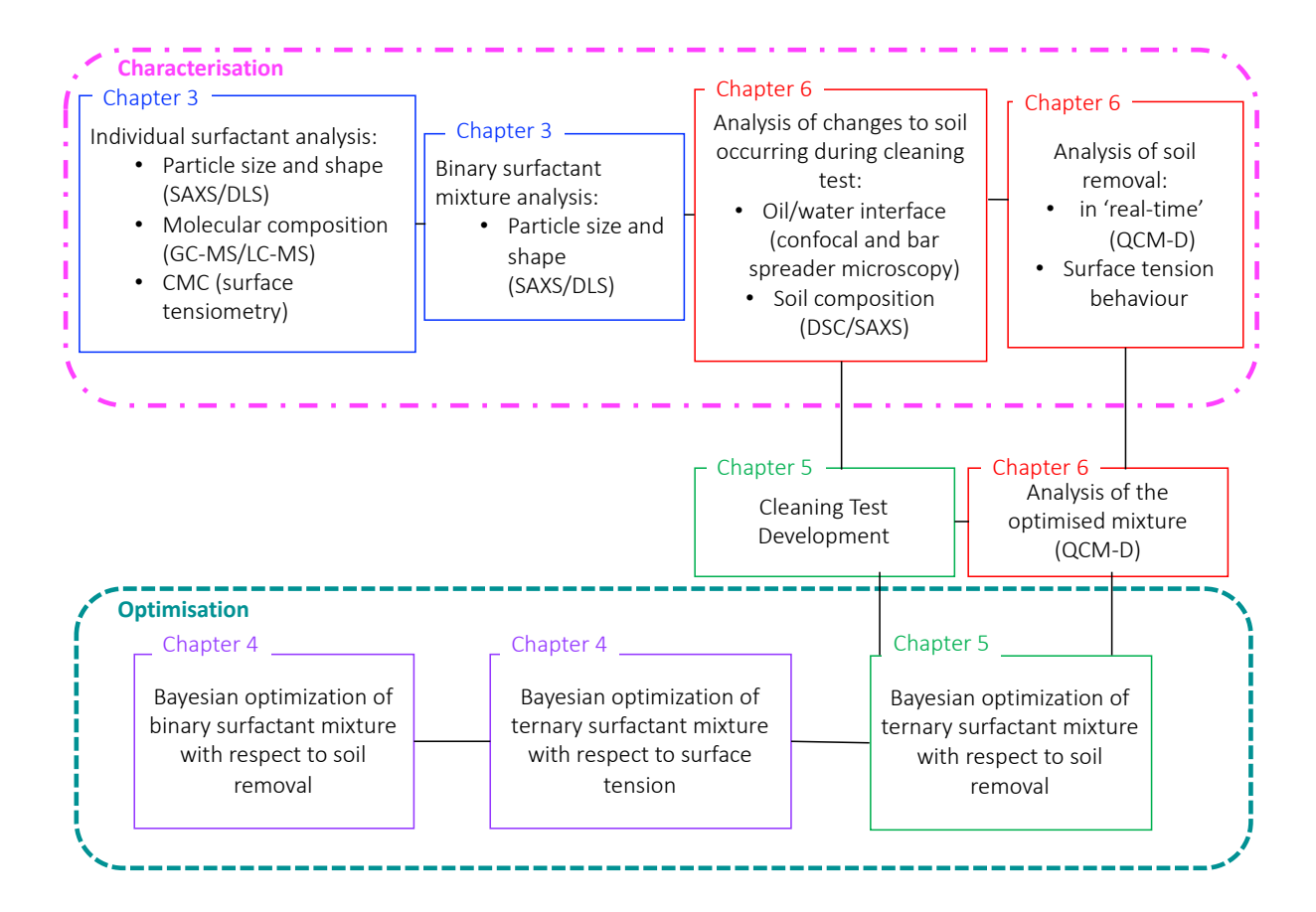


Figure 1.7: Schematic representation of the organisation of this thesis, highlighting the areas focusing on characterisation (pink) and optimisation (green). Black lines indicated the related sections. The colour of the boxes indicate their chapter locations.

1.7 References

- 1. Scheidgen, A. & Zanker, S. A.I.S.E. Activity & Sustainability Report 2017-18. (2018).
- 2. Yu, Y., Zhao, J. & Bayly, A. E. Development of Surfactants and Builders in Detergent Formulations. *Chinese J. Chem. Eng.* **16**, 517–527 (2008).
- 3. Bajpai, D. & Tyagi, V. K. K. Laundry Detergents: An Overview. J. Oleo Sci. 56, 327–340 (2007).
- 4. Flick, E. W. *Advanced Cleaning Product Formulations: Volume 3.* (Noyes Publications, 1996).
- 5. Chanwattanakit, J., Scamehorn, J. F., Sabatini, D. A. & Chavadej, S. Laundry Detergency of Solid Non-particulate Soil or Waxy Solids: Part I. Relation to Oily Soil Removal Above the Melting Point. *J. Surfactants Deterg.* **20**, 815–830 (2017).
- 6. Somasundaran, P. & Johansson, I. *Handbook for cleaning/decontamination of surfaces*. (Elsevier, 2007).
- 7. Jennings, W. G. Theory and Practice of Hard-Surface Cleaning. *Adv. Food Res.* **14**, 325–458 (1965).
- 8. Cox, M. F. Surfactants for hard-surface cleaning: Mechanisms of solid soil removal. *J. Am. Oil Chem. Soc.* **63**, 559–565 (1986).
- 9. Schwartz, A. M. Recent advances in detergency theory. *J. Am. Oil Chem. Soc.* **48**, 566–570 (1971).
- 10. Miller, C. A. & Raney, K. H. Solubilization-emulsification mechanisms of detergency. *Colloids and Surfaces A: Physicochemical and Engineering Aspects* **74**, 169–215 (1993).
- 11. Marano, A. V., Steciow, M. M. & Arellano, M. L. New records of chytridiaceous fungi (chytridiomycota) from the reserva natural selva marginal punta lara (Argentina) with comments on some previously reported species. *J. Surfactants Deterg.* **12**, 173–183 (2009).
- 12. Stellner, K. L. & Scamehorn, J. F. Hardness Tolerance of Anionic Surfactant Solutions. 1. Anionic Surfactant with Added Monovalent Electrolyte. *Langmuir* **5**, 70–77 (1989).
- 13. Koodynska, D. Chelating Agents of a New Generation as an Alternative to Conventional Chelators for Heavy Metal Ions Removal from Different Waste Waters. in *Expanding Issues in Desalination* 339–370 (InTech, 2011).
- 14. Kanegsberg, B. & Kanesberg, E. Handbook for Critical Cleaning: Cleaning agents and systems Barbara Kanegsberg, Edward Kanegsberg Google Books. (2011).
- 15. De Ketttenis, P. The historic and current use of glycol ethers: A picture of change. in *Toxicology Letters* **156**, 5–11 (Elsevier Ireland Ltd, 2005).
- 16. Block, S. S. Disinfection, sterilization, and preservation. (Williams & Wilkins, 2001).

- 17. Ioannou, C. J., Hanlon, G. W. & Denyer, S. P. Action of disinfectant quaternary ammonium compounds against Staphylococcus aureus. *Antimicrob. Agents Chemother.* (2007).
- 18. Maris, P. Modes of action of disinfectants. Rev. Sci. Tech. 14, 47–55 (1995).
- 19. Morpeth, F. F. *Preservation of Surfactant Formulations. Preservation of Surfactant Formulations* (Springer Netherlands, 2011).
- 20. Rastogi, S. C., Heydorn, S., Johansen, J. D. & Basketter, D. A. Fragrance chemicals in domestic and occupational products. *Contact Dermatitis* **45**, 221–225 (2001).
- 21. Rosen, M. J. & Kunjappu, J. T. *Surfactants and Interfacial Phenomena*. *A Wiley-Interscience publication* (Wiley, 2012).
- 22. Griffin, W. C. Classification of surface-active agents by 'HLB'. J. Soc. Cosmet. Chem. (1946).
- 23. Davies, J. T. A quantitative kinetic theory of emulsion type. I. Physical chemistry of the emulsifying agent. in *2nd International Congress Surface Activity* (1957).
- 24. Griffin, W. C. Calculation of HLB Values of Non-Ionic Surfactants. *J. Soc. Cosmet. Chem.* **5**, 249–256 (1954).
- 25. Gadhave, A. Determination of Hydrophilic-Lipophilic Balance Value. *Int. J. Sci. Res.* **3**, 573–575 (2014).
- 26. Atkins, P. & Paula, J. de. *Atkins' Physical chemistry Ninth Edition*. *Oxford University Press* (2010).
- 27. Chandler, D. Interfaces and the driving force of hydrophobic assembly. *Nature* **437**, 640–647 (2005).
- 28. Dias, C. L. et al. The hydrophobic effect and its role in cold denaturation. Cryobiology (2010).
- 29. Kronberg, B., Costas, M. & Silveston, R. Thermodynamics of the hydrophobic effect in surfactant solutions: micellization and adsorption. *Pure Appl. Chem.* **67**, 897–902 (1995).
- 30. Maibaum, L., Dinner, A. R. & Chandler, D. Micelle formation and the hydrophobic effect. *J. Phys. Chem. B* (2004).
- 31. Phillips, J. N. The energetics of micelle formation. *Trans. Faraday Soc.* **51**, 561–569 (1955).
- 32. Carroll, B. The direct study of oily soil removal from solid substrates in detergency. in *Colloids* and *Surfaces A: Physicochemical and Engineering Aspects* **114**, 161–164 (Elsevier Science B.V., 1996).
- 33. Lombardo, D., Kiselev, M. A., Magazù, S. & Calandra, P. Amphiphiles Self-Assembly: Basic Concepts and Future Perspectives of Supramolecular Approaches. *Adv. Condens. Matter Phys.* **2015**, (2015).
- 34. Zettlemoyer, A. C. Micellization, solubilization, and microemulsions. Adv. Colloid Interface Sci.

- 9, 346 (1978).
- 35. Zana, R. *Dynamics of Surfactant Self-Assemblies*. *Dynamics of Surfactant Self-Assemblies* (CRC Press, 2005).
- 36. Goddard, E. D. Surfactants and interfacial phenomena. Colloids and Surfaces 40, (1989).
- 37. Rubingh, D. N. Mixed micelle solutions. in *Solution chemistry of surfactants* 337–354 (Springer, 1979).
- 38. Khan, A. & Marques, E. F. Synergism and polymorphism in mixed surfactant systems. *Curr. Opin. Colloid Interface Sci.* **4**, 402–410 (1999).
- 39. Paye, M. *et al.* Antagonisms between surfactants: The case of laundry detergents. *Tenside, Surfactants, Deterg.* **43**, 290–294 (2006).
- 40. Jost, F., Leiter, H. & Schwuger, M. Synergisms in binary surfactant mixtures. *Kolloid-Zeitschrift und Zeitschrift für Polym.* **266**, 554–561 (1988).
- 41. Sugihara, G., Nagadome, S., Oh, S.-W. & Ko, J.-S. A Review of Recent Studies on Aqueous Binary Mixed Surfactant Systems. *J. Oleo Sci.* **57**, 61–92 (2008).
- 42. Mysels, K. J. & Otter, R. J. Thermodynamic aspects of mixed micelles—application to an empirically established equilibrium. *J. Colloid Sci.* **16**, 474–480 (1961).
- 43. Clint, J. H. Micellization of mixed nonionic surface active agents. *J. Chem. Soc. Faraday Trans.* 1 Phys. Chem. Condens. Phases **71**, 1327–1334 (1975).
- 44. Lange, H. & Beck, K. H. Zur Mizellbildung in Mischlösungen homologer und nichthomologer Tenside. *Kolloid-Zeitschrift Zeitschrift für Polym.* (1973).
- 45. Holland, P. M. & Rubingh, D. N. Nonideal multicomponent mixed micelle model. *J. Phys. Chem.* **87**, 1984–1990 (1983).
- 46. Hildebrand, J. H. Solubility. XII. Regular solutions. J. Am. Chem. Soc. 51, 66–80 (1929).
- 47. Azzam, E. M. S. Effect of Alkyl Groups in Anionic Surfactants on Solution Properties of Anionic-Nonionic Surfactant System. *J. Surfactants Deterg.* (2001).
- 48. Rubingh, D. N. & Jones, T. Mechanism of detergency in systems containing cationic and nonionic surfactants. *Ind. Eng. Chem. Prod. Res. Dev.* **21**, 176–182 (1982).
- 49. Zhu, B. Y. & Rosen, M. J. Synergism in binary mixtures of surfactants. IV. Effectiveness of surface tension reduction. *J. Colloid Interface Sci.* **99**, 435–42 (1984).
- 50. Hua, X. Y. & Rosen, M. J. Synergism in binary mixtures of surfactants. I. Theoretical analysis. *J. Colloid Interface Sci.* **90**, 212–219 (1982).
- 51. Hua, X. Y. & Rosen, M. J. Conditions for synergism in surface tension reduction effectiveness in binary mixtures of surfactants. *J. Colloid Interface Sci.* **125**, 730–732 (1988).

- 52. Hines, J. D. Theoretical aspects of micellisation in surfactant mixtures. *Current Opinion in Colloid and Interface Science* **6**, 350–356 (2001).
- 53. Shiloach, A. & Blankschtein, D. Prediction of Critical Micelle Concentrations of Nonideal Ternary Surfactant Mixtures. *Langmuir* **14**, 4105–4114 (1998).
- 54. Hines, J. D., Thomas, R. K., Garrett, P. R., Rennie, G. K. & Penfold, J. A Study of the Interactions in a Ternary Surfactant System in Micelles and Adsorbed Layers. *J. Phys. Chem. B* **102**, 9708–9713 (2002).
- 55. Ishiguro, M. & Koopal, L. K. Surfactant adsorption to soil components and soils. *Adv. Colloid Interface Sci.* **231**, 59–102 (2016).
- 56. Verma, S. & Kumar, V. V. Relationship between oil-water interfacial tension and oily soil removal in mixed surfactant systems. *J. Colloid Interface Sci.* **207**, 1–10 (1998).
- 57. Schwuger, M. J. Effects of adsorption on detergency phenomena: I. *J. Am. Oil Chem. Soc.* **59**, 258–264 (1982).
- 58. Young, T. III. An essay on the cohesion of fluids. *Philos. Trans. R. Soc. London* **95**, 65–87 (1805).
- 59. Kissa, E. Wetting and detergency. *Pure Appl. Chem.* **53**, 2255–2268 (1981).
- 60. De Gennes, P., Brochard-Wyart, F. & Quéré, D. *Capillarity and Wetting Phenomena*. (Springer, 2004).
- 61. Mahé, M., Vignes-Adler, M., Rousseau, A., Jacquin, C. G. & Adler, P. M. Adhesion of droplets on a solid Wall and detachment by a shear flow. I. Pure systems. *J. Colloid Interface Sci.* **126**, 314–328 (1988).
- 62. Carroll, B. J. The kinetics of solubilization of nonpolar oils by nonionic surfactant solutions. *J. Colloid Interface Sci.* **79**, 126–135 (1981).
- 63. Chan, A. F., Evans, D. F. & Cussler, E. L. Explaining solubilization kinetics. *AIChE J.* **22**, 1006–1012 (1976).
- 64. Shaeiwitz, J. A., Chan, A. F. C., Cussler, E. L. & Evans, D. F. The mechanism of solubilization in detergent solutions. *J. Colloid Interface Sci.* **84**, 47–56 (1981).
- 65. Sailaja, D., Suhasini, K. L., Kumar, S. & Gandhi, K. S. Theory of rate of solubilization into surfactant solutions. *Langmuir* (2003).
- 66. Favrat, O., Gavoille, J., Aleya, L. & Monteil, G. Real time study of detergent concentration influence on solid fatty acid film removal processes. *J. Surfactants Deterg.* **16**, 213–219 (2013).
- 67. Carroll, B. J. Physical aspects of detergency. *Colloids and Surfaces A: Physicochemical and Engineering Aspects* **74**, 131–167 (1993).

- 68. Kabin, J. A., Tolstedt, S. L., Sáez, A. E., Grant, C. S. & Carbonell, R. G. Removal of organic films from rotating disks using aqueous solutions of nonionic surfactants: Effect of surfactant molecular structure. *J. Colloid Interface Sci.* **206**, 102–111 (1998).
- 69. Kabin, J. A., Sáez, A. E., Grant, C. S. & Carbonell, R. G. Removal rates of major and trace components of an organic film using aqueous nonionic surfactant solutions. *Ind. Eng. Chem. Res.* **38**, 683–691 (1999).
- 70. Tongcumpou, C. *et al.* Microemulsion formation and detergency with oily soils: III. Performance and mechanisms. *J. Surfactants Deterg.* **8**, 147–156 (2005).
- 71. Phaodee, P., Attaphong, C. & Sabatini, D. A. Cold Water Detergency of Triacylglycerol Semisolid Soils: The Effect of Salinity, Alcohol Type, and Surfactant Systems. *J. Surfactants Deterg.* **22**, 1175–1187 (2018).
- 72. Shahriari, B., Swersky, K., Wang, Z., Adams, R. P. & De Freitas, N. Taking the human out of the loop: A review of Bayesian optimization. *Proc. IEEE* **104**, 148–175 (2016).
- 73. Czitrom, V. One-factor-at-a-time versus designed experiments. *Am. Stat.* **53**, 126–131 (1999).
- 74. Anderson-Cook, C. M. Response Surfaces, Mixtures, and Ridge Analyses. *J. Am. Stat. Assoc.* **103**, 888–888 (2008).
- 75. Cox, D. R. & Reid, N. The Theory of the Design of Experiments. Analysis (2002).
- 76. Box, G. E. P. & Behnken, D. W. Some New Three Level Designs for the Study of Quantitative Variables. *Technometrics* **2**, 455–475 (1960).
- 77. Omidbakhsh, N., Duever, T. A., Elkamel, A. & Reilly, P. M. Systematic Statistical-Based Approach for Product Design: Application to Disinfectant Formulations. *Ind. Eng. Chem. Res.* **49**, 204–209 (2010).
- 78. Omidbakhsh, N., Duever, T. A., Elkamel, A. & Reilly, P. M. A Bayesian experimental design approach for assessing new product performance: An application to disinfectant formulation. *Can. J. Chem. Eng.* **88**, 88–94 (2010).
- 79. Omidbakhsh, N., Duever, T. A., Elkamel, A. & Reilly, P. M. A Systematic Computer-Aided Product Design and Development Procedure: Case of Disinfectant Formulations. *Ind. Eng. Chem. Res.* **51**, 14925–14934 (2012).
- 80. Coret, J., Shiloach, A., Berger, P. & Blankschtein, D. Critical micelle concentrations of ternary surfactant mixtures: Theoretical prediction with user-friendly computer programs and experimental design analysis. *J. Surfactants Deterg.* **2**, 51–58 (1999).
- 81. Ghahramani, Z. Probabilistic machine learning and artificial intelligence. *Nature* **521**, 452–459 (2015).
- 82. Rasmussen, C. E. & Williams, C. K. I. *Gaussian Processes for Machine Learning*. (MIT Press, 2006).

- 83. Seko, A. *et al.* Prediction of Low-Thermal-Conductivity Compounds with First-Principles Anharmonic Lattice-Dynamics Calculations and Bayesian Optimization. *Phys. Rev. Lett.* **115**, 205901 (2015).
- 84. Balachandran, P. V., Xue, D., Theiler, J., Hogden, J. & Lookman, T. Adaptive Strategies for Materials Design using Uncertainties. *Sci. Rep.* **6**, (2016).
- 85. Xue, D. *et al.* Accelerated search for materials with targeted properties by adaptive design. *Nature Communications* **7**, (2016).
- 86. Li, C. *et al.* Rapid Bayesian optimisation for synthesis of short polymer fiber materials. *Sci. Rep.* **7**, 5683 (2017).
- 87. Yamashita, T. *et al.* Crystal structure prediction accelerated by Bayesian optimization. *Physical Review Materials* **2**, (2018).
- 88. Li, X. *et al.* Efficient Optimization of the Performance of Mn 2+ -Doped Kesterite Solar Cell: Machine Learning Aided Synthesis of High Efficient Cu 2 (Mn,Zn)Sn(S,Se) 4 Solar Cells. *Sol. RRL* **2**, 1870237 (2018).

2. Materials and methods

2.1 Surfactants

The commercial surfactants used in this project were: lauramine oxide (LO) (Stepan), Cocamidopropyl betaine (CB) (Solvay), Benzalkonium Chloride (BC) (Thor), Decyl Glucoside (DG) (KemCare), and a linear alcohol ethoxylate (AE) (Kao Chemicals), in addition laboratory reagent grade Sodium dodecyl sulphate (SDS)(Sigma-Aldrich) was used.

Amphoteric / Zwitterionic CH₃(CH₂)_nN Lauramine Oxide Cocamidopropyl Betaine Non-ionic OH (CH₂)_nCH₃**Decyl Glucoside** Alcohol Ethoxylate Ionic **Cationic Anionic** ,o[⊝] Na[⊕] CI⊝ Benzalkonium Chloride Sodium Dodecyl Sulphate

Figure 2.1: Structures of the commercial surfactants used in the project. m is the number of glucoside units and n is the number of CH₂ groups in the alkyl chain.

The general molecular structure of each surfactant can be seen in figure 2.1. The tradename, active content (the weight percent concentration of each surfactant in aqueous solution) and pH (at the concentration supplied), as reported by the suppliers, are summarised in table 2.1.

Table 2.1: The active content and pH of the surfactants as supplied

Generic Name	Tradename	Active Content / %	рН
Lauramine Oxide	Ammonyx LO	29-31	7-8.5
Alkyldimethyl benzalkonium Chloride	Acticide BAC50M	49-51	6-9
Decyl Glucoside	Kemgluco CEHL	50	11-12.5
Cocamidopropyl Betaine	CAB 818	28-32	4.5-5.5
Alcohol Ethoxylate	Rhodasurf B70	100	6-8

2.2 Analytical Techniques

2.2.1 Solids Content

The concentration of the surfactants was determined thermo-gravimetrically using an Ohaus MB45 halogen moisture analyser. The instrument consists of a balance unit, which measures the mass of the sample, and a halogen lamp, to heat the sample. The initial weight of the sample is measured (0.5-1.0 g). A halogen dryer heats the sample rapidly to evaporate moisture. Once the sample no longer changes in mass, the sample is considered dry, and the change in mass is measured (within the instrument) to determine water content.

Surfactant Concentration (%) =
$$\frac{\text{Final mass of sample (g)}}{\text{Initial mass of sample (g)}} \times 100 \text{ (%)}$$

2.2.2 Mass Spectrometry

Mass spectrometry separates molecules of a sample based on their mass-to-charge ratio, which can be used to determine their molecular weight. The sample is ionised to form charged molecules or fragments; commonly used methods include electron ionisation (EI) and electrospray (ESI) ionisation (both are used in this project). In EI, the sample enters the ion source in the gas phase and is bombarded with electrons. This results in positively charged ions which travel to the ioniser and are filtered by mass-to-charge ratio, the detector counts the number of ions with each mass to generate the resulting spectrum. EI is used for small, neutral, organic molecules which are volatile whereas ESI is suitable for large molecules, e.g. polymers and biomolecules, which are ionised with no dissociation. In

addition, any polar solvent can be used, e.g. water. In ESI, a solution of the sample is sprayed through an ESI capillary, a highly charged needle. The resulting charged droplets contain solvated positive and negative ions. The solvent is evaporated using heat or gas flow and the individual gas phase ions are guided towards a mass analyser.

Tandem mass spectrometry techniques were performed by the Chemistry Mass Spectrometry Facility at the University of Sheffield to calculate the molecular weight and chain length distribution of the surfactants, in the form obtained from the industrial supplier. A Perkin Elmer Turbomass instrument was used for the GC-MS of LO and AE. An Agilent 6530 Accurate-Mass Quadrupole Time-of-Flight LC-MS system was used to characterize CAB, BC and DG. The spectra obtained were analysed by considering the sequential loss of ion fragments, using average atomic weight for C (12.0 amu), H (1.0 amu), O (15.99 amu), N (14.0 amu) and Na (22.99 amu) and Cl (35.45 amu).

2.2.3 Surface Tensiometry

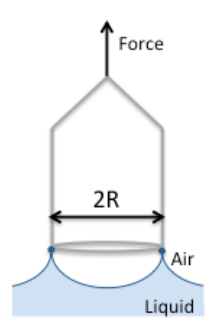


Figure 2.2 The application of a De Nöuy Ring to the surface of a solution. R is the radius of the ring.

Surface tension can be measured using a surface tensiometer. The tensiometer is comprised of a sensitive microbalance, a platform to move the sample up and down with precise control and a device with precisely known dimensions that comes into contact with the liquid to be measured. The De Nöuy Ring method measures the force required to pull a free-hanging platinum-iridium ring through the surface of a solution.³ The calculation of surface tension is dependent on the maximum pull on the ring as it is raised out of the liquid and into the air, F_{max}, and the major radius of the ring to the centre of the wire, R:⁴

$$\gamma = \frac{F_{max} - F_r}{4\pi R}$$

Where γ is the surface tension and F_r is the ring correction factor which is required because the weight of the liquid film immediately beneath the ring is raised when the ring pulls upward.

2.2.3.1 Sample Preparation

Aqueous surfactant solutions were made up using deionised water and the appropriate amount of surfactant, accounted for by the determination of solids content, from stock solutions of 0.1, 0.5 or 1 w/w% dependent on the experiment. For solutions requiring pH adjustment, either sodium hydroxide (0.1 M) or hydrochloric acid (0.1 M) was used. Surfactant solutions were kept at room temperature (20 ± 1 °C) for at least one hour before performing the surface tension measurements.

2.2.3.2 Measurement

Surface tension measurements were performed using a LAUDA TD3 tensiometer with a Du Nöuy ring attachment. Before each measurement, the ring was cleaned. First, the ring was immersed in ethanol before being subjected to a high-temperature flame, to remove any adsorbed material from previous samples. The cleaning and flaming processes were repeated with deionised water. Before each batch of measurements, the instrument was calibrated, and subsequently the cleanliness was checked by measuring the surface tension of distilled water (72 mN m $^{-1}$). All measurements were performed at room temperature (20 \pm 1 °C). For each measurement, the analysis was automated so that five or more repeats were made until a standard deviation of less than 0.1 mN m $^{-1}$ was obtained.

2.2.4 Differential Scanning Calorimetry (DSC)

DSC is a technique that is commonly used to determine the properties of a material in response to temperature. As a method of thermal analysis that measures the temperature and heat flow associated with phase transitions, it can be used to determine properties such as the melting and crystallisation temperatures and oxidative stability.^{5,6}

The DSC instrument used was a heat flux DSC which measures the heat flow to a pan containing a sample and reference, typically, an empty pan, that is needed to maintain the same temperature as they are heated and cooled.⁷ If the sample undergoes an endothermic

transition, such as the melting of a solid to a liquid, more heat will be required to maintain the temperature of the sample. Conversely, if there is an exothermic transition which generated energy, *i.e.* crystallisation, then less heat will be required to maintain the temperature.

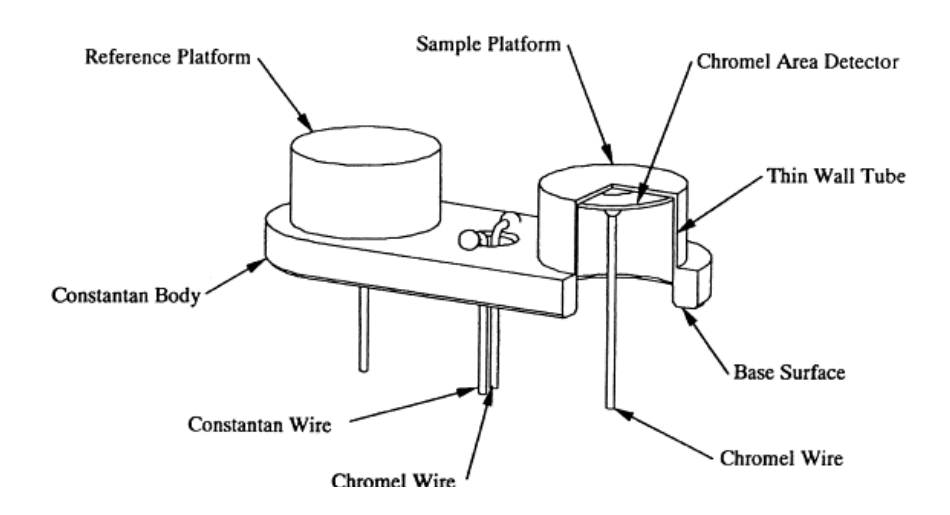


Figure 2.3: Heat flux DSC sensor assembly, diagram reproduced from "New heat flux DSC measurement technique" by Robert Danley⁷

Figure 2.3 shows a schematic of the sensor assembly in a DSC instrument.⁷ The sensor and reference calorimeters are separate so that the heat flow in one does not affect the other. The chromel area detector and wire acts as a thermocouple to measure the temperature difference between the sample and the reference. The constantan wire and body transfer heat to and from the sample and reference platforms.

2.2.4.1 Measurement

Heating and cooling curves of the oil, fats and their mixtures were made using a TA Instruments DSC-25. Samples of approximately 18 mg were weighed into Tzero aluminium hermetic pans with lids. The instrument was calibrated for heat flow and temperature using both indium and zinc standards. An empty pan was used to perform a baseline calibration. All experiments were purged with N_2 . A heating/cooling rate of 10 °C/min was used. The samples were initially heated from 20 °C to 70 °C, held at 70 °C for 5 min, cooled to -40 °C, held at -40 °C for 5 min, heated to 70 °C, held at 70 °C for 5 min and finally cooled back to -40 °C.

2.2.5 Scattering Techniques

2.2.5.1 Dynamic Light Scattering (DLS) Introduction

Dynamic light scattering can be used to characterise the size of colloidal particles in the range from nanometers to microns.⁸ The technique uses a laser beam to illuminate the dispersed particles which scatter the laser light, figure 2.4. Brownian motion is the random movement of particle in a fluid due to collisions with solvent molecules and causes smaller particles to travel faster than larger ones. Hence, the distances between particles changes constantly with time causing the intensity of the scattered light to fluctuate. By analysing the changes in the fluctuations in intensity of the scattered light, the translational diffusion coefficient can be obtained, which can be related to the hydrodynamic radius of a particle using the Stokes-Einstein equation:

$$d(H) = \frac{kT}{3\pi\eta D}$$

where d(H) is the hydrodynamic diameter, k is the Boltzmann constant, T is the temperature, η is the viscosity of the sample and D is the translational diffusion co-efficient.⁹

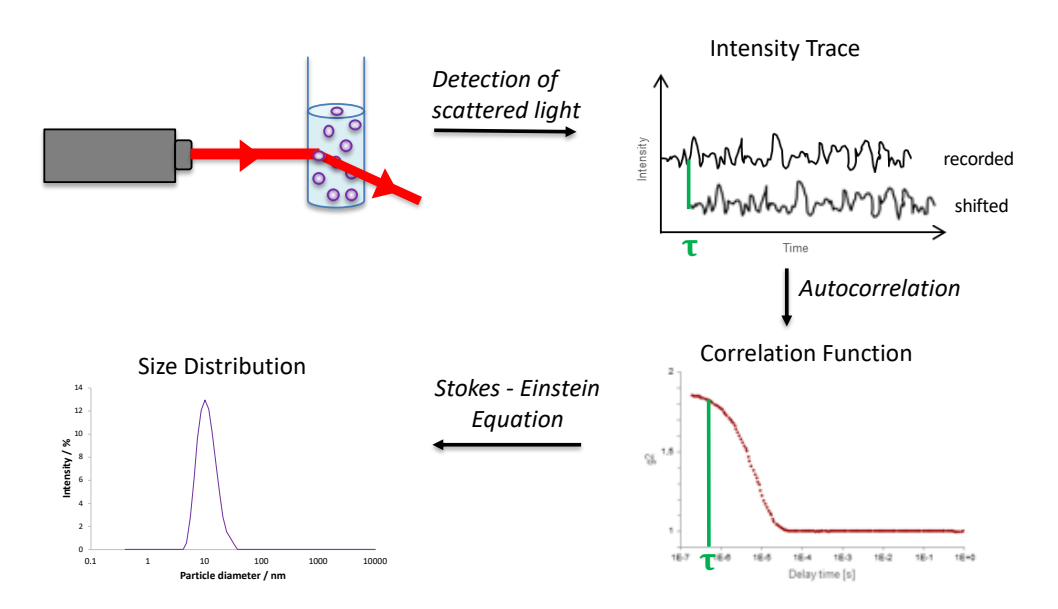


Figure 2.4: The size of the particles in a dispersion can be determined using a DLS instrument. Light scattered from a dispersion of particles, fluctuates due to the movement of particles caused by Brownian motion. The recorded fluctuations in the intensity trace are converted to a correlation function by an autocorrelator. The Stokes-Einstein equation is used to obtain a size distribution of the hydrodynamic diameters of the particles.

DLS measures the hydrodynamic diameter, which describes the effective size of a particle moving through a fluid.¹⁰ The hydrodynamic diameter is dependent on: the particle's size and surface structure, the concentration of the solution and the type of ions in the medium.

The intensity of scattering at a given scattering angle depends on the positions of the particles at a given time. However, as the particles are in motion due to diffusion from Brownian motion, the scattered intensity fluctuates, as shown schematically in the intensity trace in figure 2.4. The fluctuations are analysed by a digital signal processing device called an autocorrelator, which produces a scattered intensity correlation function, which exponentially decays with time, τ , for a solution of monodisperse, spherical particles. From the autocorrelation function, the exponential decay constant, Γ , can be derived which is related to the translational diffusion co-efficient, D:

$$\Gamma = Dq^2$$

Where q is the scattering vector:

$$q = \frac{4\pi n}{\lambda} \sin(\frac{\theta}{2})$$

Where n is the refractive index of the dispersing medium, λ is the wavelength of the laser and θ is the scattering angle (the angle between the direction of the light entering the sample and the position of the detector). From the translational diffusion co-efficient, D, the hydrodynamic diameter can be calculated using the Stokes-Einstein equation, stated previously.

To account for sample polydispersity, a cumulants analysis can be used which fits a single exponential to the correlation function to obtain the intensity weighted z-average diameter. The z-average diameter, D_z , is the intensity weighted harmonic mean size:

$$D_z = \frac{\sum S_i}{\sum \binom{S_i}{D_i}}$$

where S_i is the scattered intensity from the particle i and D_i is the diameter of particle i. The width of the distribution is estimated to obtain the polydispersity distribution.

One limitation of using DLS to measure the size of particles that are not monodisperse arises from the use of the intensity average. If there is a mixture of particles, the diameter reported is a biased towards the larger particles because they scatter more light. The

intensity of scattered light is proportional to particle diameter raised to the power six. Therefore, DLS is sensitive to dust particles and cleanliness is important.¹⁰

2.2.5.2 DLS Measurement

A Zetasizer Nano S (Malvern Instruments, UK) was used to measure the apparent hydrodynamic diameter from the Stokes–Einstein relationship. The light source was a He-Ne laser that operated at a wavelength of 533 nm at a fixed scattering angle of 173°. Each measurement was pre-set to 10 runs each of 10 seconds acquisition time at 25 °C. An average was taken from 3 measurements. The polydispersity index (PDI), z-average hydrodynamic diameter and its standard deviation, of each sample were calculated.

2.2.5.3 Small Angle X-ray Scattering (SAXS) Introduction

SAXS is used to determine the average size and structure of particles in the range of 1 to 100 nm. ^{12–14} SAXS can be used to study solid or liquid matrices containing solid liquids or gases including the shape and size of surfactants in aqueous solution. ^{15–18} The applications of SAXS are broad, including study of: the ordering of liquid crystals used in displays, mesoporous materials for catalysis, nanostructure of biological materials and self-assembly in cosmetics, food and pharmaceutical products. ^{19–24} The advantages of analysis using SAXS include its accuracy, the minimal sample preparation required, and that the sample is not destroyed.

SAXS can measure the size of particles in the nanometre range due to the short wavelengths of x-rays, which are high energy, electromagnetic waves with a wavelength of 0.1 to 10 nm. Most x-rays directed at a material pass through, though some are absorbed or scattered. The elastic scattering of these x-rays is recorded at small scattering angles (0.1 - 10°). The x-ray beam is sensitive to differences in electron density, which causes a change in the intensity of the scattered light, which can be used to obtain information about the average particle structure. The greater the difference in electron density, the greater the scattering intensity.

Figure 2.6 shows a schematic of the components in a SAXS instrument. Most experiments are performed in transmission mode, where X-rays are directed at a sample of particles and the scattering from the atoms in the sample is detected on the opposing side. In the x-ray source, a microfocus tube produces a beam of electrons which strike a liquid metal-jet generating an x-ray beam. The x-rays are emitted accompanying the electrons in the metal atoms to dropping down from higher energy levels to fill vacancies formed by ejection of

elections from the inner shells of the metal due to the high-speed electrons in the beam. As the angles between the incident and the scattered beam are very small, the divergence of the incoming beam must be minimised. The beam is narrowed by passing it through using slits or pinholes. The sample holder can vary depending on the sample type run and whether there is a need to study the behaviour of the sample under a changing environment such as temperature or flow. For a static study, a liquid sample can be placed in a thin-walled capillary.

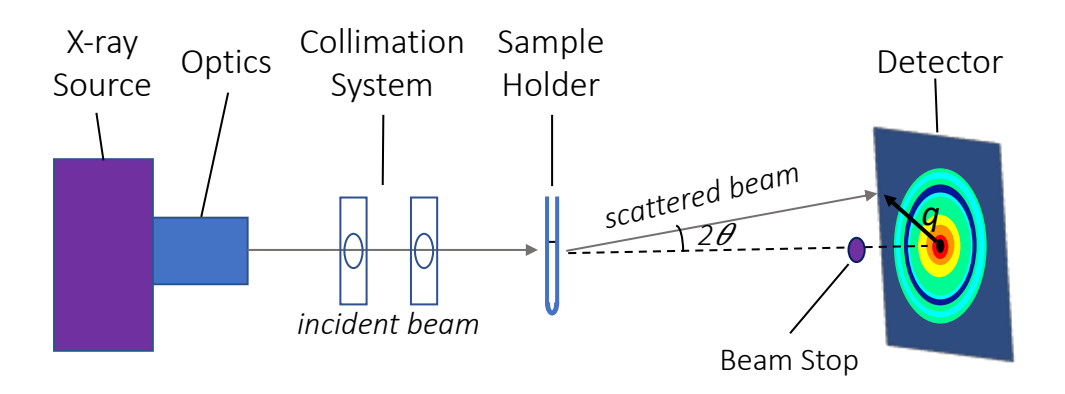


Figure 2.5: The components of a SAXS instrument

Once the beam hits the sample, some will be scattered and collected by the detector. As the unscattered beam is still intense, it can be problematic if it hits the detector as either the strong backscatter from the detector can hide the weak scattered signal or the detector itself could be damaged. Therefore, a lead or tungsten beamstop can be used to block the direct beam. Detectors count the number of particles hitting an area over time to generate a 2D interference pattern showing the variation in intensity of the absorbed radiation, due to the constructive and destructive interference.

A two-dimensional scattering pattern is recorded in the plane of detection. This is converted into a one-dimensional scattering pattern by taking the circular average which also improves the statistical quality of the data. At this point, the scattering of the matrix (e.g. a solvent in an aqueous surfactant solution) needs to be taken into consideration. The 1D pattern from the solvent capillary and the sample is subtracted from the pattern of the solvent, sample and capillary, to obtain the particles alone. This requires the transmittance of the solvent and particles to be the same because if the particles absorb more than the solvent, the scattering of the particles will be reduced. To take the fact that, in most cases, the transmittance of the solvent and particles differs, the 1D scattering patterns are normalised

using a scaling factor. Normalised, background subtracted, scattering patterns can be analysed to gain information about the shape, size and distribution of the particles.

The scattering vector, q, which is inversely proportional to the characteristic length scale, can be calculated from the scattering angle, 2θ , and the wavelength of the incident radiation, λ :

$$q = \frac{4\pi}{\lambda}\sin(\theta)$$

2.2.5.4 SAXS Measurement

SAXS experiments were conducted using a laboratory SAXS instrument (Xeuss 2.0, Xenocs, France), with a liquid gallium X-ray source (MetalJet, Excillium, Sweden) at a wavelength of 0.134 nm, with motorized scatterless slits for beam collimation and a Dectris Pilatus 1M pixel detector with a sample-to-detector distance of 0.55 m. Patterns were recorded over the scattering vector (q) range of 0.013 to 1.426 A⁻¹, where $q = 4\pi sin\theta$ and θ is half the scattering angle. Samples were pipetted in to a 1.7 nm glass capillary.

To obtain SAXS of surfactant solutions, all SAXS patterns were corrected for background scattering by initially measuring the scattering of a capillary containing deionised water. Intensity calibrations were obtained by using the SAXS patterns of the empty and water filled capillaries. The excess scattering associated with the surfactant micelles was extracted from the SAXS data by subtraction of the SAXS pattern of a capillary containing water. Data was reduced using the Foxtrot software package and further analysed using SasView software.²⁶

2.2.5.5 SAXS Models

The scattering intensity, I, as a function of q, the scattering wave vector, is:

$$I(q) = c P(q) S(q, c)$$

where c is the concentration of the particles in the matrix, P(q) is the form factor based on the orientationally average scattering profile of one particle and S(q,c) is the structure factor which expresses the interactions of the particles in solution.²⁷ At low q, the structure factor affects I(q) more strongly. The scattering intensity of the form factor alone can be found by using a low concentration of the particles so S(q) tends to 1.

Where there are 2 regions of differing electron density (spheres of uniform electron density suspended in a different phase) such as in the case of benzalkonium chloride surfactant micelles, the form factor of the scattering vector is:

$$P(q) = \left[3 V_{sph}(\rho - \rho_s) \frac{\sin(qR) - qR\cos(qR)}{(qR)^3}\right]^2 = \left[3 V_{sph}(\rho - \rho_s) \frac{j_1(qR)}{qR}\right]^2$$

Where R is the radius of the sphere, ρ and ρ_s are the electron densities of the sphere and the solvent, V_{sph} is the volume of the sphere i.e. $\frac{4 \pi R^3}{3}$ and j_1 is the first order spherical Bessel function $\frac{\sin(x)}{x^2} - \frac{\cos(x)}{x}$.

Where there are 3 regions of differing electron density, a core surrounded by a shell immersed in a solvent, a core-shell sphere (figure 2.6 a)), such as in the case of decyl glucoside surfactant micelles, the form factor is:

$$P(q) = \frac{1}{V} \left[\frac{3 V_c(\rho_c - \rho_s) j_1(qR_c)}{qR_c} + \frac{3 V_c(\rho_c - \rho_{solv}) j_1(qR_s)}{qR_s} \right]^2$$

where R_c is the radius of the core, R_s is the shell thickness and ρ_c , ρ_s and ρ_{sol} are the electron densities of the core, shell and solvent respectively.

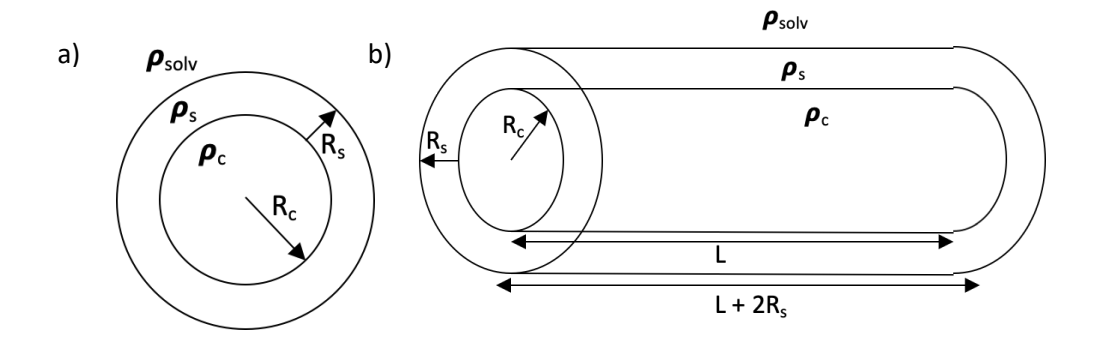


Figure 2.6: Defining the dimensions in the SAXS models for: a) a core-shell sphere and b) a core-shell cylinder

A number of surfactants have been shown to form long, worm-like micelles.^{28–30} The form factor fo these cylindrical particles with a core-shell structure is given by:

$$P(q) = \frac{1}{V_{\rm s}} f^2(q)$$

Where:

$$V_S = \pi (R_C + R_S)^2 \cdot (L + 2t)$$

$$f(q) = 2(\rho_c - \rho_s)V_c \sin\left[\frac{qL\cos\alpha}{2}\right] \frac{j_1[qR_c\sin\alpha]}{[qR_c\sin\alpha]} + \frac{2(\rho_s - \rho_{solv})V_s \sin\left[\frac{q(L+2R_s)\cos\alpha}{2}\right]}{\left[\frac{q(L+2R_s)\cos\alpha}{2}\right] \frac{j_1[q(R_c+R_s)\sin\alpha]}{[q(R_c+R_s)\sin\alpha]}}$$

 V_c is the volume of the core, V_s is the volume of the shell, α is the angle between the major axis and the q vector and L is the length of the core. The total length of the outer shell is expressed as $L + 2R_s$ and the outer radius of the shell is $R_c + R_s$.

For some of the micelles studied, such as SDS, by consideration of the shape of the 1D scattering pattern, it was identified that they formed an ellipsoid shape in aqueous solution with a shell containing hydrophilic head groups, surrounding the hydrophobic tails in the core. As the hydrophilic head groups are the same size, it was assumed the shell would be equal round the circumference of the ellipsoid and so the shell thickness was fixed. The ellipsoid core–shell form factor can be expressed as:

$$P(q) = \frac{1}{V} \int_0^1 \left| F(q, R_{min}, R_{maj}, \alpha) \right|^2 d\alpha$$

$$|F(q, R_{min}, R_{maj}, \alpha)| = V\Delta\rho \cdot (3j_1(u)/u)$$

$$u = q \left[R_{maj}^{2} \alpha^{2} + R_{min}^{2} (1 - \alpha^{2}) \right]^{\frac{1}{2}}$$

where R_{min} and R_{maj} are the minor and major radii of the ellipse, respectively, α is the angle between the major axis and the q vector and V is the volume of the ellipse calculated from $V = \frac{4\pi R_{min}^2 R_{maj}}{3}.^{31,32}$ The contrast, $\Delta \rho$, is the scattering length density difference between the scattering object (e.g. a surfactant micelle) and the solvent.

2.2.6 Quartz Crystal Microbalance and Dissipation (QCM-D)

2.2.6.1 Principles

A quartz crystal microbalance (QCM) measures frequency and dissipation of a quartz crystal sandwiched between two electrodes.³³ When a voltage is applied, the sensor electrodes change shape, depending on the direction of the voltage and the cut of the crystal because of the piezoelectric property of the quartz crystal. If an alternating voltage is applied to a crystal, at a frequency close to its resonant frequency, the crystal oscillates, figure 2.7.

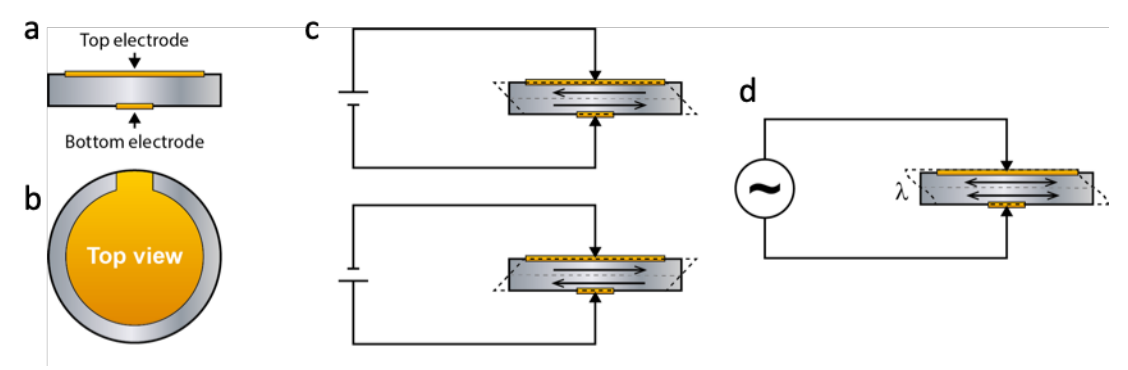


Figure 2.7: Piezoelectricity is the basis for QCM-D, taken from blog.biolinscientific.com. The QCM-D sensor as viewed from a) the side and b) the top. c) The deformation of the disk on the application of a voltage is dependent on the direction of the applied voltage and the cut of the crystal. d) The quartz crystal oscillates on the application of an alternating voltage.

QCMs work because frequency change in the oscillations of the crystal can be related to the mass adsorbed on the surface. When nothing is adsorbed to the surface of the sensor, the crystal oscillates at its resonant frequency. Lowering of the resonant frequency to maintain a constant driving force, is observed as material is adsorbed and conversely, an increase in oscillation frequency indicates mass loss. By measuring this change in frequency, Δf , the mass adsorbed per unit surface, Δm , can be determined by the Sauerbrey equation:

$$\Delta m = \frac{-C\Delta f}{n}$$

where *C* is the mass sensitivity constant, 17.7 ng cm⁻² Hz⁻¹ for 5 MHz AT-cut quartz, which describes the sensitivity of a device to changes in mass.³⁴ The assumptions of this model are the mass adsorbed is small relative to the mass of the crystal and the mass adsorbed is rigid and evenly distributed in a thin layer over the surface. If the applied film is thin and rigid, the decay rate of the oscillation will be low, and the harmonic overtones will overlap. In cases where the film is not rigid, the decay rate of the oscillation is much higher due to dissipation of energy in the adsorbed layer and the higher overtones will not overlap with the resonant frequency. Therefore, the decay rate is related to the viscoelastic properties of materials. In this case, models such as the Voinova-Voigt can be used to relate the frequency and dissipation shifts to parameters of the adsorbed layer such as: thickness, density, viscosity and elasticity.^{35,36}

2.2.6.2 Measurement

To investigate the mechanism of the removal of the TAG soil, adapted for use in the film removal test, 37 by surfactant solutions, a method to coat SiO $_2$ coated quartz sensors (Biolin Scientific) was developed. Before each use, the sensors were placed in a Bioforce UV/ozone cleaner for 30 minutes to remove any organic contaminants. Subsequently, sensors were submerged in a 1% alconox detergent (Sigma-Aldrich), and then placed in a sonic bath for 10 minutes, then washed with deionised water, and the sonication process repeated in deionised water. The adapted TAG (triacyl glyceride) mixture was prepared by mixing linseed oil (8.33 w/w%), vegetable oil (25 w/w%), lard (Sainsburys own brand, 33.3 w/w%) and Vegetable shortening (Crisco, 33.3%) at 50 °C. Once molten, the mixture was pipetted onto a glass slide before baking in an oven at 200 °C for 60 minutes. The baked TAG was removed from the slide and dissolved in toluene (5 w/w%) by stirring at room temperature. Precleaned SiO $_2$ coated sensors were coated with TAG by spin coating the TAG solution (20 µL) at a rate of 500 rpm for 9 seconds followed by 40 seconds at 2000 rpm using an Ossila spin coater to form level films of ~ 1 µm. Coated sensors were subsequently baked in an oven for 1 hour at 50 °C to remove any residual solvent.

QCM measurements were performed on a Q-SENSE E4 system, comprising of 4 flow cells, comprising of 4 flow cell, each holding one sensor such that measurements were obtained from four separate sensors simultaneously. Initially, the sensors were equilibrated in air overnight. Deionised water was initially flowed over the coated chips until a stable baseline was obtained. Next, surfactant (or mixture of surfactants) solutions of interest (one per channel) were flowed through the QCM. The frequency was monitored until a plateau was reached indicating the end of the soil removal process or over a reasonable time scale. All solutions were passed through the QCM at a rate of 0.1 mL min⁻¹ using an Ismatec peristaltic pump.

2.2.7 Microscopy

2.2.7.1 Confocal Microscopy

Confocal microscopy has been widely used to visualise colloidal systems. ³⁸ Its rise in popularity arose from its increase in resolution and contrast compared to widefield fluorescence microscopes and the ability to image a slice of a sample at a selected depth enabling the construction of 3D images from collecting multiple slices. ³⁹ In conventional fluorescence microscopy, the whole sample is illuminated so the image detected contains both in-focus (from in the focal plane) and out-of-focus (from other focal planes) light. In confocal microscopy, the noise is reduced by only illuminating one point in the sample at a time and using a pinhole in front of the detector to block out any out-of-focus fluorescence. As only one point in the sample is excited at a time, light from a laser is raster scanned across a sample using directing mirrors. Different materials within a sample can be made to fluoresce by using fluorophores. Fluorophores are chemical compounds that, when excited with light at a specific wavelength, absorb and re-emit light at a greater wavelength. The fluorescent light from the sample is focused onto a pinhole aperture, the light that makes it through the pinhole is measured by a detector, a photomultiplier tube. A schematic of a confocal microscope can be seen in figure 2.8.

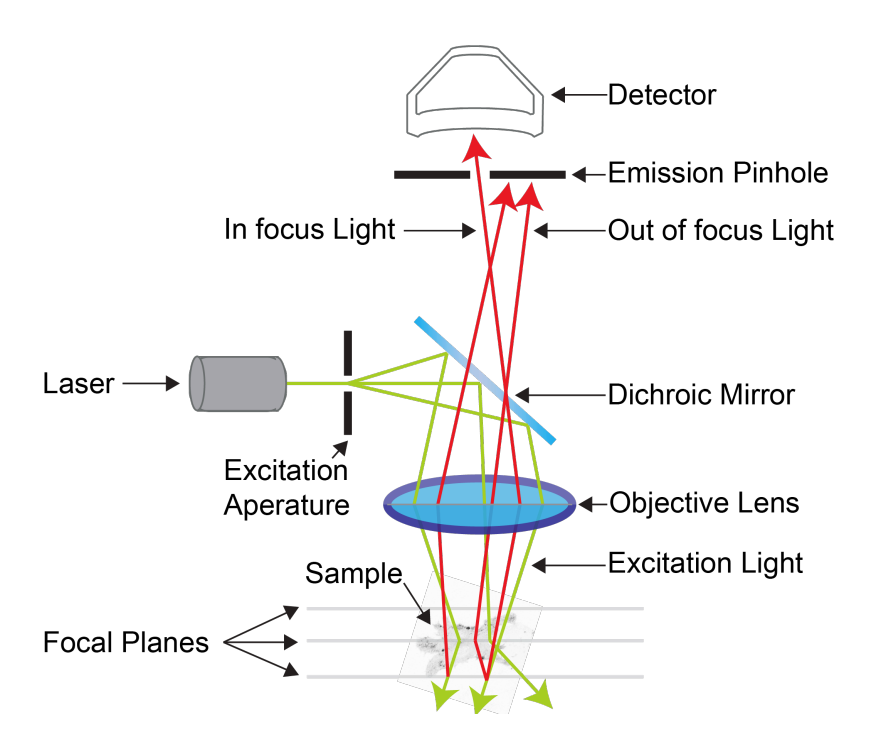


Figure 2.8: The pathways of light in confocal microscopy to image different sections of a fluorescent sample.

The schematic is taken from imb.uq.edu.au/facilities/microscopy/

Imaging work was performed by Darren Robinson at the Wolfson Light Microscopy Facility, using the Nikon A1 confocal microscope equipped with Nikon elements software. Samples of 0.1 mg ml $^{-1}$ Nile Red in vegetable oil (Tesco's own brand) and oleic acid (Sigma-Aldrich) were prepared and stirred overnight. To study the surfactant-oil interface, a drop of the dyed oil and 1% SDS solution was pipetted onto a clean glass slide. A coverslip was placed on the top of the two drops to form an interface and then the edges of the glass slide were sealed using dental wax. The optical beam path was set to radiate the sample at the characteristic excitation wavelength of Nile Red, 553 nm, in order to only illuminate the oil. The microscope was focused on the interface of the oil droplet and images of 425 μ m by 425 μ m were collected every 0.2 seconds, until any changes were complete.

2.2.7.2 Bar-spreader Microscopy

A bar-spreader is an instrument that applies an even layer of a solution to a substrate by passing a moving bar across its surface at a pre-defined distance to form a film. The method was developed to study the phase separation of bar-spread polymer films *in situ* by placing the bar-spreader within a laser reflectance microscope. ⁴⁰ The same method can be used to mimic the process of cleaning a hard surface, figure 2.9. Firstly, the surface is "soiled" by the application of an oil film: a blade draws the oil at a fixed height across the surface of the slide. The blade is returned to its original location and a surfactant solution is pipetted onto the film and images are recorded from above the oil film as the blade is again drawn over surface to spread the solution.

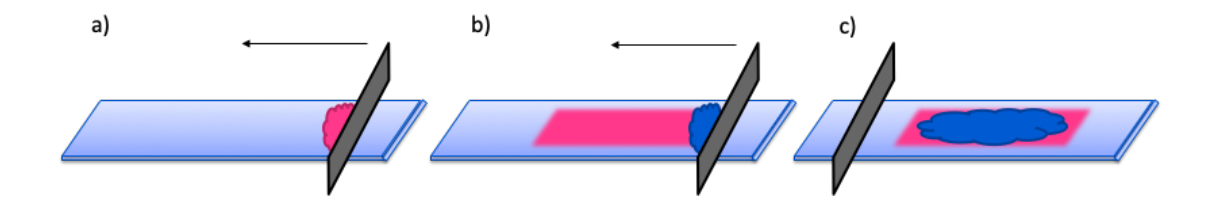


Figure 2.9: Process for drawing a surfactant solution (dark blue) across the surface of an oil (pink) in barspreader microscopy. a) Oil drawn across the surface using a blade 50 µm above the surface to create a film b) Surfactant solution drawn across the oil film c) Images taken by microscope positioned above the slide

A bar-spreader microscopy set-up developed and built by Toolan et al.⁴⁰ was used to observe the application of a surfactant solution to an oil film in a model of hard surface cleaning. A motorised bar coater was placed in a reflection mode microscope equipped with a Nikon 10x objective. The bar-coater was fitted with a razor blade to draw the oil and surfactant solutions across the surface of a glass slide. Firstly, the oil, oleic or vegetable, was

micropipetted onto the glass slide at the centre of the razor (20 μ L). The razor was drawn across the slide at a speed of 25 mm s⁻¹ at a height of 50 μ m from the surface to form a film. The razor was returned to its initial position. The surfactant solution (20 μ L) was micropipetted onto top. Images were taken at a rate of 20 s⁻¹ for 30 seconds.

2.3 Film removal test

To optimise the removal of a soil from a substrate, an appropriate soil, substrate, and a reproducible method of making, applying, and removing the soil are needed. A test detailed by Dunstan and Fletcher was adapted for use in this project.³⁷ A number of changes were made to this test to run the experiments in batches. Therefore, an investigation of stirring rate, slide position in the cleaning solution, measurement of soil removal loss by area and mass loss and the composition of the model soil, was performed. The following details the preparation of the reproducible soil and the resulting method to perform the soil removal test.

2.3.1 Film Preparation

Firstly, glass slides were cleaned by sonication for 15 mins in 1 w/w% Micro-90 cleaning solution followed by 15 minutes sonication in deionised water. The TAG mixture was prepared using the same method and materials as that used for QCM-D, discussed in section 2.2.6.2, from 33.3 w/w% lard, 25 w/w% vegetable oil, 33.3 w/w% vegetable shortening and 8.3% linseed oil, resulting in a yellow homogenous liquid. This molten TAG mixture was pipetted onto pre-weighed clean glass slides. The slides were thermally aged by being placed in a 200 °C oven for 1 hour to convert the soil from a liquid into a viscous semi-solid which is resistant to removal by surfactant. After this time, the slides were removed, left to cool and re-weighed.



Figure 2.10: Prepared glass slide coated in a TAG film containing a mixture of 33.3 w/w% lard, 25 w/w% vegetable oil, 33.3 w/w% vegetable shortening and 8.3% linseed oil.

2.3.2 Film removal measurement

TAG coated glass slides (either individually or in batches of 3) were held vertically in a glass beaker containing 250 ml of test surfactant solution while vigorously stirred, figure 2.11. The slides were immersed for 24 hours, as this was enough time to observe removal of approximately half of the soil by a formulated cleaning formulation. Next, the slides were removed and rinsed gently with deionised water. Subsequently, the slides were dried under reduced pressure in a vacuum desiccator for 24 hours and re-weighed. The percentage change by mass and area of the TAG film (as shown in the following section 2.3.3) was measured.

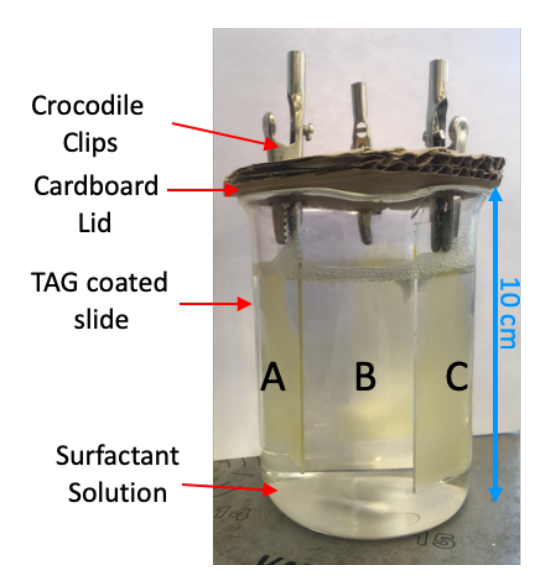


Figure 2.11: A three sample setup (labelled A, B, C) of the cleaning test where a model soil, consisting of TAG, was applied to a surface and thermally treated was placed in a cleaning solution and the subsequent mass loss was measured.

2.3.3 Area change measurement

Photographs of the slides were taken using an iPhone camera (12 megapixel, 1.22 μ m pixel size) after thermal aging of the films and after testing, once the slides had been washed and dried. Image analysis software, Fiji, was used to colour threshold the images and calculate the area of the TAG film (ranging from 1200 to 1800 mm²).⁴¹







Outline of TAG film in image created in Fiji

Figure 2.12: Determination of area change by conversion of an iPhone photograph of the TAG film before cleaning into an image outlining the TAG remining on the surface of the slide only, using the image processing software, Fiji.

2.4 Machine Learning

Machine learning is the use of known data to learn a function which allows prediction about data that is unknown.⁴² Without explicit programming, algorithms are used which allow computers to learn from data and improve their predictions. The main types of machine learning are: supervised learning, where the empirical data set comprises of inputs and outputs and the aim is to discover their relationship, and unsupervised learning, where the input data has no corresponding target data, so the algorithms analyse the data without prior training. Machine learning is able to analyse large numbers of parameters and large data sets so has found multiple industrial uses, including image recognition, prediction systems and medical diagnoses.^{42–45}

The machine learning techniques utilized in this thesis were possible due to a collaboration with experts in the Machine Learning group at the University of Sheffield: Neil Lawrence, Javier Gonzalez and Alan Saul. These computational scientists used the Python programming language to implement machine learning algorithms, including Bayesian Optimisation, which was used to perform the optimisations in this thesis.^{46–48}

2.4.4 Bayesian Optimisation

Situations where the mathematical relationship between input and output variables is unknown are called black-box functions. If they are expensive to evaluate, for example to obtain the required data requires a lot of time or financial cost, and the aim is to identify the optimal parameters for finding either the maximum or minimum result, one method that can be utilised is a Bayesian Optimisation. For example, the black-box problem considered in this thesis is the relationship between the concentrations of a number of surfactants in an aqueous mixture and the properties of the resulting solution: surface tension and soil removal efficacy. Bayesian optimisation is a machine learning method for globally optimising black-box functions by modelling through a stochastic process as follows.^{49,50}

A global optimization problem, targeting the maximum of the function, f, within the possible values of x, can be expressed as:

$$x^* = \arg\max f(x), \qquad x \in X$$

where X is the range of values within which x can be.⁵¹ Arg max, or the arguments at the maximum, are the points, or inputs, for the largest possible values of a function. In the case of Bayesian optimization, f is a black-box function, and f is observed by stochastic (randomly determined) outputs, y. The algorithm sequentially searches for where the maximum value is likely to be based on previous observations. For each iteration, x, this location is selected, x, and y, is observed to query f. In this thesis, for example, one global optimization problem is to minimise the surface tension (y), with the input parameters (x) of: concentration of the surfactants between 0 and 1 x

Bayesian optimization approximates an unknown function using prior knowledge, which is updated with new evidence, in order to find the best model. This idea is based on Bayes Rule, which introduced the ability to assign probability to an unknown event using known information. The idea originated from the Reverend Thomas Bayes and appeared in an equivalent form in Laplace's 1814 essay. ^{52,53}

$$P(y|x) = \frac{P(x|y)P(y)}{P(x)}$$

The equation states that our belief about a hypothesis, y, can be updated in the light of new evidence, x. The posterior belief, P(y|x), is calculated by multiplying our prior belief, P(y), by the likelihood, P(x|y), that x will occur if y is true.

This idea of updating beliefs based on new data can be applied to the case of approximating an unknown function, where the 'posteriors' are a probability distribution of all the possible curves (functions) that pass through all the points that have been previously measured, the 'priors'. With the next point measured, the number of possible functions that pass through all the points decreases so the probability distributions can be updated, figure 2.13. This is called a Gaussian process.⁵⁴

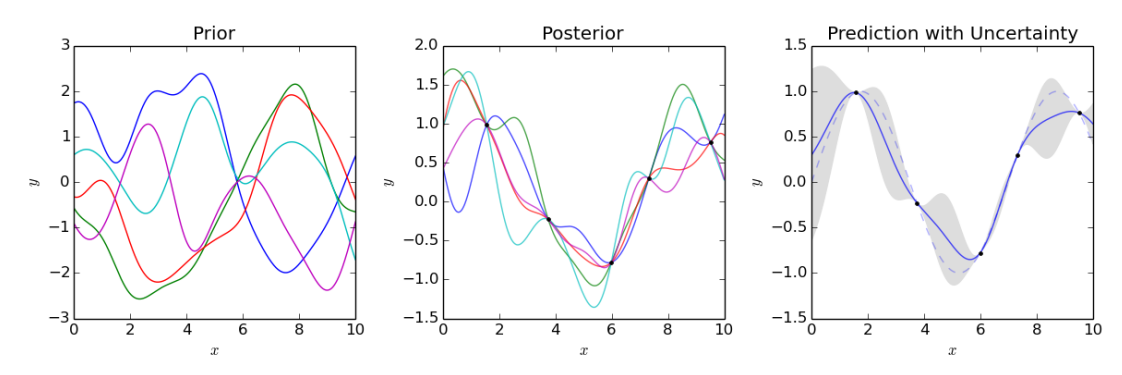


Figure 2.13: An example of Gaussian Process regression taken from presentation "Introduction to Bayesian Optimisation" given by Javier Gonzalez at the Gaussian Processes Summer School, Sheffield, 2017. The first plot shows a sample of the possible functions from the prior function distribution. The second plot shows the posterior distribution of functions which must pass through the five data points (black dots). The third plot is a prediction of the uncertainty: the mean of all functions that can pass through the points is shown by the blue line and the shaded section shows one standard deviation.

In Bayesian Optimisation, a prior assumption is made about the shape of the function by the choice of kernel function. ⁵⁵ This takes any two data points, and outputs the covariance between them. The data analyst's selection of kernel will be dependent on whether they perceive the model might be linear, exponential, periodic or cyclic. As a check that the kernel is adequate, a test set of data can be used to try out different kernels to minimise the prediction error. ⁵⁶

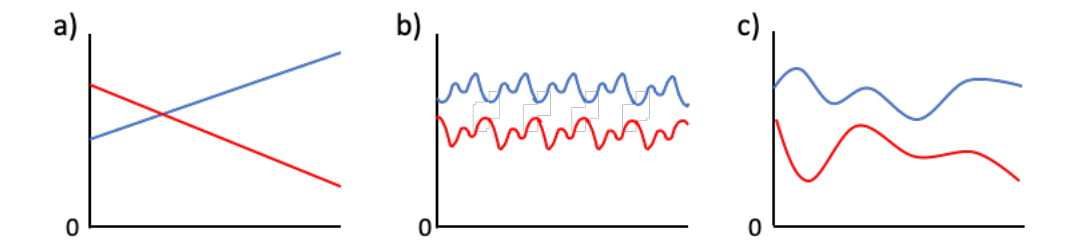


Figure 2.14: The functions from commonly used kernels used for Gaussian Processes, adapted from "The Kernel Cookbook" by David Duvenaud: a) A linear function obtained from a linear kernel b) A periodic kernel that generates functions with a repeating structure c) A squared exponential kernel.⁵⁷

Once the analyst has selected a kernel, the prediction uncertainty from the Gaussian process is used to drive the selection of the next set of experiments. In order to maximise *x* for the unknown function, *f*, the next data to be acquired should be selected where the mean is high and the variance is low, which is directed by the acquisition function. The most common acquisition function is "Expected Improvement" and describes the balance between exploration and exploitation; exploration probes the areas in the space where there is most uncertainty due to lack of previous data whereas exploitation probes the areas where the maximum is most likely and previous data shows high values. A key advantage of this is importance is placed on sampling areas close to the current maximum to reduce the number of data points required. In comparison, the alternative, a grid search, gives equal importance to all points, regardless of previous results, and so measurements will be directed across the entire range of the parameters, even though the optimum is likely to be in a small region. Hence, to find the optimum using a grid search would require a larger number of experiments, with a greater possibility of the optimum being passed over.

In summary, the aim of a Bayesian Optimisation is to design sequential experiments to optimise physical processes. A prior assumption is made about the shape of the function, via the kernel, incorporating epistemic uncertainty about the system. The prior and the likelihood distributions are combined, given observations or data, to give a posterior over the uncertain function. This posterior is used to decide where next to query (*i.e.* which experiments to perform next) in order to maximise the acquisition function, figure 2.15.

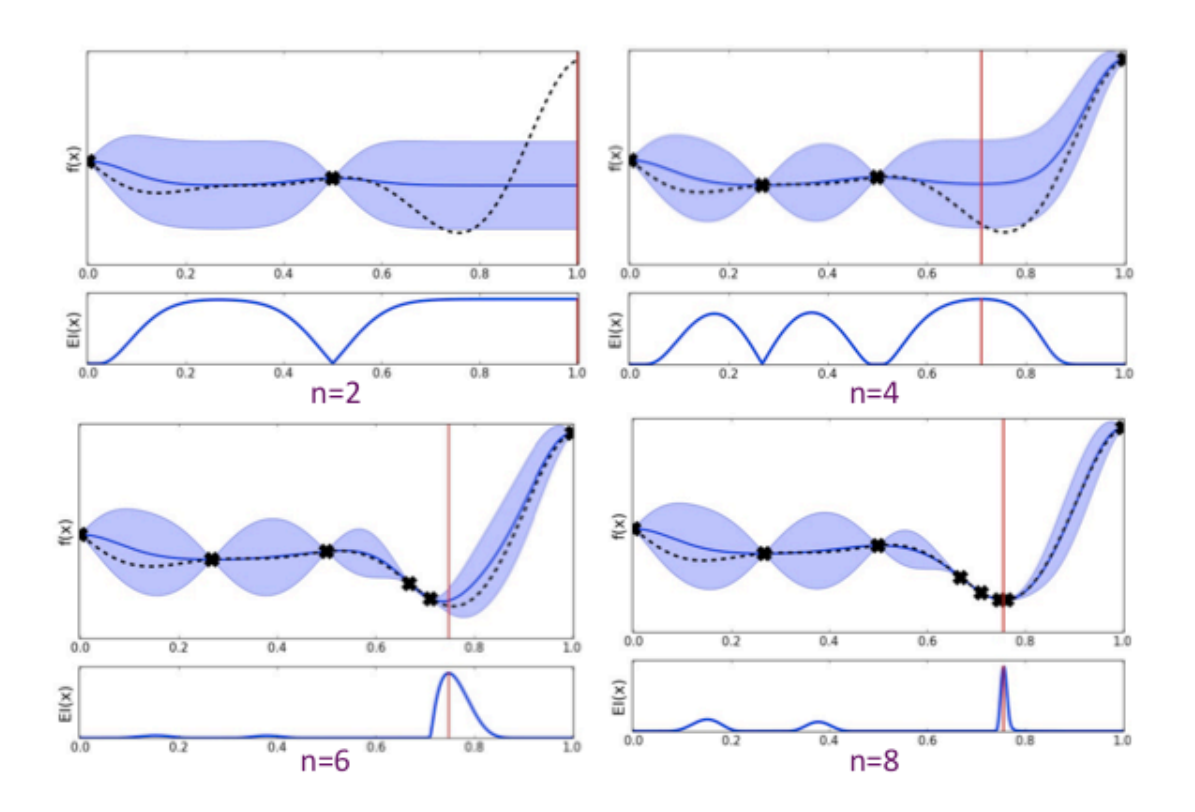


Figure 2.15: An example of a one-dimensional Bayesian optimisation with the aim of finding the minimum in the function f(x). Observations are performed (black crosses) sequentially and n is the number of iterations performed in each case. The blue shaded areas show the confidence or uncertainty associated with the posterior mean function. The black dotted line shows the objective function and the blue line shows the posterior mean of the function. The bottom graph in each case shows the acquisition function, El(x), in this case 'expected improvement', which is high where the posterior gives most uncertainty and high where there is a low mean (as the minimum is the target in this case). The red line shows the peak in the acquisition function which provides the most important point to evaluate next. In this way, Bayesian methods can be used to guide measurement efficiently by obtaining the most information from each subsequent measurement.

2.4.4 Optimisation Process

Herein, Bayesian optimisation was used to optimise a mixture of two, as well as three, surfactants with regards to finding the minimum surface tension, as a lower surface tension aids hard surface cleaning by increased surface wetting and aiding the detergency mechanism, as well as the maximum soil removal. The independent variables were surfactant concentration and pH. For simplicity, only the process of optimisation for minimising surface tension is now described. The process for soil removal is the same except the number of experiments in each batch is four times lower and the soil removal is maximised instead of minimised. The first step was selection of an initial batch of 20 experiments by using a random sampling algorithm given initial constraints of surfactant concentration (0-2 w/w%) and pH (2-11). The surface tension of each solution was

measured. This data was used to model the unknown function via a Gaussian Process. By maximising the acquisition function, the next set of 20 experiments were suggested and subsequently their surface tension was measured. This process was repeated until no further improvement was seen in the measurement of surface tension, i.e. the values of surface tension predicted were not lower than those previously measured. The process is summarised in figure 2.16.

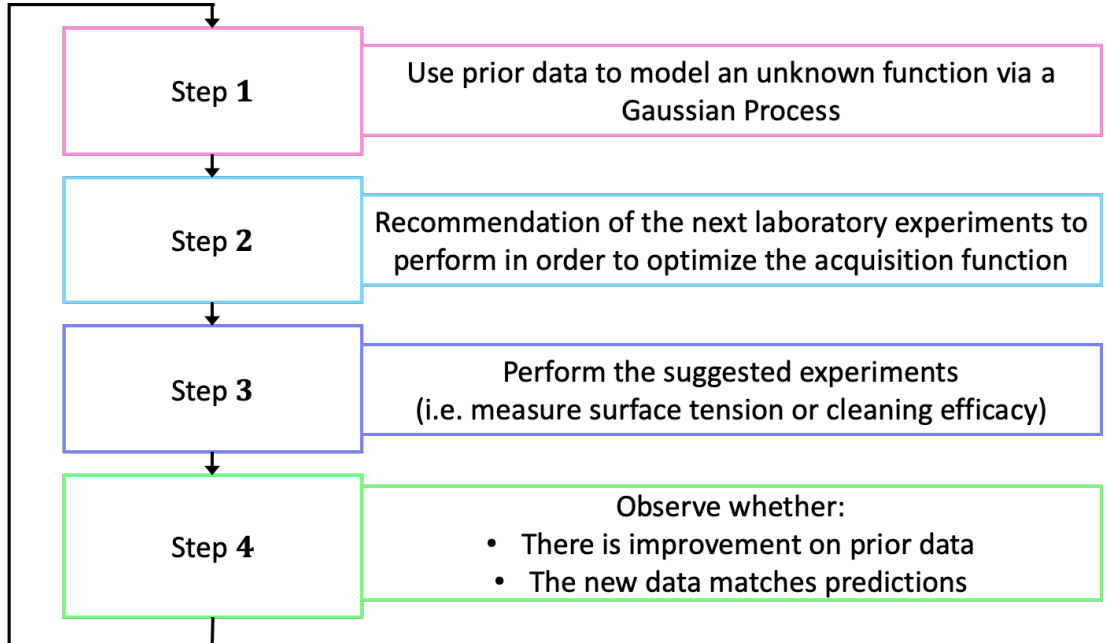


Figure 2.16: The cyclic process to optimise a formulation using a Bayesian optimisation.

2.4.4.1 Computation

The Bayesian optimisation computation was performed in GPyOpt, which is an open-source library for Bayesian optimization. GPyOpt uses the Python programming language to implement machine learning algorithms and was developed by the Machine Learning group at the University of Sheffield who collaborated on this research. The Bayesian optimisation algorithm used was illustrated previously by Shahriari et al.⁵⁰ A random sampling algorithm in GPyOpt determined the initial batch of experiments to be run. The results were computed into a Jupyter Notebook⁵⁹ (an interactive, open-source application for developing code) and the Bayesian optimisation was used to select the next batch of experiments to be run until the solution with optimised properties was found.

2.5 References

- 1. Sparkman, O. D., Penton, Z. & Kitson, F. G. *Gas Chromatography and Mass Spectrometry: A Practical Guide. Gas Chromatography and Mass Spectrometry: A Practical Guide* (2011). doi:10.1016/C2009-0-17039-3
- 2. Banerjee, S. & Mazumdar, S. Electrospray Ionization Mass Spectrometry: A Technique to Access the Information beyond the Molecular Weight of the Analyte. *Int. J. Anal. Chem.* (2012). doi:10.1155/2012/282574
- 3. Lecomte Du Noüy, P. An interfacial tensiometer for universal use. *J. Gen. Physiol.* **7**, 625–632 (1925).
- 4. Harkins, W. D. & Jordan, H. F. A method for the determination of surface and interfacial tension from the maximum pull on a ring. *J. Am. Chem. Soc.* (1930).
- 5. Kodre, K., Attarde, S., Yendhe, P., Patil, R. & Barge, V. Differential Scanning Calorimetry: A Review. Kodre. *Res. Rev. J. Pharm. Anal.* (2014).
- 6. Gabbott, P. A Practical Introduction to Differential Scanning Calorimetry. in *Principles and Applications of Thermal Analysis* (2008).
- 7. Danley, R. L. New heat flux DSC measurement technique. *Thermochim. Acta* **395**, 201–208 (2002).
- 8. Pecora, R. Dynamic light scattering measurement of nanometer particles in liquids. *J. Nanoparticle Res.* **2**, 123–131 (2000).
- 9. Woolard, E. W., Einstein, A., Furth, R. & Cowper, A. D. Investigations on the Theory of the Brownian Movement. *Am. Math. Mon.* **35**, 318 (1928).
- 10. Stetefeld, J., McKenna, S. A. & Patel, T. R. Dynamic light scattering: a practical guide and applications in biomedical sciences. *Biophysical Reviews* **8**, 409–427 (2016).
- 11. Provencher, S. W. & Štěpánek, P. Global analysis of dynamic light scattering autocorrelation functions. *Part. Part. Syst. Charact.* **13**, 291–294 (1996).
- 12. Glatter, O. & Kratky, O. *Small Angle X-ray Scattering*. *Acta Polymerica* (Academic Press Inc., 1982).
- 13. Anderson, A. Canonical Transformations in Quantum Mechanics. *Ann. Phys. (N. Y).* **232**, 292–331 (1994).
- 14. Guinier, A. & Fournet, G. *Small-Angle Scattering of X-rays*. (John Wiley & Sons, 1955).
- 15. Jensen, G. V., Lund, R., Gummel, J., Narayanan, T. & Pedersen, J. S. Monitoring the Transition from Spherical to Polymer-like Surfactant Micelles Using Small-Angle X-Ray Scattering. *Angew. Chemie Int. Ed.* **53**, 11524–11528 (2014).

- 16. Gubaidullin, A. T. *et al.* Structure and dynamics of concentrated micellar solutions of sodium dodecyl sulfate. *Russ. Chem. Bull.* **65**, 158–166 (2016).
- 17. Lipfert, J., Columbus, L., Chu, V. B., Lesley, S. A. & Doniach, S. Size and shape of detergent micelles determined by small-angle X-ray scattering. *J. Phys. Chem. B* **111**, 12427–12438 (2007).
- 18. Oliver, R. C. *et al.* Dependence of Micelle Size and Shape on Detergent Alkyl Chain Length and Head Group. *PLoS One* **8**, e62488 (2013).
- 19. Silva, H. D., Cerqueira, M. Â. & Vicente, A. A. Nanoemulsions for Food Applications: Development and Characterization. *Food and Bioprocess Technology* **5**, 854–867 (2012).
- 20. MacMillan, S. D. *et al.* In Situ Small Angle X-ray Scattering (SAXS) Studies of Polymorphism with the Associated Crystallization of Cocoa Butter Fat Using Shearing Conditions. *Cryst. Growth Des.* **2**, 221–226 (2002).
- 21. Dong, Y. Da & Boyd, B. J. Applications of X-ray scattering in pharmaceutical science. *International Journal of Pharmaceutics* **417**, 101–111 (2011).
- 22. Svergun, D. I. & Koch, M. H. J. Small-angle scattering studies of biological macromolecules in solution. *Reports Prog. Phys.* **66**, 1735–1782 (2003).
- 23. Flodström, K., Teixeira, C. V., Amenitsch, H., Alfredsson, V. & Lindén, M. In situ synchrotron small-angle X-ray scattering/X-ray diffraction study of the formation of SBA-15 mesoporous silica. *Langmuir* **20**, 4885–4891 (2004).
- 24. Ignat, M., Sacarescu, L., Cool, P. & Harabagiu, V. Glycerol-derived Mesoporous Carbon: N2-sorption and SAXS Data Evaluation. in *Materials Today: Proceedings* **2**, 3836–3845 (2015).
- 25. Rice, S. A. Small angle scattering of X-rays. A. Guinier and G. Fournet. Translated by C. B. Wilson and with a bibliographical appendix by K. L. Yudowitch. Wiley, New York, 1955. 268 pp. \$7.50. *J. Polym. Sci.* **19**, 594–594 (1956).
- 26. Doucet, M. et al. SasView version 4.1. SasView version 4.1, Zenodo (2017).
- 27. Pedersen, J. S. Analysis of small-angle scattering data from colloids and polymer solutions: Modeling and least-squares fitting. *Adv. Colloid Interface Sci.* **70**, 171–210 (1997).
- 28. Yang, J. Viscoelastic wormlike micelles and their applications. *Current Opinion in Colloid and Interface Science* **7**, 276–281 (2002).
- 29. Velinova, M., Sengupta, D., Tadjer, A. V. & Marrink, S. J. Sphere-to-rod transitions of nonionic surfactant micelles in aqueous solution modeled by molecular dynamics simulations. *Langmuir* **27**, 14071–14077 (2011).

- 30. Varade, D., Rodríguez-Abreu, C., Shrestha, L. K. & Aramaki, K. Wormlike micelles in mixed surfactant systems: Effect of cosolvents. *J. Phys. Chem. B* **111**, 10438–10447 (2007).
- 31. Kotlarchyk, M. & Chen, S. H. Analysis of small angle neutron scattering spectra from polydisperse interacting colloids. *J. Chem. Phys.* **79**, 2461–2469 (1983).
- 32. Berr, S. S. Solvent isotope effects on alkyltrimethylammonium bromide micelles as a function of alkyl chain length. *J. Phys. Chem.* **91**, 4760–4765 (1987).
- 33. Sakai, K. Quartz Crystal Microbalance with Dissipation Monitoring (QCM-D). in *Measurement Techniques and Practices of Colloid and Interface Phenomena* 45–50 (2019).
- 34. Sauerbrey, G. Verwendung von Schwingquarzen zur Wägung dünner Schichten und zur Mikrowägung. *Zeitschrift für Phys.* **155**, 206–222 (1959).
- 35. Voinova, M. V., Jonson, M. & Kasemo, B. 'Missing mass' effect in biosensor's QCM applications. *Biosens. Bioelectron.* **17**, 835–841 (2002).
- 36. Voinova, M. V., Rodahl, M., Jonson, M. & Kasemo, B. Viscoelastic Acoustic Response of Layered Polymer Films at Fluid-Solid Interfaces: Continuum Mechanics Approach. *Phys. Scr.* **59**, 391–396 (1999).
- 37. Dunstan, T. S. & Fletcher, P. D. I. The removal of thermally aged films of triacylglycerides by surfactant solutions. *J. Surfactants Deterg.* **17**, 899–910 (2014).
- 38. Prasad, V., Semwogerere, D. & Weeks, E. R. Confocal microscopy of colloids. *J. Phys. Condens. Matter* **19**, (2007).
- 39. Pawley, J. B. Confocal and two-photon microscopy: Foundations, applications and advances. *Microsc. Res. Tech.* **59**, 148–149 (2002).
- 40. Haq, E. U. *et al.* Real time laser interference microscopy for bar-spread polystyrene/poly(methyl methacrylate) blends. *J. Polym. Sci. Part B Polym. Phys.* **52**, 985–992 (2014).
- 41. Schindelin, J. *et al.* Fiji: An open-source platform for biological-image analysis. *Nature Methods* (2012).
- 42. Bishop, C. M. Machine Learning and Pattern Recognition. *Def. Sci. J.* **60**, 345–347 (2010).
- 43. Krizhevsky, A., Sutskever, I. & Hinton, G. E. ImageNet classification with deep convolutional neural networks. in *Advances in Neural Information Processing Systems* (2012).
- 44. Lecun, Y., Bengio, Y. & Hinton, G. Deep learning. *Nature* (2015).

- 45. Xiong, H. Y. & Alipanahi et al., B. The human splicing code reveals new insights into the genetic determinants of disease. *Science* (80-.). **347**, 144 (2015).
- 46. González, J., Osborne, M. & Lawrence, N. D. GLASSES: Relieving the myopia of Bayesian optimisation. in *Proceedings of the 19th International Conference on Artificial Intelligence and Statistics, AISTATS 2016* (2016).
- 47. González, J., Dai, Z., Hennig, P. & Lawrence, N. Batch bayesian optimization via local penalization. in *Proceedings of the 19th International Conference on Artificial Intelligence and Statistics, AISTATS 2016* (2016).
- 48. González, J., Longworth, J., James, D. C. & Lawrence, N. D. Bayesian Optimization for Synthetic Gene Design. (2015).
- 49. Ghahramani, Z. Probabilistic machine learning and artificial intelligence. *Nature* **521**, 452–459 (2015).
- 50. Shahriari, B., Swersky, K., Wang, Z., Adams, R. P. & De Freitas, N. Taking the human out of the loop: A review of Bayesian optimization. *Proc. IEEE* **104**, 148–175 (2016).
- 51. Malherbe, C. & Vayatis, N. Global optimization of Lipschitz functions. in *34th International Conference on Machine Learning, ICML 2017* (2017).
- 52. Bayes, T. An essay towards solving a problem in the doctrine of chances. 1763. *MD. Comput.* **8**, 157–171 (1991).
- 53. Laplace, P. S. Essai philosophique sur les probabilités. (Mme. Ve Courcier, 1814).
- 54. Rasmussen, C. E. & Williams, C. K. I. *Gaussian Processes for Machine Learning*. (MIT Press, 2006).
- 55. Wilson, A. G. & Adams, R. P. Gaussian process kernels for pattern discovery and extrapolation. in *30th International Conference on Machine Learning, ICML 2013* (2013).
- 56. Schulz, E., Speekenbrink, M. & Krause, A. A tutorial on Gaussian process regression: Modelling, exploring, and exploiting functions. *J. Math. Psychol.* **85**, 1–16 (2018).
- 57. Duvenaud, D. K. *PhD Thesis: Automatic Model Construction with Gaussian Processes. Thesis* (2014).
- 58. Mockus, J., Tiesis, V. & Zilinskas, A. The application of Bayesian methods for seeking the extremum. *Towar. Glob. Optim.* (1978).
- 59. Kluyver, T. et al. Jupyter Notebooks—a publishing format for reproducible computational workflows. Positioning and Power in Academic Publishing: Players, Agents and Agendas (2016).

3. Physical Chemistry of Surfactant Structures

3.1 Introduction

Commercial "ready-to-use" hard-surface cleaning formulations are complex mixtures of small concentrations of surfactants and additives in a relatively large amount of solvent. A considerable amount of time and effort by product development scientists goes into the selection of the right surfactants in the right quantities to get optimal cleaning efficacy (among other ingredients, such as solvents or cosurfactants).

To gain an understanding of how a cleaning formulation performs and in what way it can be optimised, the surfactants chosen for this project needed to reflect those used in commercial formulations. The choice of surfactants was based on those frequently found in commercial cleaning solutions and included a range of surfactant classes i.e. non-ionic (decyl glucoside (DG) and alcohol ethoxylate (AE)), zwitterionic (lauramine oxide (LO) and cocamidopropyl betaine (CAB)), cationic (alkyldimethyl benzylalkonium chloride (BC)) and anionic (sodium dodecyl sulphate (SDS)). It is important to note that LO and BC both have antimicrobial properties as well as being detergents.

Use of these commercial grade surfactants could be problematic as they are not highly purified, and typically contain mixtures of surfactants with different hydrophobic alkyl chain lengths or different numbers of repeating units in the hydrophilic group. Minimal information about each product is given by the suppliers, presumably to obscure the identity from competitors. Therefore, a greater understanding of the characteristics and composition of each mixture is required in order to aid later formulation.

In this chapter, analysis of the industrial surfactants is presented. Firstly, the concentration and structure of the surfactants is determined. Secondly, light and X-ray scattering experiments are detailed to determine the aggregation behaviour of the surfactants in aqueous solution. The characterisation of the surfactants alone is important for mixture optimisation in subsequent chapters.

3.2 Surfactant Characterisation

In order to prepare mixtures for experiments in later chapters, it was necessary to calculate the concentration of the surfactants alone. Initially, the aim was to calculate the molar

concentration of the surfactants based on their weight percentage concentrations (w/w%) and molar mass, determined by thermal gravimetry and mass spectrometry, respectively. SDS and the AE were obtained as neat surfactant, whereas the other four surfactants were obtained at various concentrations in aqueous solutions. A moisture analyser was used to measure weight percentage gravimetrically, by heating the sample incrementally to a maximum of 150 °C until constant mass was reached (i.e. the point at which all the water has been removed). A comparison between the concentrations quoted by the supplier and those measured gravimetrically can be seen in table 2.1. In some cases, the measured values are higher than those quoted, which may be due to the hygroscopic nature of the surfactants making complete removal of the water difficult. Another possibility is that heating causes autoxidation of the surfactants, causing surfactant degradation, which has previously been shown to occur at temperatures above 100°C.^{1,2}

Table 3.1: The weight percent quoted vs. measured by a moisture analyser

Surfactant	Concentration given by Supplier / w/w%	Measured Concentration / w/w%		
Lauramine Oxide	20-40	31.8 ± 2.08		
Benzalkonium Chloride	50	$\textbf{52.1} \pm \textbf{0.53}$		
Decyl Glucoside	55	$\textbf{55.5} \pm \textbf{0.11}$		
Cocamidopropyl Betaine	30	$\textbf{33.3} \pm \textbf{2.71}$		

Chain length analysis was performed on each of the surfactants in order to determine the distribution of chain lengths. Due to the different structures and properties of the surfactants, different methods of mass spectrometry and chromatography were used as appropriate. The commercial LO sample was specified to be a mixture of alkyldimethyl, Noxide amines with chain lengths from C10-C20. The general structure is shown in figure 3.1.

$$\begin{array}{c} \mathsf{CH_3} \\ |_{\oplus} & \ominus \\ \mathsf{CH_3}(\mathsf{CH_2})_\mathsf{n} \mathsf{N} \overline{\qquad} \mathsf{O} \\ | \\ \mathsf{CH_3} \end{array}$$

Figure 3.1: General structure of LO

Gas Chromatography – Mass Spectrometry (GC-MS) showed seven fractions, the most abundant fraction had a chain length of 14 carbons. A summary of the fractions is presented in table 4.2.

Table 3.2: Fragment data for LO from the GC mass spectrum. M+ is the molecular ion peak and Mr is the molar mass.

Fraction	Number of C in alkyl chain	M+	Mr / g mol ⁻¹	Relative Abundance / %
1	10	184	201	6.7
2	12	212	229	3.4
3	14	240	257	47.2
4	16	268	271	15.7
5	17	285	299	18.0
6	18	297	313	4.5
7	20	325	341	4.5

For larger or more polar molecules that could not be separated by GC-MS, Liquid Chromatography – Mass Spectroscopy (LC-MS) was used. Analysis of the BC sample showed there were two chain lengths present: one of twelve carbons and one of 14 carbons which matches the specification provided by the supplier. The relative ratios were approximately 50% of each, by mass.

Figure 3.2: General structure of BC

Table 3.3: Fragment data for BC from the LC mass spectrum. M+ is the molecular ion peak and Mr is the molar mass.

Fraction	Number of C in alkyl chain	M+ / g mol ⁻¹	Mr / g mol ⁻¹	Relative Abundance / %	
1	12	304	304	52.9	
2	14	332	332	47.1	

The DG sample was analysed using LC-MS, which gave a complicated spectrum. Some fractions could not be assigned which was in part due to a large number of fractions isolated and therefore, the relative abundance could not be calculated. The main fractions are detailed in the table below. The spectrum showed there were mixed glucosides with different length alkyl chains, C8-C14, and between 1 and 3 glucoside units. The data sheet provided by the supplier did not give any values for comparison.

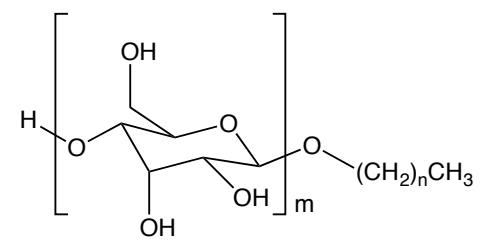


Figure 3.3: General structure of DG

Table 3.4: Fragment data for DG from the LC mass spectrum. M+ is the molecular ion peak and Mr is the molar mass.

Fraction	Molecular	Number of	Number of C in	M+/	Mr/
	Formula	Glucoside Units	alkyl chain	g mol ⁻¹	g mol ⁻¹
1	$C_{14}H_{28}O_6$	1	8	291	292
2	$C_{16}H_{32}O_6$	1	10	319	320
3	$C_{18}H_{36}O_{6}$	1	12	347	348
4	$C_{20}H_{38}O_{11}$	2	8	453	454
5	$C_{22}H_{36}O_{11}$	2	10	481	480
6	$C_{24}H_{40}O_{11}$	2	12	509	508
7	$C_{26}H_{44}O_{11}$	2	14	537	536
8	$C_{28}H_{52}O_{16}$	3	10	640	644
9	$C_{30}H_{56}O_{16}$	3	12	668	672
10	$C_{32}H_{60}O_{16}$	3	14	696	700

The zwitterionic ammonium compound, CAB, contained seven fractions (there were no details in the supplier's data sheet for comparison). The most abundant fraction having a chain where n=10. Other fractions had an even number for n ranging from n=4 to n=16.

Figure 3.4: General structure of CAB

Table 3.5: Fragment data for CAB from the LC mass spectrum. M+ is the molecular ion peak and Mr is the molar mass.

Fraction	Molecular Formula	n	M+ /g mol ⁻¹	Mr /g mol ⁻¹	Relative Abundance / %
1	$C_{13}H_{30}N_2O_3$	4	261	262	1.6
2	$C_{15}H_{34}N_2O_3$	6	289	290	13.7
3	$C_{17}H_{38}N_2O_3\\$	8	317	318	13.2
4	$C_{19}H_{40}N_2O_3$	10	345	346	22.6
5	$C_{21}H_{44}N_2O_3$	12	373	374	18.4
6	$C_{23}H_{48}N_2O_3$	14	401	402	15.3
7	$C_{25}H_{52}N_2O_3$	16	429	430	15.3

The structure of the AE proved difficult to determine from its spectra, as there were over 30 fractions. There was a common fragment of 163 g mol⁻¹, which corresponds to a C12 alkyl chain, i.e. m=11 (figure 3.5a)). By subtracting this fragment from the largest molecules, the ethoxy length was determined to range from 14 to 18 ethoxy units.

SDS was selected because it has been studied comprehensively and is also found in many cleaning products. For comparison with a previous study, the SDS used was laboratory grade. The supplier's specification details that the purity was >99% determined by NaOH titration and >96% determined by GC.³

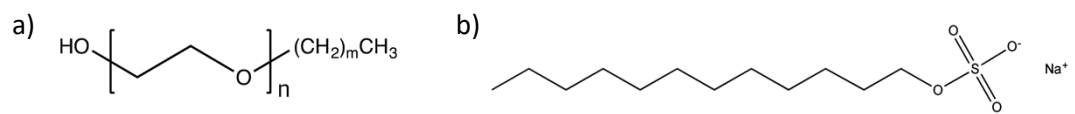


Figure 3.5: General structure of a) AE (tradename Rhodasurf B7) b) SDS

In conclusion, the chain length distribution of some fractions in the AE and the DG could not be determined due to the complexity of the spectra and the number of fractions. Several fractions were also found for the CAB and LO samples. As a result, determination of the molar concentration of each surfactant solution based on molecular weight would be either impossible or imprecise, and therefore the measured weight percent concentrations were used in all subsequent dilutions or mixtures used in this thesis.

3.3 Critical micelle concentration determination

The surface tension isotherms of six surfactants were measured in order to determine the CMC (table 3.9) by using the point of inflection in the surface tension data with increasing surfactant concentration.^{4,5} This data was then compared to the previous literature, unless specified, all the CMC data was obtained from Rosen and Kunjappu's: *Surfactants and Interfacial Phenomena*.⁶

The critical micelle concentration (CMC) measured for DG, calculated by point of inflection in the surface tension isotherm, was 0.014 w/w%. As mass spectrometry showed the DG used herein has a distribution of 8-14 C chain lengths, this result is used to compare with single chain length glucosides found in the literature. The value of 0.014 w/w% is an intermediate between the literature values found for the pure fractions. The literature value of CMC for dodecyl glucoside (C12) was much lower (0.006 w/w%), whilst CMC for octyl (C8) and decyl glucoside (C10) were higher (0.073 and 0.075 w/w%, respectively). The measured CMC supports the general trend that CMCs for surfactants in aqueous solutions decrease with increasing hydrophobic character, which in this case is an increasing carbon chain length. This rule is demonstrated in the literature for the C12 and C14 chain lengths in BC, which were reported at 0.20 and 0.052 w/w% respectively. The experimentally determined CMC value for commercial BC was 0.1 w/w%, which is an intermediate value between the CMC of the two component surfactants.

Table 3.9: Comparison of the critical micelle concentrations (CMCs) obtained experimentally vs those found in the literature.^{6,7}

			Measured		Literature Values			Measured vs. Literature
Surfactant Type	Surfactant	Trade Name	Surface Tension Minima / mN/m	CMC / w/w %	Surfactant	CMC / mM	CMC / w/w%	Discrepancy in CMC / %
Non-ionic	DG	Kemgluco CEHL	28.54	0.014	octyl-β-D-glucoside	2.5	0.073	80
					decyl-β-D-glucoside	2.2	0.075	81
					dodecyl-β-D-glucoside	0.19	0.0066	79
Anionic	SDS		26.23	0.20	C ₁₂ H ₂₅ SO ₄ -Na ⁺	8.2	0.23	13
Zwitterionic	CAB	Mackam CAB-818	28.56	0.015	RCONH(CH ₂) ₃ N ⁺ (CH ₃) ₂ CH ₂ COO ⁻	0.28	0.0096	56
Zwitterionic	LO	Ammonyx LO	33.49	0.0015	C ₁₂ H ₂₅ N(CH ₃) ₂ O	1.6	0.036	95
Cationic	ВС	Acticide BAC50M	28.66	0.10	$C_{12}H_{25}N^{+}(CH_{2}C_{6}H_{5})(CH_{3})_{2}CI^{-}$	8.8	0.20	50
					$C_{14}H_{29}N^{+}(CH_{2}C_{6}H_{5})(CH_{3})_{2}CI^{-}$	2.0	0.052	81
Non-ionic	AE	Rhodasurf B7	28.42	0.0050	C ₁₂ H ₂₅ (OC ₂ H ₄) ₇ OH	0.1	0.0041	22

For three of the surfactants, AE, CAB and SDS, the values measured were comparable with those in the literature and were within experimental error (table 3.9). The CMC of the AE was 0.005 w/w%, similar to 0.0041 w/w% quoted by Rosen.⁶ The CMC of CAB was 0.015 w/w%, which is marginally higher than the value originally quoted by Staszak *et al.*⁷ However, the discrepancy can be justified by the number and relative ratios of different chain length fractions between surfactant suppliers. The CMC of SDS was very similar, 0.2 w/w% determined experimentally versus 0.23 w/w% in the literature, as would be expected due to its high purity (95%). Conversely, the measured CMC of LO is considerably lower than found in literature, 0.0015 w/w% versus 0.036 w/w%. This discrepancy could be due to difference in purity as the literature values are obtained from pure samples whereas the commercial sample supplied was shown to be a mixture of multiple alkyl chain lengths (C10 to C20).

In the following experiment, figure 3.11, the three most industrially relevant surfactants were used (LO, BC, DG) and the pH was kept constant for comparison purposes (pH 7). The CMCs were all in the region of 0.01 w/w%. DG caused the largest decrease in surface tension of an aqueous solution ($28.36 \pm 0.05 \text{ mN m}^{-1}$) whereas BC lowers the surface tension of the solution the least ($33.73 \pm 0.08 \text{ mN m}^{-1}$). The surface tension at the CMC of LO was $32.23 \pm 0.19 \text{ mN m}^{-1}$.

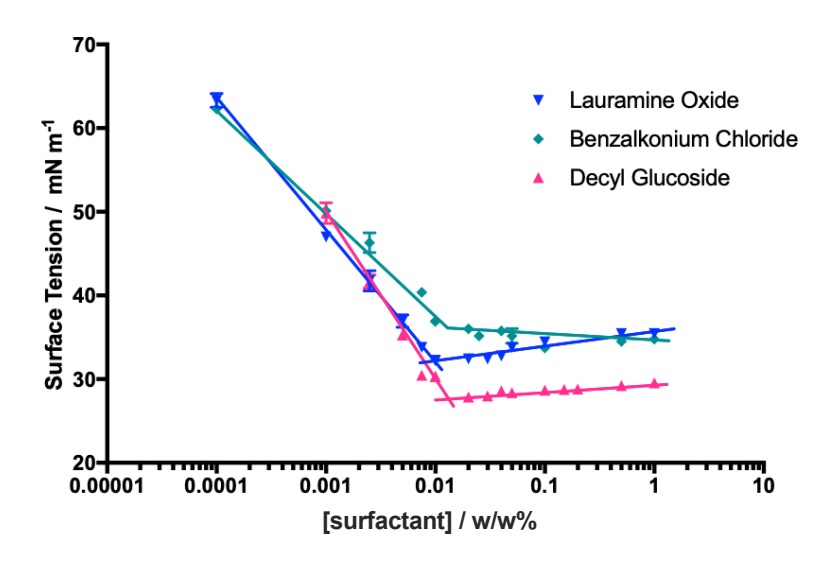


Figure 3.11: Effect of surfactant concentration on the surface tension for LO, BC, DG at pH 7

The CMCs of the three industrial surfactants, at pH 7, were within a similar range however the reduction in surface tension differed significantly, in the order BC < LO < DG. The surface

tension reduction effectiveness is dependent on the relative sizes of the hydrophilic and hydrophobic groups in a surfactant molecule. The finding that the DG reduces the surface tension more than LO and BC is likely to be related to the superior packing of the surfactant molecules. The packing in BC will be less efficient due to the bulky benzyl groups and repulsion of the ionic groups. The previous analysis of the DG sample showed a high number of fractions, including those of lower molecular mass meaning there are smaller molecules which would be able to orientate themselves around the larger molecules leading to more efficient packing and lower surface tension. The surface tension, and CMC, of surfactant solution are affected by the pH due to changes is micelle formation due to the changes in hydrogen bonding and ionization of surfactant headgroups or tails, depending on surfactant class. This led to the decision to include pH as a parameter to be optimised in the subsequent chapters.

3.4 Micelle Size and Shape Characterisation

At concentrations above the CMC, amphiphiles form micelles due to entropic and enthalpic contributions to free energy.⁶ In water, burial of hydrophobic moieties in a micelle core is favourable and the continuation of this process should eventually lead to large aggregates or phase separation. However, by definition being amphiphilic means the hydrophobic section of a surfactant is covalently linked to the hydrophilic section. Bringing these hydrophilic headgroups into close proximity is energetically unfavourable, and these two opposing effects balance each other to form micelles of finite size. Surfactant micelles can be 2 to 50 nm in diameter;⁸ within the range of Dynamic Light Scattering (DLS) and Small Angle X-ray Scattering (SAXS). DLS is a fast technique to determine the size of the micelles, *i.e.* hydrodynamic radius, whereas SAXS is a technique that uses static scattering to provide insight into the shape, as well as size, of the micelles, although an electron density contrast is required.⁹ Hence, both DLS and SAXS were used as complimentary techniques.

3.3.1 DLS

The size of micelles formed by the six surfactants was characterised by DLS. The concentration of the aqueous surfactant solutions used for DLS was 1 w/w% as this is the higher than the CMC for all surfactants of interest, presented in section 3.3. The hydrodynamic diameter of the micelles is shown in table 3.6.

Table 3.6: Hydrodynamic diameter of surfactant micelles determined by DLS for 1 w/w% aqueous solutions

Surfactant	Z-average diameter / nm	PDI
LO	5.6 ± 0.0	0.03
ВС	2.9 ± 0.1	0.22
DG	20 ± 0.2	0.16
CAB	6.3 ± 0.0	0.11
SDS	8.6 ± 0.0	0.45
AE	10 ± 0.1	0.03

Interestingly, the data in table 3.6 reveals that one of the surfactants with the broadest distributions of molecules, LO, shown previously by mass spectrometry, has one of the lowest PDI. A possible explanation for this may be that the mixture of chain lengths in the LO sample is beneficial as the rearrangement of the different sized surfactants will lead to towards the formation one size of micelle at equilibrium. In contrast, the larger PDIs from samples with less variability in the size of the hydrophobic section of the surfactant indicates that only micelles of specific sizes can be formed depending on the most favourable number of surfactant molecules in the micelle, *i.e.* the aggregation number.

BC, a cationic surfactant, formed the smallest micelles according to DLS. It is important to note that BC had one of the fewest number of components in their mixture, two: C12 and 14. At the opposite end of the scale, the largest micelles were formed by DG and AE. Both of these surfactants comprised of mixtures of multiple alkyl chain lengths (C8 to C12) which could lead to less efficient packing of chains within the micelle core and causing the chains to occupy a greater volume. An effective hydrodynamic sphere is assumed for DLS particle size analysis; therefore, the samples were analysed by SAXS in order to determine if this was an accurate assumption.

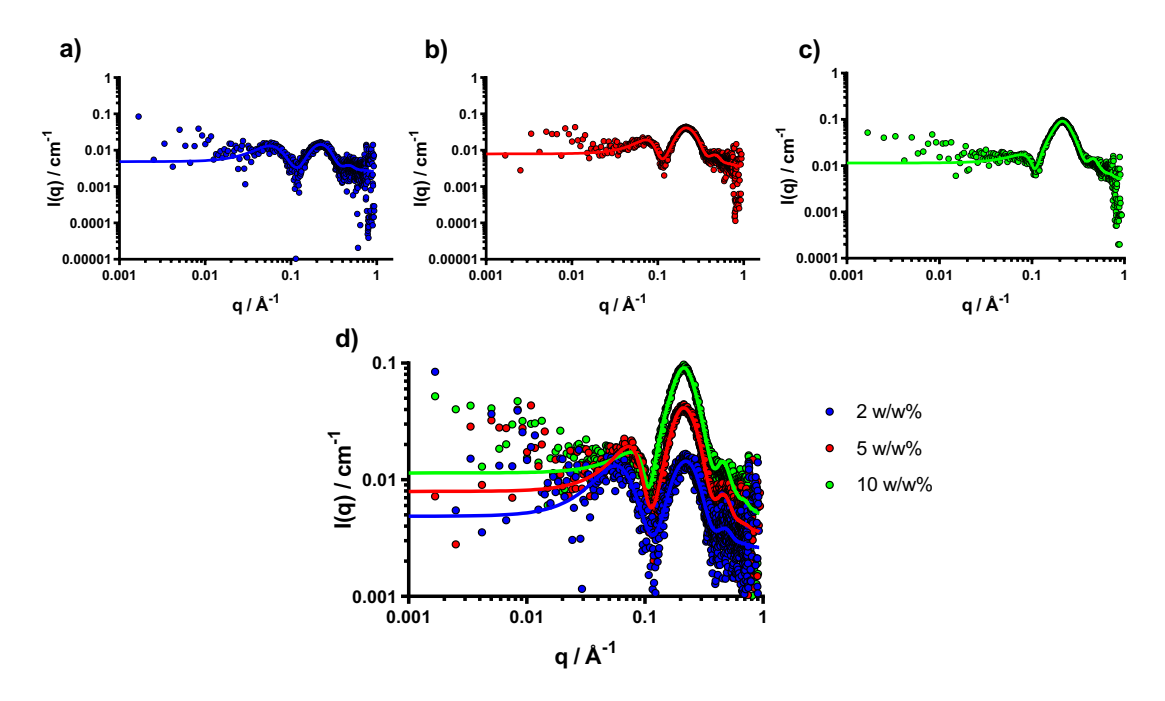


Figure 3.6: q dependence of the normalised scattering intensity for SDS as a function of concentration:

a) 2 w/w% b) 5 w/w% c) 10 w/w% d) Comparison of all 3 concentrations. The circles are the collected data and the solid lines indicate fit with a model describing core shell ellipsoids.

SAXS can be used to characterise the size and shape of the surfactant micelles. SAXS data was first obtained for SDS in deionised water at three concentrations (2, 5 and 10 w/w%) as shown in figure 3.6. The scattering intensity, corrected for background scattering by subtraction of the scattering of a deionised water capillary, is plotted against the scattering vector, q. The position of the intensity minima at 0.1 A⁻¹, is not affected by increasing concentration, which suggests that the dimensions of the micelles remain constant. However, the local maxima in intensity at approximately 0.07 A⁻¹ grows with increasing SDS concentration and is indicative of interactions between micelles. As the size of the micelles is independent of concentration, this maximum is due to a decreasing intermicellular distance at higher concentrations, leading to a structure factor. The scattering for SDS is well described by modeling the system as a mixture of core-shell ellipsoidal particles and a hard sphere structure factor.

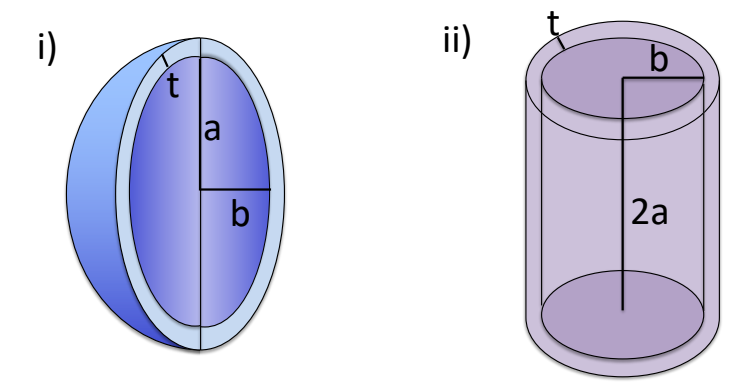


Figure 3.7: The SAXS model fits used here were for: i) a spheroid core-shell ellipsoid particle, where a is the axial radius of the core and b is the equatorial radius of the core and t is the thickness of the shell, and ii) a circular core-shell cylinder, where a is half the length of the core, b is the radius of the core and t is the thickness of the shell.

The chosen model fits the scattering data well and are in agreement with previous studies of the shape of SDS micelles. ^{10–12} SDS micelles were modelled as prolate ellipsoids where the axial radius of the core (figure 3.7i)), the polar radius divided by the equatorial radius, is greater than 1. ¹⁰ (Prolate describes an ellipsoid where the two equal axes are larger than the remaining axis, whilst oblate describes an ellipsoid where the two equal axes are smaller than the remaining axis.) Is It is commonly accepted that this non-spherical shape is to account for thermal fluctuations. ¹³

Table 3.6: Dimension of SDS surfactant micelles determined by small angle X-ray scattering with data fitted to a core-shell prolate ellipsoid model.

Surfactant	a/Å	b/Å	Shell Thickness / Å
SDS	26.9	15.9	4.0

The shell thickness was assumed to be constant around the circumference of the particles. Since there is only one type of surfactant present in the SDS sample, all the surfactant headgroups should be the same size. The core equatorial radius of the micelles was $15.9 \pm 0.1 \,\text{Å}$, which accounts for the hydrophobic tail length (a stretched C12 chain has a theoretical length of $16.9 \,\text{Å}^{14}$).

Table 3.7: Dimension of LO surfactant micelles determined by small angle X-ray scattering with data fitted to a core-shell prolate ellipsoid model.

Concentration of LO / w/w%	a/Å	b/Å	Shell Thickness / Å
1	37.5	16.9	2.4
2	42.7	17.6	2.4

The SAXS analysis for LO is shown in table 3.7. The non-ionic surfactant, N,N-Dimethyldodecylamine-N-oxide (DDAO), has been shown in multiple previous small angle neutron scattering (SANS) studies to form elongated prolate ellipsoid micelles. ^{15,16} The sample of LO surfactant used in this study contains DDAO, which has a C12 tail group, in addition to six other fractions with differing tail lengths. The prolate, core-shell ellipsoid model fits well to the scattering pattern of the commercial LO sample. To make sure the shape and size of LO micelles are concentration independent two concentrations of surfactant were prepared: 1 and 2 w/w%. Barlow *et al.* showed that DDAO formed micelles of axial radius 16.2 ± 0.5 Å and axial ratio of the core 1.89 ± 0.21 . ¹⁵ The parameters calculated for this surfactant are in agreement with these values: the axial radii obtained were 16.9 Å and 17.6 Å and the axial ratios of the core were 2.23 and 1.90, corresponding to 1 and 2 w/w% respectively.

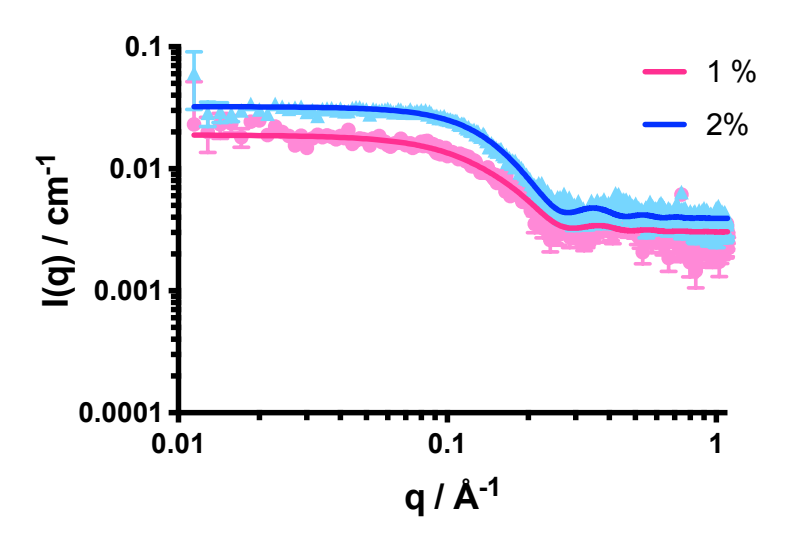


Figure 3.8: q dependence of the normalised scattering intensity for 1 and 2 w/w% LO. Lines indicate fit with a model describing core shell ellipsoids.

The SAXS pattern of 2 w/w% BC is shown in figure 3.9. Having a best fit to a model of spherical particles, with a uniform scattering length density, suggests the radius of BC is 8.3 Å. Although the spherical model has the best fit, the fit is not perfect. The SAXS pattern shows a high noise at $0.05 \text{ Å}^{-1} > q$ and $q > 0.5 \text{ Å}^{-1}$ and the model is a poor fit to the data. In addition, the SAXS of samples below 2 w/w% resulted in high noise with very little variation in intensity. These results taken together might be due to low contrast as the difference between the scattering length density of the micelle and the solvent is small: SLD of BC is $9.18 \times 10^{-6} \text{ Å}^2$ and SLD of water is $9.42 \times 10^{-6} \text{ Å}^2$. Alternatively, the cause could be that the micelle is highly solvated which means the scattering length density difference between the micelle and the solvent would be decreased.

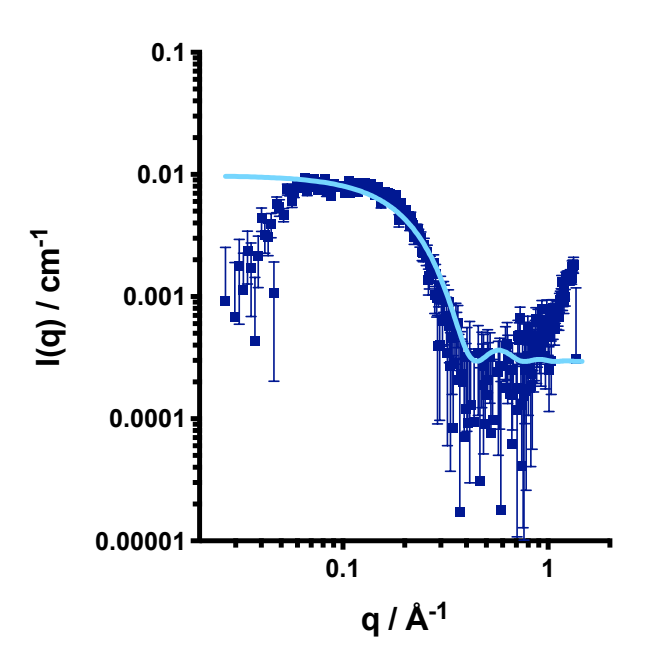


Figure 3.9: q dependence of the normalised scattering intensity for 2 w/w% BC. Lines indicate fit with a model describing spherical particles.

SAXS of 1 w/w% DG fits well to both a core-shell ellipsoid and a core-shell cylinder, suggesting similar values for shell thickness and radius in both cases. A comparison of the fits can be found in table 3.8. The radius and shell thickness determined by each model are in agreement; however, there is an 18% discrepancy between the longest axis in the particle determined by each model. The conversion between the shape of a cylinder to a sphere could be considered as the curving or rounding of the bases of the cylinder. Therefore, for the total area of the two shapes to the same, with the same equatorial diameter: an ellipsoid would be longer than a cylinder.

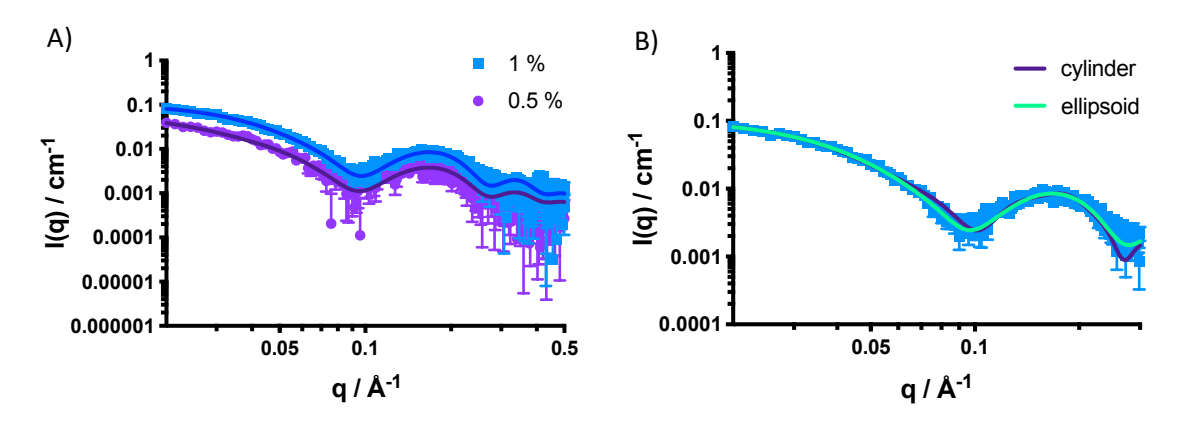


Figure 3.10: q dependence of the normalised scattering intensity for DG with the comparison of: A) concentration and B) fitting of different shaped models.

Previous SAXS studies of alkylpolyglucosides have described the micelles as both ellipsoids and cylinders. Oliver et~al. validated the use of a two-component micelle model to fit experimental SAXS data for DG by comparing its derived parameters to model-free derived parameters rather the micelles are short rods which 'interact via excluded volume interactions'. ^{17,18} Zhang et~al. showed that simpler core-shell ellipsoid models fit octyl- and nonyl- glucoside micelles at lower q but at q values ≥ 0.3 Å, cylinder fits are more appropriate. ¹⁹ Lipfert et~al. also performed small angle scattering experiments with alkylpolyglucosides and found octyl and nonyl glucosides to fit prolate ellipsoid models. ²⁰ As expected, the values they obtained for the core micelle radius increase with increasing carbon tail length. For example, the axial radii at the equator, b, for octyl glucoside was 12-13.2 Å (i.e. 8 C) and for nonyl glucoside was 13.5-15 Å (i.e. 9 C), a difference of 2 Å. The DG radii was 16 Å, showing an increase of the same increment. Difficulties in running scattering experiments of DG was reported due to its poor solubility, high viscosity and the complexity of the DG phase diagram. In comparison, our sample of alkyl polyglucoside showed no solubility issues at any of the concentrations tested.

Table 3.8: Comparison of the dimensions of DG surfactant micelles determined by fitting of small angle x-ray scattering data using a core-shell ellipsoid model and a spherical cylinder model where a is half the length of the core, b is the radius of the core and t is the thickness of the shell.

Surfactant	a/Å	b/Å	t/Å	Model shape
2% DG	$\textbf{72.0} \pm \textbf{0.1}$	$\textbf{17.0} \pm \textbf{0.1}$	$\textbf{7.6} \pm \textbf{0.1}$	prolate ellipsoid
2% DG	59.2 ± 1.7	$\textbf{16.0} \pm \textbf{0.1}$	7.2 ± 0.1	short cylinder

3.3.3 Comparison of DLS and SAXS

As SAXS and DLS are complimentary techniques, SAXS measures the static properties whilst DLS measures dynamic properties. Another difference is that DLS probes the hydrodynamic diameter, indicating the size of the hydrated or solvated micelle, whereas SAXS gives the size based on the electron density contrast. The size and shape data from the two techniques can be techniques is compared in table 3.9.

Table 3.9: Comparison of the size and shape of LO, BC, DG, and SDS micelles determined by DLS and SAXS. The dimensions of LO, DG and SDS surfactant micelles were determined by fitting of small angle x-ray scattering data using a core-shell ellipsoid model, where a is half the length of the core, b is the radius of the core and t is the thickness of the shell. The dimensions of BC surfactant micelles were determined by fitting of small angle x-ray scattering data using a core-shell model for spherical particles.

	DLS	SAXS			
Surfactant	Hydrodynamic Radius / Å	a/Å	b/Å	t/Å	Model Shape
LO	28	37.5	16.9	2.4	prolate ellipsoid
BC	10	8.3			sphere
DG	100	72.0	17.0	7.6	prolate ellipsoid
SDS	43	26.9	15.9	4.0	prolate ellipsoid

SAXS has the advantage of being able to identify the shape of the micelles, LO, DG and SDS are ellipsoidal whereas BC is spherical. The spherical radius determined by both methods is comparable for BC, 10 Å by DLS and 8.3 Å by SAXS. The radii determined for LO was smaller by DLS than SAXS, however the value is between the small and long axis determined in the ellipsoid. However, the radius of SDS was larger than that determined by SAXS, which may be due to a higher degree of solvation. Furthermore, the radii determined by SAXS for DG are of the same order of magnitude as the diameter determined by DLS; the Z-average diameter was 20.33 ± 0.21 nm. In summary, SAXS has been used to initially confirm the data obtained by DLS and further investigate the sizes and shapes of the micelles which highlighted the differences between the surfactants.

3.5 Characterisation of micelles in binary mixtures

Apart from a small angle neutron study of SDS and dodecyldimethylamine oxide, there is little published data on the characterisation of the micelles in aqueous mixed surfactant solutions for the surfactants of interest in this project.²¹ Hence, the micelles in the binary mixtures optimised previously, LO/BC and LO/DG, were analysed, by DLS and SAXS. As mentioned in the previous chapter, the SAXS pattern obtained for BC was very noisy and therefore, SAXS was not performed on mixtures of LO and BC.

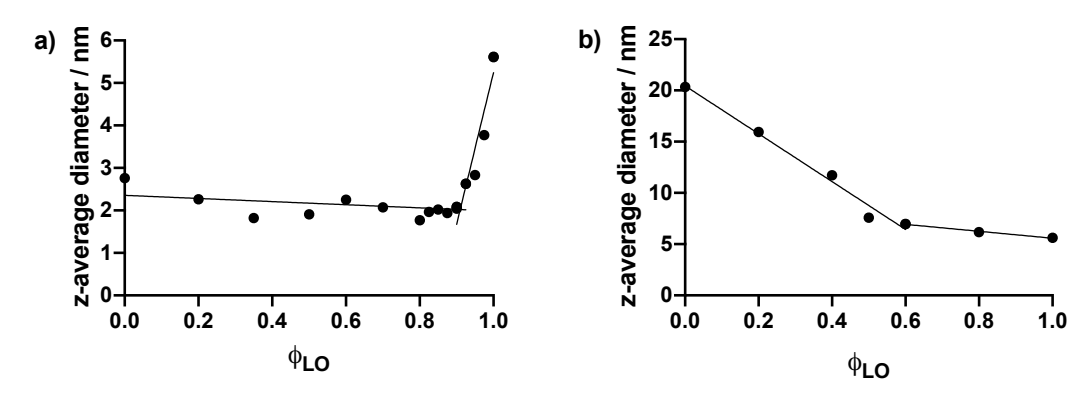


Figure 3.11: The intensity averaged hydrodynamic diameter of micelles in aqueous mixtures of a) LO and BC and b) LO and DG, measured by DLS. The black lines show a linear regression fitted to the two sections of each data set.

Figure 3.11 shows DLS of surfactant mixtures of LO/BC and LO/DG at 1 w/w% total surfactant concentration, which is above the CMC for all 3 surfactants. For the duration of this discussion, Φ_{LO} is the ratio of LO to the other surfactant, either BC or DG. The mixed LO/BC systems are of similar diameter to solely BC micelles until Φ_{LO} is above 0.9. As discussed previously, LO micelles are much larger than the BC micelles, 2.9 nm (at $\Phi_{LO}=0$) and 5.6 nm (at $\Phi_{LO}=1$) respectively. The small size of cationic BC micelles reflects the strong repulsive electrostatic interactions between the charged headgroups. As LO is zwitterionic, the small size of the micelles may suggest that the LO is incorporated into the BC micelles in its positively charged form causing no change in the repulsive interactions between headgroups. The second binary mixture, LO and DG, was studied by DLS and SAXS. Earlier DG was shown to be a mixture of multiple alkyl chain lengths forming larger micelles whereas there were only 2 chain lengths in the sample of BC and DG micelles (20.3 nm at $\Phi_{LO}=0$) are much larger than the LO micelles (5.6 nm at $\Phi_{LO}=1$). DLS of the mixture showed the micelle diameters decrease linearly with increasing LO concentration and there is a decrease in gradient when $\Phi_{LO}=0.6$. With higher LO concentrations higher than this, the rate of change

in micelle diameter decreases shown by the smaller gradient of the regression line in figure 3.11a).

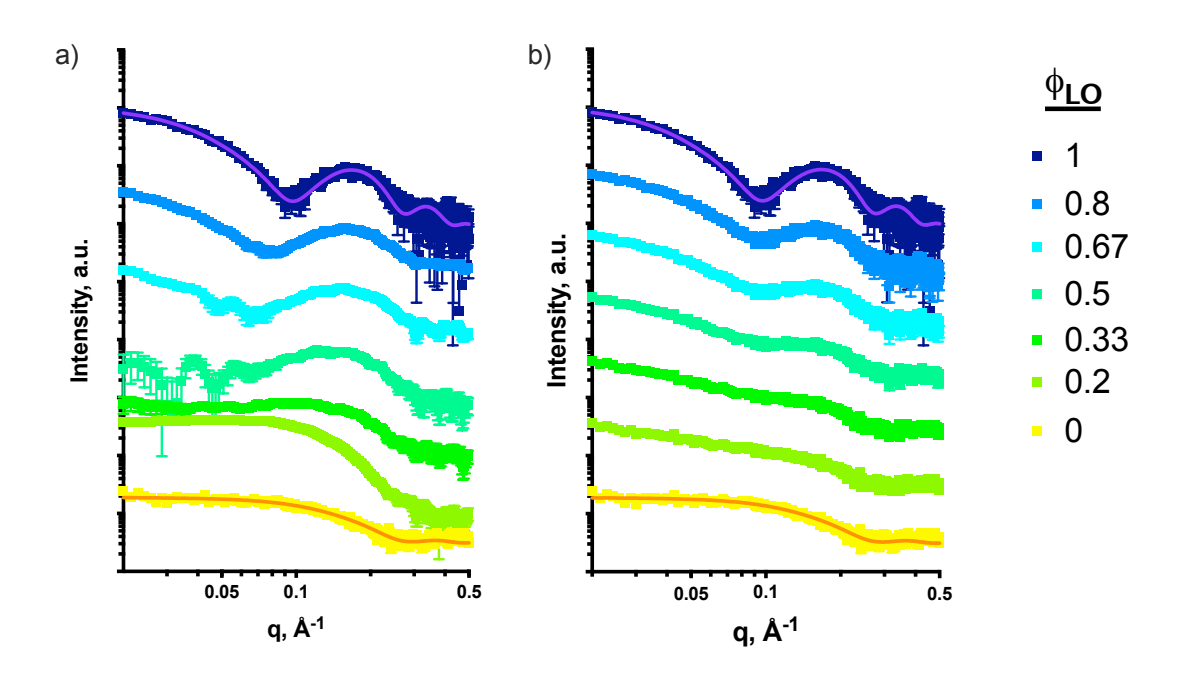


Figure 3.12: The 1D scattering patterns for aqueous mixtures of LO and DG showing the formation of mixed micelles where a) shows the scattering patterns obtained experimentally and b) shows the mixing of two populations of single surfactant micelles, LO and DG, simulated by adding their individual SAXS patterns together in relative proportions.

The SAXS patterns collected for the mixtures of DG and LO, figure 3.12 a), suggest the formation of mixed micelles. This can be shown by weighted addition of the SAXS patterns for the individual surfactants (Φ_{LO} = 0 and Φ_{LO} = 1). For example, the scattering pattern for Φ_{LO} = 0.5 is a combination of the SAXS pattern from half the LO pattern (Φ_{LO} = 1) and half the DG pattern (Φ_{LO} = 0). For two populations of micelles, the minima would be expected to be gradually lost with increasing DG concentration (as in figure 3.12 b)). However, this is not the case; comparison of the position of the minima at q ~ 0.1 Å in figures 3.12 a) and b) show a significant difference and the shape of the patterns' changes (*i.e.* the minimum shifts to lower Å in the patterns for Φ_{LO} = 1, 0.8 and 0.67 in figure 3.12 a)).

3.6 Conclusions

In this investigation, the aim was to assess the physical characteristics of six commercial surfactants (LO, BC, DG, CAB, AE and SDS) through the determination of their native concentration, molar mass and fraction composition, micelle shape and size and CMC. This study has shown that many of these commercial surfactants are complex mixtures, meaning that the molar concentrations could not be precisely determined using moisture analysis and chromatography. The shape and size of the micelles formed by these surfactants were analysed by applying different micelle models, namely spherical, ellipsoidal and cylindrical, to SAXS data, and were broadly in agreement with the literature. Surface tension is used as an indicator of surfactant efficiency, therefore determination of the CMC of these surfactants was measured and compared to literature values. Binary mixtures of LO/BC and LO/DG were analysed by DLS to investigate the behaviour of the mixed micelles and SAXS was used to identify the formation of mixed micelles in the mixture of LO and DG.

These findings suggest that when using industrial grade surfactants to formulate solutions with targeted properties, i.e. cleaning solutions, each surfactant component should be regarded as a mixture of different molar masses. The results in this chapter have informed the design of initial optimisation experiments later on in this project with regards to initial boundary conditions.

3.7 References

- 1. Liu, X., Zhao, Y., Li, Q., Jiao, T. & Niu, J. Adsorption behavior, spreading and thermal stability of anionic-nonionic surfactants with different ionic headgroup. *J. Mol. Liq.* **219**, 1100–1106 (2016).
- 2. Mansur, C. R. E., González, G. & Lucas, E. F. Calorimetry and thermogravimetry as tools for the assessment of the thermal stability of polyoxide-based nonionic surfactants. *Polym. Degrad. Stab.* **80**, 579–587 (2003).
- 3. Sigma-Aldrich. *Product Specification: Sodium Dodecyl Sulphate.* (2019).
- 4. Powney, J. & Addison, C. C. The properties of detergent solutions. *Trans. Faraday Soc.* (1937).
- 5. Chakraborty, T., Chakraborty, I. & Ghosh, S. The methods of determination of critical micellar concentrations of the amphiphilic systems in aqueous medium. *Arab. J. Chem.* (2011).
- 6. Rosen, M. J. & Kunjappu, J. T. *Surfactants and Interfacial Phenomena. A Wiley-Interscience publication* (Wiley, 2012).
- 7. Staszak, K., Wieczorek, D. & Michocka, K. Effect of sodium chloride on the surface and wetting properties of aqueous solutions of cocamidopropyl betaine. *J. Surfactants Deterg.* **18**, 321–328 (2015).
- 8. Ben-Naim, A. & Stillinger, F. H. Critical micelle concentration and the size distribution of surfactant aggregates. *J. Phys. Chem.* (1980).
- 9. Schwamberger, A. et al. Combining SAXS and DLS for simultaneous measurements and time-resolved monitoring of nanoparticle synthesis. *Nucl. Instruments Methods Phys. Res. Sect. B Beam Interact. with Mater. Atoms* (2015).
- 10. Jensen, G. V., Lund, R., Gummel, J., Narayanan, T. & Pedersen, J. S. Monitoring the Transition from Spherical to Polymer-like Surfactant Micelles Using Small-Angle X-Ray Scattering. *Angew. Chemie Int. Ed.* **53**, 11524–11528 (2014).
- 11. Itri, R. & Amaral, L. Q. Distance distribution function of sodium dodecyl sulfate micelles by X-ray scattering. *J. Phys. Chem.* **95**, 423–427 (1991).
- 12. Duplâtre, G., Ferreira Marques, M. F. & Da Graça Miguel, M. Size of sodium dodecyl sulfate micelles in aqueous solutions as studied by positron annihilation lifetime spectroscopy. *J. Phys. Chem.* **100**, 16608–16612 (1996).
- 13. Ljunggren, S. & Eriksson, J. C. Thermal shape fluctuations of spherical surfactant micelles. *J. Chem. Soc. Faraday Trans. 2 Mol. Chem. Phys.* **85**, 1553–1574 (1989).
- 14. MacKerell, A. D. Molecular dynamics simulation analysis of a sodium dodecyl sulfate micelle in aqueous solution: Decreased fluidity of the micelle hydrocarbon interior. *J. Phys. Chem.* **99**, 1846–1855 (1995).
- 15. Barlow, D. J., Lawrence, M. J., Zuberi, T., Zuberi, S. & Heenan, R. K. Small-angle neutron-scattering studies on the nature of the incorporation of polar oils into aggregates of N,N-dimethyldodecylamine-N-oxide. *Langmuir* **16**, 10398–10403 (2000).
- 16. Baglioni, M. *et al.* An amine-oxide surfactant-based microemulsion for the cleaning of works of art. *J. Colloid Interface Sci.* **440**, 204–210 (2015).

- 17. Oliver, R. C. *et al.* Dependence of Micelle Size and Shape on Detergent Alkyl Chain Length and Head Group. *PLoS One* **8**, e62488 (2013).
- 18. Stradner, A., Glatter, O. & Schurtenberger, P. Hexanol-induced sphere-to-flexible cylinder transition in aqueous alkyl polyglucoside solutions. *Langmuir* **16**, 5354–5364 (2000).
- 19. Zhang, R., Marone, P. A., Thiyagarajan, P. & Tiede, D. M. Structure and molecular fluctuations of n-alkyl-β-D-glucopyranoside micelles determined by X-ray and neutron scattering. *Langmuir* **15**, 7510–7519 (1999).
- 20. Lipfert, J., Columbus, L., Chu, V. B., Lesley, S. A. & Doniach, S. Size and shape of detergent micelles determined by small-angle X-ray scattering. *J. Phys. Chem. B* **111**, 12427–12438 (2007).
- 21. Kakitani, M., Imae, T. & Furusaka, M. Investigation of mixed micelles of dodecyldimethylamine oxide and sodium dodecyl sulfate by SANS: Shape, size, charge, and interaction. *J. Phys. Chem.* (1995).

4 Bayesian Optimisation with respect to Surface Tension

4.1 Introduction

Mixtures of surfactants are used in many applications, such as detergents, coatings, cosmetics and personal care, due to synergistic effects, where the properties of the mixture are greater than that of either pure surfactant. In addition, commercial surfactants are mixtures of different isomers, lengths of the alkyl chain and headgroup orientation, due the process of their manufacture. Properties of surfactant mixtures, such as adsorption, shape and size of self-assembled structures, can be difficult to predict due to the synergistic, or antagonistic, behaviour of surfactant mixtures.¹

Surfactant mixing has been previously studied using surface tension to quantify one aspect of the physical chemistry of the mixture.² Prediction of the CMC, the point of inflection in a surface tension isotherm, for some surfactant mixtures has been achieved using regular solution theory or, more recently, molecular thermodynamics.^{3,4} Surface tension plays a role in the removal of soil from a surface. By reducing the surface tension of a solution, its wetting ability is increased leading to a greater coverage of the soiled surface. Above the CMC, there is more surfactant available (as monomer or in micelles) to perform the mechanisms of cleaning discussed previously: roll-up and emulsification. In addition, the surfactant micelles are able to aid in prevention of re-deposition of the soil on the surface. Thus, the minimum in surface tension was the parameter chosen to optimise as it has importance in the cleaning ability of a surfactant mixture with minimal difficulty in measurement. Computational methods to optimise mixtures of surfactants are limited and, so far, the models only extend to surfactant mixtures of three parameters.^{4–6} Furthermore, these approaches require detailed characterisation of the surfactant that are difficult to obtain for commercial surfactants because they are complex mixtures as shown in in the previous chapter.

Due to the complexity of formulations, formulators use their years of expertise coupled with general guiding principles. As discussed in Chapter 2, this has driven the use of traditional design of experiment (DOE) approaches in product formulation.^{7,8} DOEs target finding an empirical model for the system of interest using an experimental design to more efficiently cover the formulation space. However, these methods rely on the ability to fit a suitable model which may not be the case if there is high nonlinearity in the data collected.^{9,10} An

alternative method is adaptive experimental optimisation, which guides an experimenter to find the optimum by suggesting the next experiment to perform based on Bayesian rules of probability. The advantage of this method is that importance is placed on areas in the formulation space close to the "best" previous results, in order to reduce the number of experiments required to find the optimum.

This chapter explores the use of Bayesian optimisation to optimise a mixture of surfactants with multiple variables (surfactant concentrations, water concentration and pH). As discussed in a previous chapter (section 2.4), Bayesian optimisation is a data-driven iterative approach to deal with black-box problems: the mathematical relationship between the input and target variables is unknown. In this case, the black box problem is the optimisation of a surfactant mixture where the target output variable is the minimum in surface tension optimised by finding the right combinations of surfactants and the right concentrations in an aqueous mixture. In summary, this chapter investigates the extent to which the lowest surface tension of an aqueous mixture of surfactants can be identified using a Bayesian optimisation methodology.

4.2 Design Loop

The first step in the design of the Bayesian optimisation is to select the input and output parameters and boundary conditions and whether the unknown function is to be maximized or minimized. Next, an initial batch of experiments (surface tension measurements) was selected which randomly cover the formulation space previously defined. Upon acquiring the data for the initial batch of experiments, the unknown function is modelled using a Gaussian process. The next set of experiments are suggested in order to optimise the acquisition function derived from the Gaussian process. The suggestions have a high chance of improving on previous results or are in unexplored areas of the formulation space. The collected data is compared to the predictions and the process is repeated until no further improvement is observed.

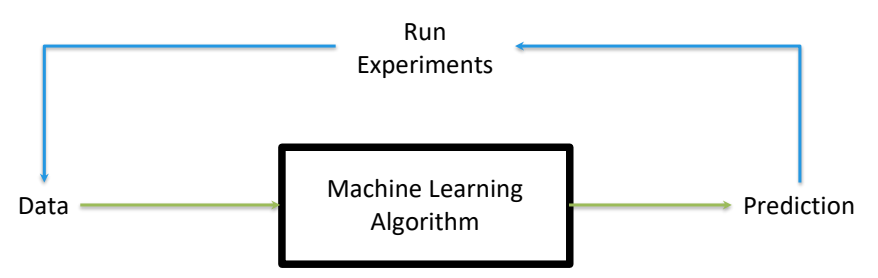


Figure 4.1: The optimisation process using a machine learning algorithm

4.3 Bayesian Optimisation of LO and BC

The target of the first optimisation was to find the pH and concentrations of LO and BC in an aqueous mixture with the lowest surface tension. To begin the iterative optimisation process, an initial experimental design was chosen to select a preliminary batch of 20 experiments. A randomised sampling algorithm with a bias was used to select the preliminary batch with half the experiments having a water concentration between 99.8% and 100% and the other 10 between 99% and 100%, figure 4.2. This was due to the knowledge, from chapter 3, that the CMC of the individual surfactants were within the range 0.0015 to 0.2 w/w% surfactant and the formulation space could be reduced.

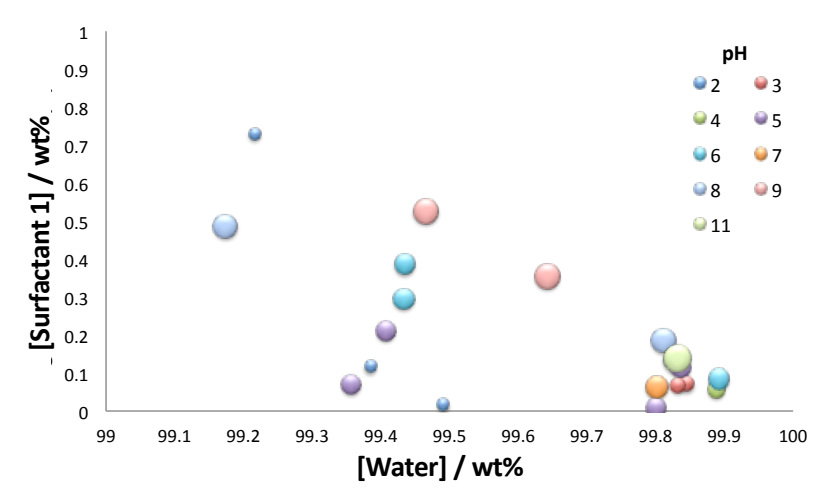


Figure 4.2: The initial experimental design selected by a random sampling algorithm within the following parameters that define the formulation space: 99-100 w/w% water, 0-1 w/w% of each surfactant and pH of integer values between 2 and 11. The size and colours of the bubbles indicate the pH.

The surface tension of the twenty created solutions were measured. There was a range in the surface tension measured, as would be expected for a random sample. The optimisation algorithm was used to select the next batch of 20 experiments. The experiments suggested were predicted to have a low surface tension based on the data previously collected or were associated with a high uncertainty due to being in areas of the formulation space not previously explored (figure 2.15 in section 2.4.4).

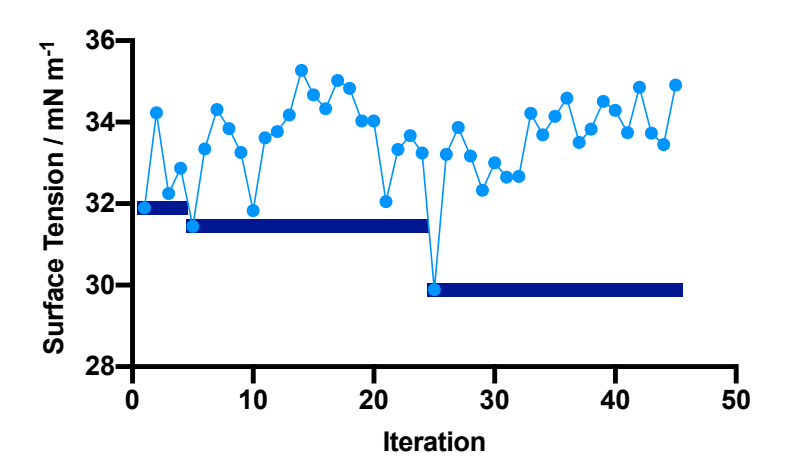


Figure 4.3: Surface tension through the optimisation process of an aqueous binary mixtures of LO and BC. For comparison, the surface tension of water is 72 mN m⁻¹ at 25 °C. The lowest surface tension at each iteration is shown by the dark blue line and the surface tension measured at that iteration is shown by a light blue circle.

No further improvement was seen after 23 iterations indicating the optimum had been identified.

Figure 4.3 shows the lowest surface tension observed with each iteration of the optimisation, *i.e.* after each surface tension was measured. There is no further decrease in the surface tension after iteration 23 which was the lowest surface tension observed for the mixture of LO and BC, 29.89 mN m⁻¹. The subsequent experiments probed the previously identified optimal region of the formulation space, in addition to other areas, but did not observe any lower values of surface tension. The optimisation was terminated after 45 iterations (surface tension measurements) to be confident the minimum value of surface tension had been identified as multiple experiments had not shown any improvement.

Figure 4.4 shows the concentrations of surfactant, pH and corresponding surface tension for each solution measured, as suggested by the Bayesian optimisation. Due to the difficulty of creating a graph with 6 axes, the data is shown as a matrix of graphs indicating there pairwise relationahips. As all the surfactants used in this study have different critical micelle concentrations, to be able to make a comparison between the concentration of surfactant needed to lower the surface tension for the surfactant alone and in a binary mixture, the units of surfactant concentration are given as normalised to the CMC. The effect of pH on surface tension of this mixture was explored by the optimisation. First, the 3 pH vs. surface tension graph (purple crosses) shows alignment of points around surface tensions of 33-34 mN m⁻¹ and the pH vs LO concentration (orange square) and BC concentration (pink diamond) show experiments across the pH range. Second, by looking at the experiments

suggested by the optimisation, 10 pH's, between 2 and 11, were measured for a solution with the same surfactant concentrations. However, there was little variation in surface tension, \pm 0.5 mN m⁻¹, which indicates that pH does not minimise surface tension for this surfactant combination. The points clustered at low concentration in the graph of LO vs BC concentration indicate the convergence of the optimisation, which is corroborated by the concentrations of the surfactants in the optimum mixture, table 4.1.

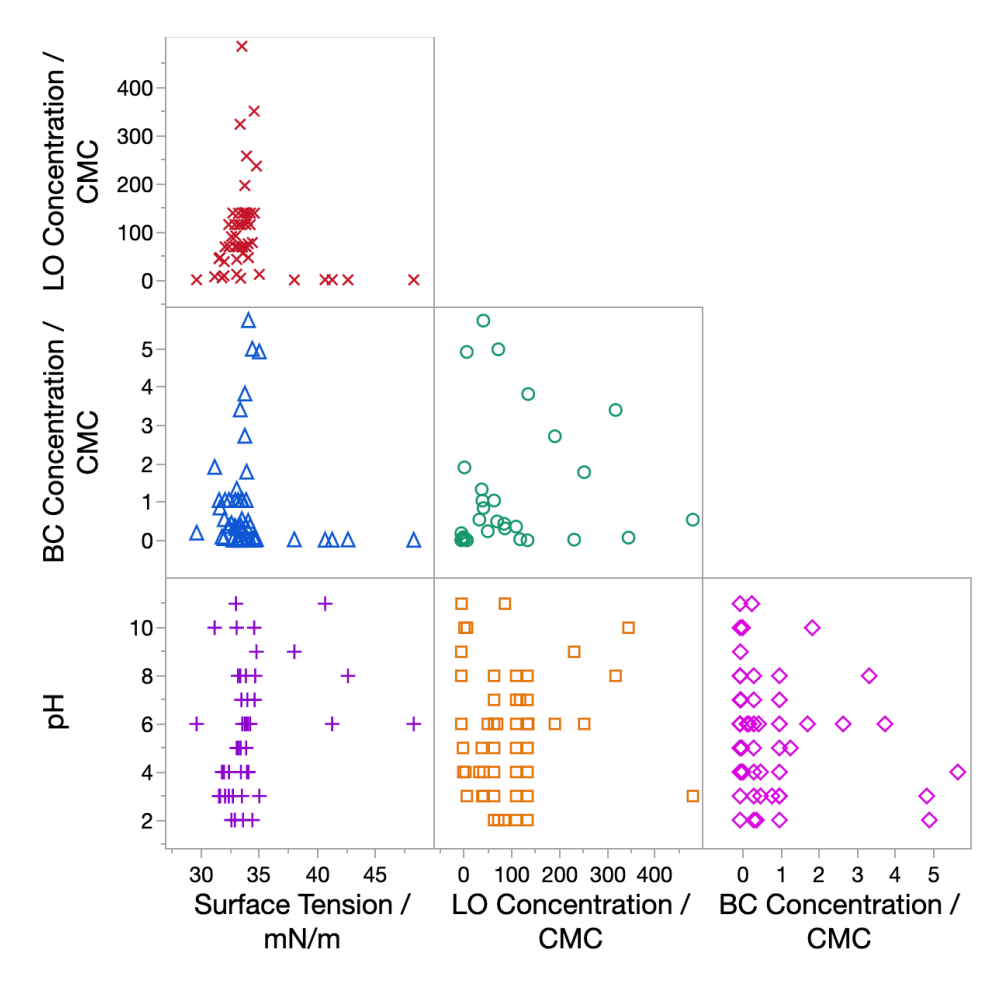


Figure 4.4: Experiments performed in a Bayesian optimisation of an aqueous binary mixture of LO and BC, with regards to minimising the surface tension. For comparison, the surface tension of water is 72 mN m⁻¹ at 25 °C. The boundary conditions were: 0-2 w/w% of each surfactant, 98-100 w/w% water and pH 2-11. Each point represents a single experiment, of which there were 45. The concentration of the surfactants is given in units normalised to their CMC concentration, as an indication of surfactant synergism. In the graph of LO vs BC concentration, there are points clustered at low concentration indicating convergence of the optimisation. The alignment of points on the pH graphs (bottom row) was due to the optimisation selecting experiments to test out pH dependence i.e. fixing the concentrations of BO and LO while changing pH.

In the mixture with lowest surface tension, in table 4.1, there are two interesting observations. First, the concentration of both surfactants was lower than either CMC individually: LO was 70% of its CMC and BC was 18.8% of its CMC. Second, the surface tension of the optimal mixture ($29.89~\text{mN}~\text{m}^{-1}\pm0.07$) was lower than the surface tension either surfactant was able to achieve individually, LO $33.49\pm0.25~\text{mN}~\text{m}^{-1}$ for LO and $35.17\pm0.05~\text{mN}~\text{m}^{-1}$ for BC. The increase in efficiency of the surfactants at reducing surface tension shows that these surfactants are exhibiting synergism which has been seen before, for example, in a previous study of the mixing behaviour of a BC surfactant and non-ionic, polyoxyethylene alkyl ether surfactants by Nandni *et al.*¹⁴ There is an increase in surface activity due to the formation of electrostatically stabilised mixed micelles as the non-ionic LO molecules insert themselves into the cationic BC micelles, which shields the repulsion between charged headgroups in addition to possible ion-dipole interactions between the ionic and cationic headgroups.¹⁴

Table 4.1: Result of the optimisation of a LO, BC surfactant mixture with respect to the minimum in surface tension.

LO	ВС	Water		Surface
Concentration	Concentration	Concentration	pН	Tension
(/CMC)	(/CMC)	(w/w%)		(mN m ⁻¹)
0.7	0.188	99.98	6	29.89 ± 0.07

A final observation was the total amount of surfactant that is required to be effective in lowering the surface tension in the optimal aqueous surfactant mixture, 0.02 w/w%, is much lower than the amount typically used in cleaning formulations, 2-5%. This is significant as the surfactant is one of the most expensive components in a cleaning formulation.

4.4 Bayesian Optimisation of LO and DG

As the iterative optimisation process to minimize surface tension efficiently found the optimal mixture for a binary mixture of a zwitterionic and cationic surfactant, the optimisation was implemented on a zwitterionic – non-ionic surfactant mixture, LO and DG. Except for the type of surfactants, the initial batch of 20 experiments chosen was identical to the previous optimisation with the same ratios of surfactants and boundary conditions: 99-100 w/w% water, 0-1 w/w% of each surfactant and pH of integer values between 2 and 11. Once the surface tension for these initial 20 experiments was measured, the data was used to suggest subsequent experiments using a Bayesian Optimisation.

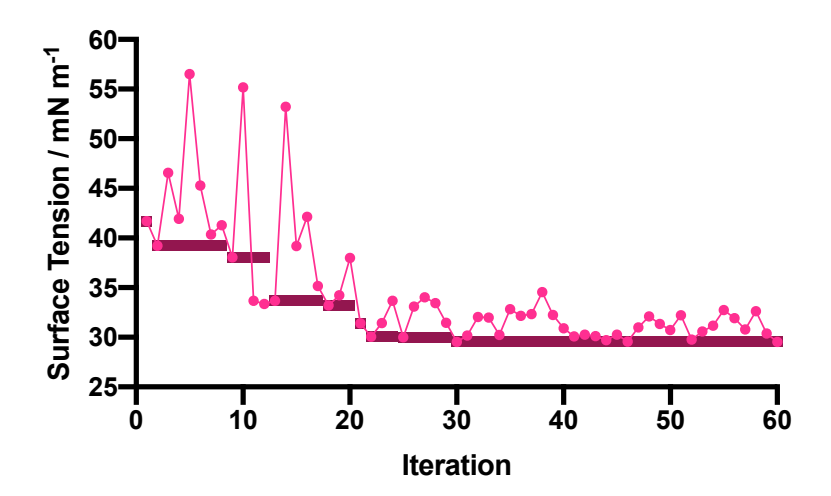


Figure 4.5: Surface tension through the optimisation process of an aqueous binary mixtures of LO and DG. For comparison, the surface tension of water is 72 mN m⁻¹ at 25 °C. The lowest surface tension at each iteration is shown by the burgundy line and the surface tension measured at that iteration is shown by a pink circle. No further improvement was seen after 30 experiments indicating the optimum had been identified.

The optimisation was terminated after 60 experiments as no further improvement was expected. Figure 4.5 shows the experiment iteration number vs surface tension. There was a reduction in surface tension on those previously measured at the thirtieth iteration which was the lowest surface tension measured for the combination of LO and DG, 29.54 mN m⁻¹. Further experiments probed this region of the formulation space, in addition to other areas, but no lower values of surface tension were observed.

In this second optimisation of a binary mixture, pH did have an effect. The graphs in figure 4.6 for pH vs LO concentration (yellow circles) and DG concentration (pink diamonds) reveals that solutions with lower surface tension are found with low pH. In the second round of the optimisation, all of the suggested experiments were at pH 2 indicating the algorithm had found the minimum at pH 2 which was the minimum boundary of the formulation space. Previous investigation of the surface properties of amine oxides showed a high pH-dependence, which was theorised to be due to formation of cationic species due to the protonation of the oxygen at high pH which forms hydrogen bonds with other cationic or ionic species. ^{16,17}

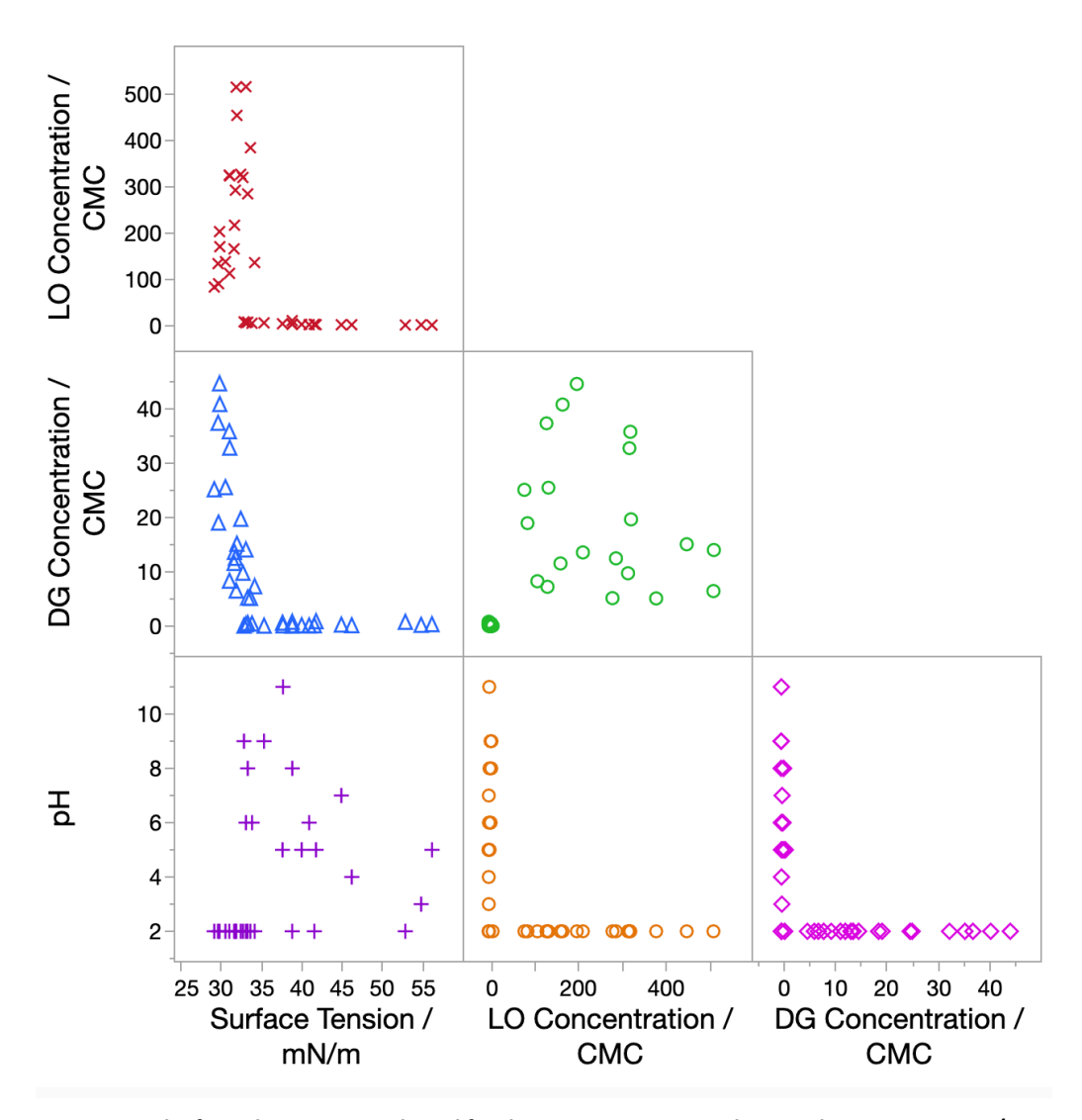


Figure 4.6: The formulation space selected for the optimisation. Boundary conditions were 0-1 w/w% surfactant, 0-98 w/w% water and pH 2-11. For comparison, the surface tension of water is 72 mN m⁻¹ at 25 °C. Each point represents a single experiment, of which there were 60. The concentration of the surfactants is given in units normalised to their CMC concentration, as an indication of surfactant synergism. In the graph of LO vs DG concentration, there are points clustered at low concentration indicating convergence of the optimisation. In the graphs of surfactant concentration vs surface tension for LO (red crosses) and DG (blue triangles), a plateau of the surface tension at high surfactant concentrations is observed. The pH vs surfactant concentration graphs show a large proportion of the selected experiments were at pH 2.

In the graphs of surfactant concentration vs surface tension for LO (red crosses) and DG (blue triangles), a plateau of the surface tension at high surfactant concentrations is observed. The total concentration of each surfactant in the mixture is much higher that their individual CMCs, table 4.2.

Table 4.2: Result of the optimisation of a LO and DG surfactant mixture with respect to the minimum in surface tension.

LO Concentration (/CMC)	DG Concentration (/CMC)	Water Concentration (w/w%)	рН	Surface Tension (mN m ⁻¹)
137.34	25.5	99.44	2	29.54 ± 0.03

It was surprising that the surface tension at the CMC for the optimum mixture was higher than that of DG alone and therefore an effort was made to figure out why. This result may be explained by errors caused by a new De Nouy ring (used in the measurement of the individual surfactants whilst the old ring was used for the optimisation). By re-measuring some of the test solutions and comparing the results from the two De Nouy rings, it was found that surface tensions of the samples measured with the new ring were all lower than that measured previously. The surface tension of the optimum sample measured using the new De Nouy ring was 28.21 mN m⁻¹.

4.5 Bayesian Optimisation of a Binary Mixture Conclusions

The purpose of both of these optimisations (LO/BC and LO/DG) was to determine whether the Bayesian Optimisation can optimise a surfactant mixture efficiently. The LO/BC and LO/DG mixtures were optimised with regards to four parameters: two surfactant concentrations, water concentration and pH. For both binary mixtures studied, the optimum was reached within 30 iterations, which is a much-reduced number compared to one-factor-at-a-time optimisation. In addition, this number is comparable to the number of runs required for full factorial or Box-Behnken experimental designs, which are frequently used in detergent optimisation. The number of experiments required to optimise four parameters is 30 for a central composite design and 27 for a Box-Behnken design.

4.6 Bayesian Optimisation of a Ternary Mixture

After optimising two binary mixtures of surfactants in aqueous solution, the optimisation was extended to three surfactants: LO, BC and DG. Commercial cleaning solutions can contain more than two surfactants so if a surfactant was added to a synergistic system, determination of whether the extra surfactant would show increased synergy or be detrimental to the system would be required. Furthermore, the addition of another parameter introduces complexity therefore, it was predicted that more iterations would be required.

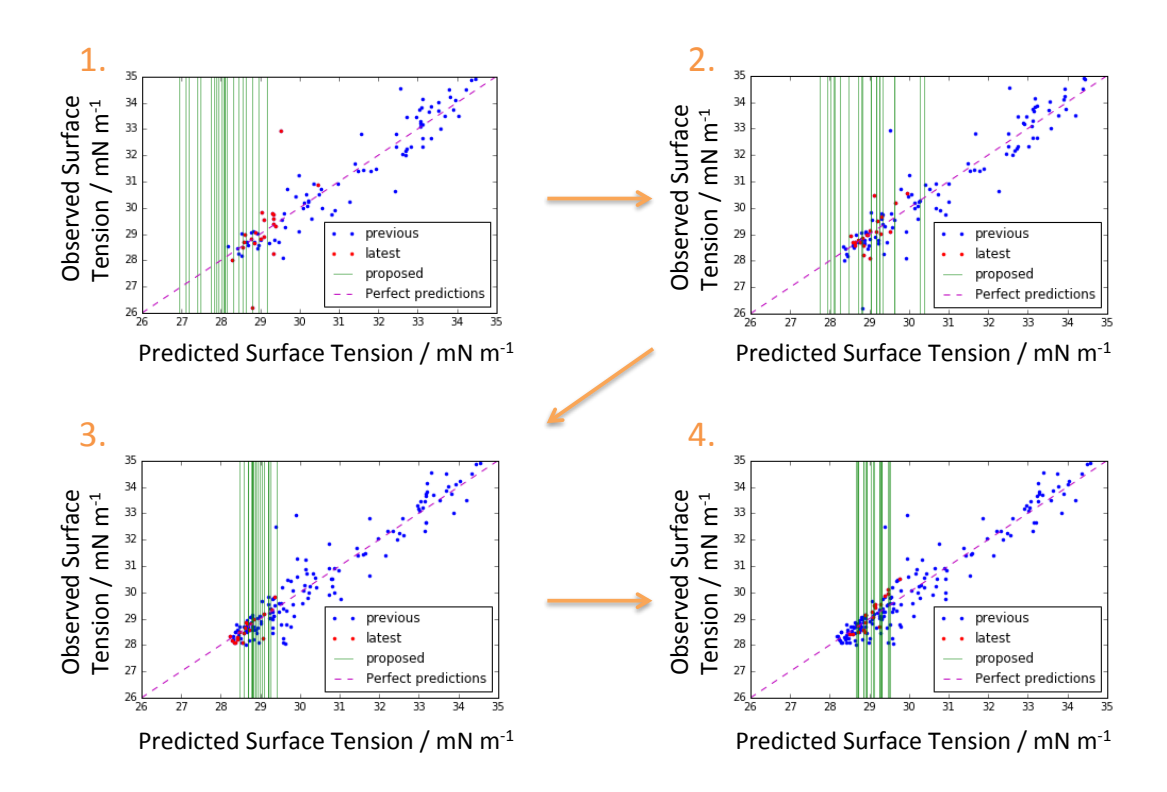


Figure 4.9: Iterations of the optimisation process of a ternary surfactant mixture with regards to surface tension of a surfactant mixture of LO, BC and DG with respect to the minimum in surface tension. The observed (measured) surface tension is compared to the surface tensions predicted by the model for the most recent data collected (red circles), the next proposed experiments (green lines) and the previously measured experiments (blue circles). The previous data collected in (1) is from the binary mixtures of LO/BC and LO/DG, optimised previously.

The additional surfactant was added to the previous binary mixtures to take advantage of the results already obtained. The Bayesian optimization iteration process for the three-surfactant mixture is shown in figure 4.9. The green lines show the predicted values of surface tension associated with suggested experiments. The blue dots show the surface tension of previously measured ternary mixtures. The red dots are the surface tension values of the most recent batch of measurements. Therefore, if the predictions for all experiments are perfect, the green lines in graph 1 would correspond to the red points in graph 2.

To identify when the optimum surface tension has been reached, the position of the predicted surface tensions relative to previous data is used. In graphs 1 and 2, the proposed batch of experiments include a number that are predicted to have lower surface tensions than those previously measured *i.e.* green lines at lower values than the blue/red dots. In graphs 3 and 4, data collected prior has lower surface tension than any predicted of the proposed batch of experiments. Therefore, the next iterations are to investigate any areas of

the formulation space with some uncertainty, for example, outliers due to physical measurement error or areas with less measurements. The optimal mixture has been identified by this point and it is unlikely further batches will show improvement.

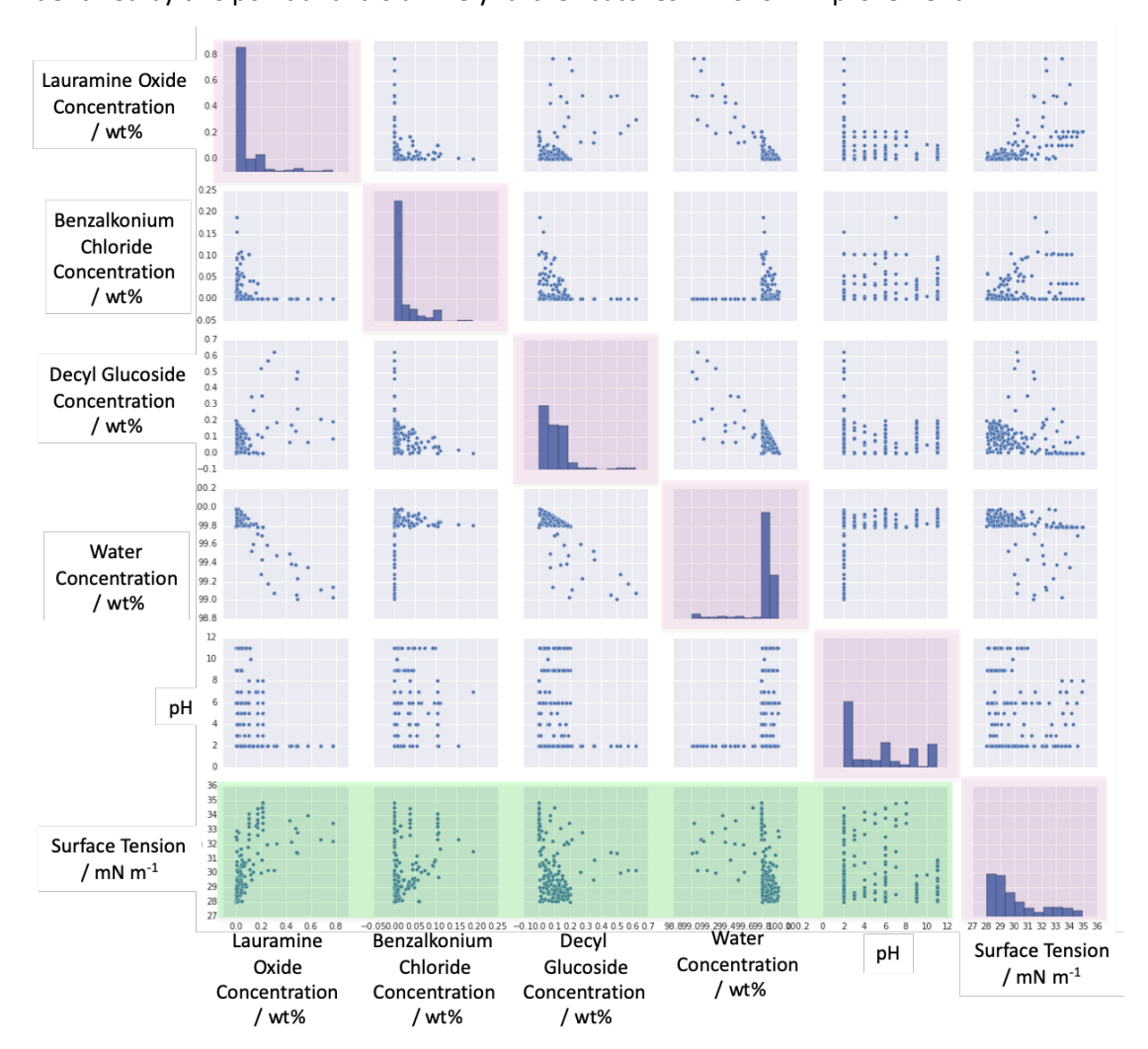


Figure 4.10: Graph matrix for the optimisation of a ternary mixture of LO, BC and DG surfactant mixture with respect to the minimum in surface tension. The graphs along the diagonal highlighted in pink show the number of experiments than have been performed with each proportion of surfactants, showing a greater number of experiments with higher decyl glucoside concentration. The peaks where the concentration of surfactant is zero in the histograms are due to the inclusion of the binary mixtures in the optimisation. The graphs highlighted in green on the bottom row of the matrix show the effect of surfactant concentration and pH on the surface tension, with low surface tensions found across the pH range.

Figure 4.10 shows a matrix of graphs to compare the all the surfactant solutions in the optimisation of the ternary mixture of LO, BC and DG. Little linear correlation is observed between all input variables. However, two key ranges of graphs are highlighted. First, the diagonal in the matrix (highlighted in pink) gives an indication of the relative number of experiments selected in different concentration ranges with regards each parameter (*i.e.* surfactant concentration, pH and surface tension). The histogram for the experiments at

different Decyl Glucoside concentrations shows the model selected more experiments with higher DG concentration, relative to the other surfactants. This is in agreement with the surface tensions of the individual surfactant, DG reduce the surface tension of water the most. The incorporation of the binary mixtures (LO/BC and LO/DG) in the data is shown by the peak at 0 w/w% in the surfactant concentration. The histogram for the number of solutions showed the model had a tendency towards solutions of pH 2. This peak at pH 2 is most likely due to the inclusion of the LO, DG binary mixtures which had lower surface tensions at pH 2.

Table 4.3: The four lowest surface tension values found by a Bayesian Optimisation of a ternary mixture of a LO, BC and DG surfactant mixture.

LO Concentration (/CMC)	BC Concentration (/CMC)	DG Concentration (/CMC)	Water Concentration (w/w%)	рН	Surface Tension (mN m ⁻¹)
1.4	0.582	0.338	99.935	6	28.04 ± 0.20
2.27	0.019	5.746	99.914	6	28.09 ± 0.04
7.73	0.031	7.356	99.911	9	28.08 ± 0.02
11.33	0.002	8.855	99.870	9	28.09 ± 0.01

Second, the scatterplots of each parameter against surface tension are highlighted in green. Low surface tensions are found right across the pH range and with a high proportion of water and therefore a low surfactant concentration. Interestingly, the optimisation found that the four lowest surface tension values were within 0.05 mN m⁻¹. In table 4.3, the results show that low surface tensions mixture were found for solutions with the major component being LO or DG. The surface tensions all had water concentrations above 99.8%. In addition, the surface tension of all four mixtures was lower than for each surfactant individually; the differences were 5.4 mN m⁻¹ for LO, 0.6 mN m⁻¹ for BC and 0.5 mN m⁻¹ for DG. For all three of the four lowest surface tension mixtures, the amount of LO and DG are higher than their concentrations at the CMC. However, for the lowest surface tension measured, the concentration of DG is lower than the CMC and LO is 40% greater than its CMC.

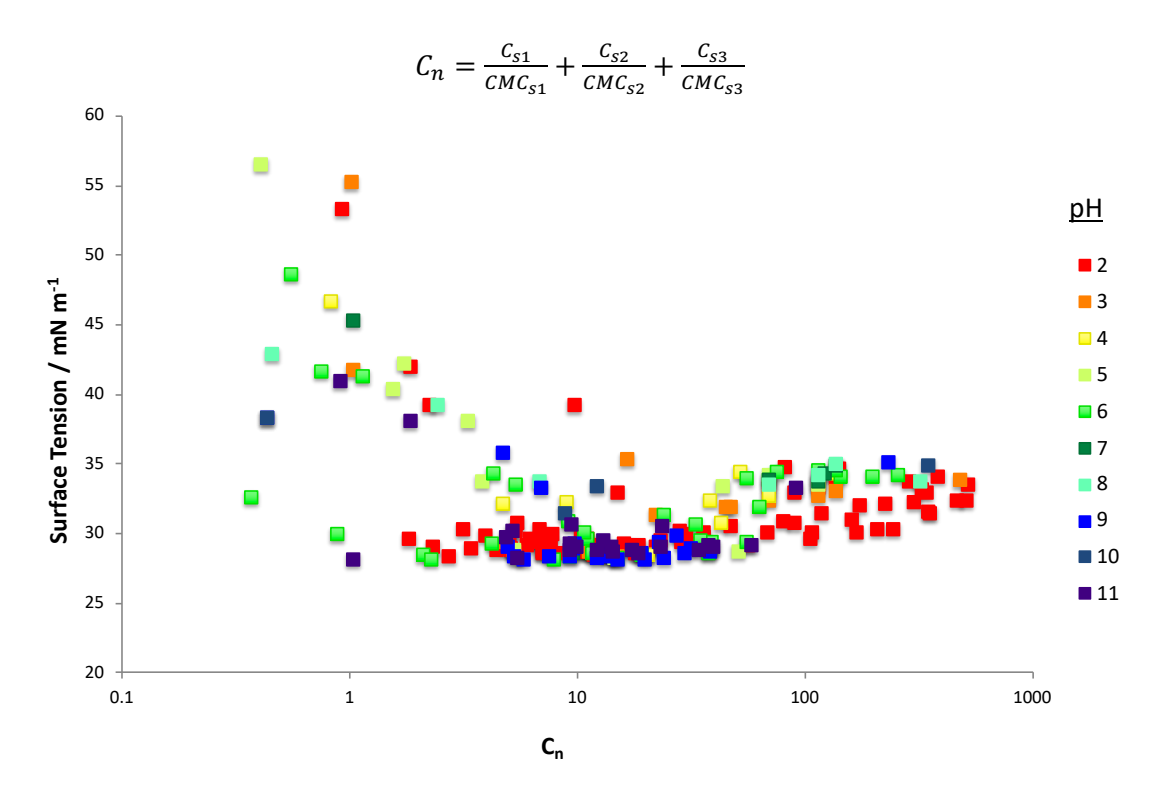


Figure 4.11: Surface tension of aqueous mixtures of LO, BC and DG with respect to total surfactant concentration normalised to the CMC of the individual surfactants. The colours indicate the pH of each surfactant solution.

Figure 4.11 shows the surface tensions of the all the surfactant mixtures measured against the total surfactant concentration normalised to the critical micelle concentration of each surfactant. There is a variation of ~ 5 mN m⁻¹ at $C_n > 100$ showing that the total surfactant concentration does not directly determine surface tension. In general, there is no further decrease above a C_n of 10 which is approximately the concentration of surfactant used in commercial cleaning formulations. There is also the indication that surface tension is independent of pH.

The iterative optimisation process does not conclude of its own accord. The process continuously searches for better results (lower surface tension values in this case). However, there is a point when the values suggested are not lower than those predicted and the values over all the iterations show a long time since the lowest value was found. The optimisation of a ternary mixture is an increase of one parameter in comparison to the binary mixture optimisation and therefore, an increase in the number of experiments required to identify the optimal formulation would be expected. In total, 140 experiments were performed during this optimisation, however, the 43rd experiment showed a low surface tension that was not improved upon in later solutions, shown in Figure 4.12. The number of experiments is much lower than would be expected from trial-and-error testing

(in which the optimum may not be found).¹⁰ In addition, this number is an improvement over the number of runs required to optimise a formulation with regards to five parameters using a full factorial or Box-Behnken experimental design, which would be 52 and 46 respectively.¹⁸ Although this method has many advantages, there are a few limitations that must be considered. First, is the inability to make predictions in the cases of antagonistic surfactant mixtures that cause precipitation, i.e. if a cationic and anionic surfactant were mixed. Second, the optimisation is specific to the selected surfactant so predictions cannot be made about similar surfactant mixtures and the process has to be repeated for each new surfactant formulation. Finally, formulators are able to learn and run a full factorial or Box-Behnken experimental design, however, in contrast, to set up a Bayesian optimisation would require a highly trained computer scientist.

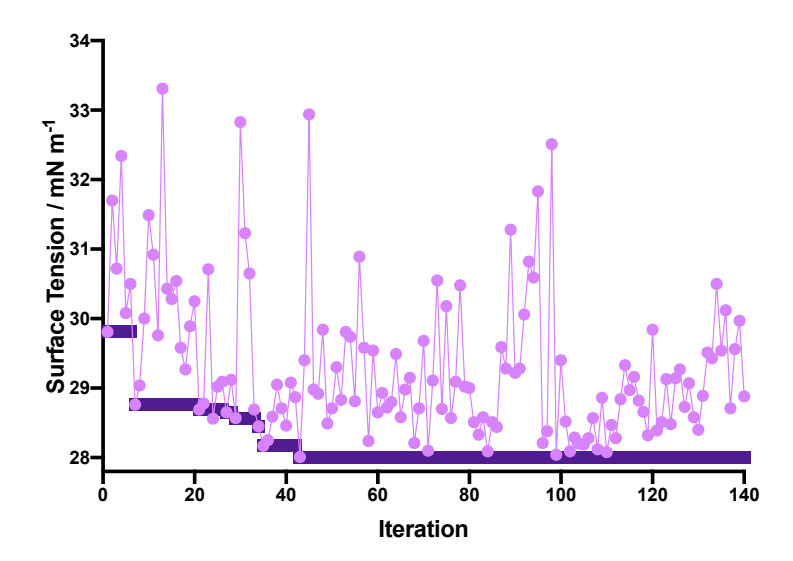


Figure 4.12: Surface tension through the optimisation process of an aqueous ternary mixture of LO, BC and DG.

The lowest surface tension at each iteration is shown by the purple line and the surface tension measured at that iteration is shown by a pink circle. No further improvement was seen after 43 iterations indicating the optimum had been identified.

4.7 Conclusions

The surface tension of binary and ternary surfactant mixtures was minimised using Bayesian Optimisation, reducing the number of required experiments compared to the use of a factorial or matrix method. In the optimised binary mixture of LO and BC, the concentration of surfactants was lower than their individual CMCs, $0.7~\rm CMC^{-1}$ of LO and $0.188~\rm CMC^{-1}$ of BC, and the surface tension was lower than either surfactant's minimum, $29.89 \pm 0.07~\rm mN~m^{-1}$. Another binary mixture was optimised, LO and DG, and the concentration of the surfactants in the optimised was higher than their CMC, $137.34~\rm CMC^{-1}$ and $25.5~\rm CMC^{-1}$, and the minimum is surface was $29.54 \pm 0.03~\rm mN~m^{-1}$. In the case of LO and BC, pH did not have an effect. In contrast, a lower pH leads to a lower surface tension in the mixture of LO and DG.

For the optimisation of a ternary mixture of surfactants, low surface tensions were found across the pH range and there was a tendency towards higher decyl glucoside concentrations to obtain lower surface tensions. In the system with the lowest surface tension, the value of surface tension was lower than both the surfactants alone and the optimised binary mixtures, 28.04 ± 0.20 mN m⁻¹, with concentrations of surfactants being 1.4 CMC⁻¹ of LO, 0.582 CMC⁻¹ of BC, 0.338 CMC⁻¹ of DG. This is firstly interesting as it suggests that the critical micelle concentration of the mixture is at a much lower concentration than any surfactant alone. Hard surface cleaning formulations have total surfactant concentrations typically in the range of 1 to 5 w/w%, whereas the optimised surfactant solutions here have less than 0.2 w/w%. If less surfactant was used in these formulated products, this could reduce the cost of production. However, this assumes that the surface tension is related to the cleaning efficacy which will be discussed in Chapters 5 and 6.

4.8 References

- 1. Khan, A. & Marques, E. F. Synergism and polymorphism in mixed surfactant systems. *Curr. Opin. Colloid Interface Sci.* **4**, 402–410 (1999).
- 2. Rosen, M. J. & Kunjappu, J. T. *Surfactants and Interfacial Phenomena*. A Wiley-Interscience publication (Wiley, 2012).
- 3. Hines, J. D. Theoretical aspects of micellisation in surfactant mixtures. *Current Opinion in Colloid and Interface Science* **6**, 350–356 (2001).
- 4. Shiloach, A. & Blankschtein, D. Prediction of Critical Micelle Concentrations of Nonideal Ternary Surfactant Mixtures. *Langmuir* **14**, 4105–4114 (1998).
- 5. Coret, J., Shiloach, A., Berger, P. & Blankschtein, D. Critical micelle concentrations of ternary surfactant mixtures: Theoretical prediction with user-friendly computer programs and experimental design analysis. *J. Surfactants Deterg.* **2**, 51–58 (1999).
- 6. Hines, J. D., Thomas, R. K., Garrett, P. R., Rennie, G. K. & Penfold, J. A Study of the Interactions in a Ternary Surfactant System in Micelles and Adsorbed Layers. *J. Phys. Chem. B* **102**, 9708–9713 (2002).
- 7. Omidbakhsh, N., Duever, T. A., Elkamel, A. & Reilly, P. M. A Systematic Computer-Aided Product Design and Development Procedure: Case of Disinfectant Formulations. *Ind. Eng. Chem. Res.* **51**, 14925–14934 (2012).
- 8. Jurado Alameda, E., Bravo Rodriguez, V., Bailón Moreno, R., Núñez Olea, J. & Vaz, D. A. Fatty soils removal from hard surfaces in a clean-in-place system. *J. Food Process Eng.* **34**, 1053–1070 (2011).
- 9. Omidbakhsh, N., Duever, T. A., Elkamel, A. & Reilly, P. M. A Bayesian experimental design approach for assessing new product performance: An application to disinfectant formulation. *Can. J. Chem. Eng.* **88**, 88–94 (2010).
- 10. Omidbakhsh, N., Duever, T. A., Elkamel, A. & Reilly, P. M. Systematic Statistical-Based Approach for Product Design: Application to Disinfectant Formulations. *Ind. Eng. Chem. Res.* **49**, 204–209 (2010).
- 11. Xue, D. *et al.* Accelerated search for materials with targeted properties by adaptive design. *Nature Communications* **7**, (2016).
- 12. Shahriari, B., Swersky, K., Wang, Z., Adams, R. P. & De Freitas, N. Taking the human out of the loop: A review of Bayesian optimization. *Proc. IEEE* **104**, 148–175 (2016).
- 13. Ghahramani, Z. Probabilistic machine learning and artificial intelligence. *Nature* **521**, 452–459 (2015).
- 14. Nandni, D. & Mahajan, R. K. Micellar and interfacial behavior of cationic benzalkonium chloride and nonionic polyoxyethylene alkyl ether based mixed surfactant systems. *J. Surfactants Deterg.* **16**, 587–599 (2013).

- 15. Flick, E. W. *Advanced Cleaning Product Formulations: Volume 3.* (Noyes Publications, 1996).
- 16. Maeda, H. *et al.* Effects of ionization on the critical micelle concentration and the surface excess of dodecyldimethylamine oxide in salt solutions. *J. Colloid Interface Sci.* (1995).
- 17. Schellmann, K., Preisig, N., Claesson, P. & Stubenrauch, C. Effects of protonation on foaming properties of dodecyldimethylamine oxide solutions: A pH-study. *Soft Matter* (2015).
- 18. NIST/Sematech. e-Handbook of Statistical Methods. (2012).

5. Optimisation of soil removal

In Chapter 4, optimization of a surfactant formulation with regards to surface tension was performed. However, surface tension alone does not describe how a soil is removed from a surface and a test for soil removal was sought, and later optimised.

5.1 Soil removal tests used in academic and industrial research

In the development of effective cleaning products, it is important to be able to quantify soil removal. A number of methods have been used previously to measure the ability of detergents to remove soil from a hard surface, for many different types of soils^{1–3} and surfaces^{4–6}. The first examples used radioactively labelled fatty acids to model soils.^{1,7} These soils were applied to laminate disks by a pellet press before immersion and rotation in the cleaning solution to be tested. Aliquots of the cleaning bath were removed periodically, and the radiolabelled fatty acid concentration was measured by a liquid scintillation counter to indicate the amount of soil removed from the surface. An alternative test using a similar system was performed by Kabin² but instead used abietic acid as the model soil. The concentration of abietic acid in the washing solution could be measured using a UV detector.⁸ Subsequently, other tests have been developed for different cleaning applications e.g. dishwashing, sprays, sponges.

A method to test a hard surface cleaning solution was developed in which a soiled panel was rotated between two nozzles spraying surfactant solutions. These panels were then rinsed and dried and the soil removal was determined gravimetrically. To analyse the detersive capability of mechanical cleaning systems, such as floor washing machines and clean-in-place systems, a method called bath-substrate-flow was developed. In this case, the soil is not statically immersed in the cleaning solution; instead, there is cyclic and continuous flow of the cleaning solution over the glass beads covered in the soil. The soil used to coat the beads was a mixture of oleic, palmitic and stearic acids and the acidity index of samples of the washing bath was determined by acid-base titration to indicate soil removal. A schematic of the system is given in figure 5.1.

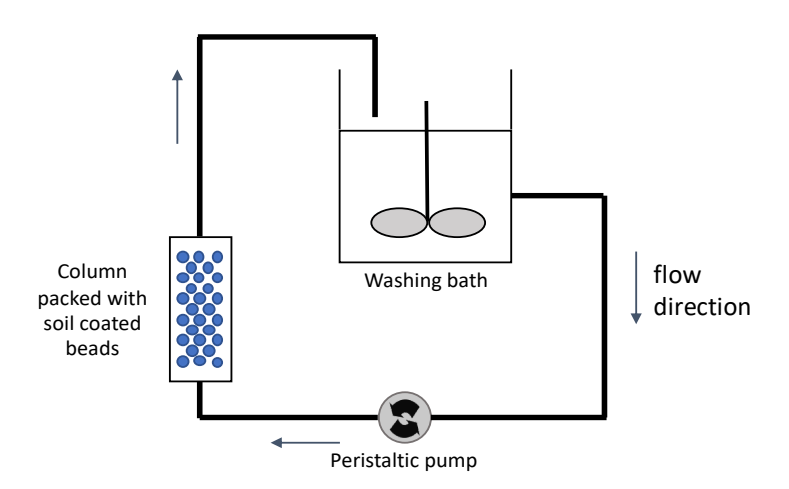


Figure 5.1: A schematic of the bath-substrate-flow system as detailed by Almeda. A peristaltic pump flows a cleaning solution from a washing bath over soil-coated beads packed into a column. The soil removal is measured by calculating the amount of fatty acids in the washing bath, using acid-base titration. ¹⁰

Flow cells have been used to assess the cleaning efficacy of solutions on different polymer coatings. The first example of this was a laminar flow cell where a detergent was flowed between a top layer of glass and a bottom layer of soiled surface. In the second case, a radial flow cell was used, consisting of two parallel disks with a narrow spacing in between. Cleaning fluid was pumped through the centre of one disk and flowed radially outwards between a narrow gap in between the two disks. The shear stress at the surface decreases from the centre to the edge of the disk so the test evaluated the wall shear stress required for cleaning, Figure 5.2.⁵

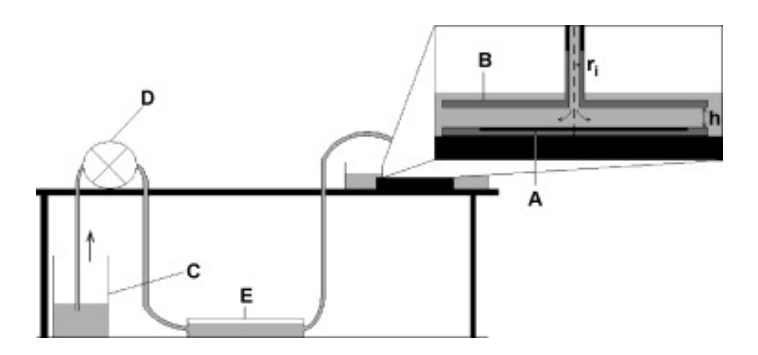


Figure 5.2: A schematic of the radial-flow cell reproduced from Detry *et al.*⁵ where: A is the sample, B is the radial-flow cell, C is the cleaning fluid tank, D is the pump, E is the glass container, ri is the inlet radius and h is the disk spacing.

In 2014, Dunstan and Fletcher investigated the removal of triacylglyceride (TAG) films from surfaces using a variety of surfactants.¹¹ TAG films are formed during food preparation and are made difficult to remove due to the hydrolysis, oxidation and polymerisation reactions

that occur during cooking at high temperatures. Their TAG removal test does not require calibration against a known cleaning formulation and the TAG mixture is a ternary mixture of vegetable oil, lard and vegetable shortening. The test involves the production of a thermally TAG film which is immersed in a stirred surfactant solution. The soil removal over time is measured quantitatively by mass loss, figure 5.3.

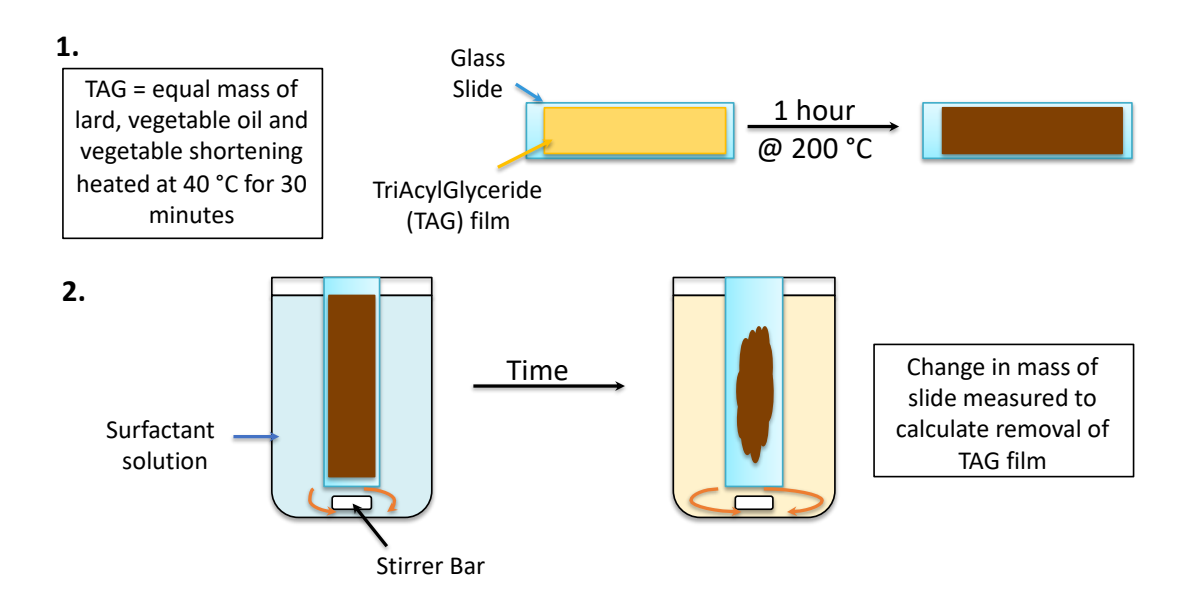


Figure 5.3: Removal of a TAG film by surfactant solutions as described by Dunstan and Flecther.¹¹ 1) A TAG mixture of 1/3 lard, 1/3 vegetable oil and 1/3 vegetable shortening is prepared by heating at 40 °C for 30 minutes with stirring. TAG is pipetted onto a glass slide and baked at 200 °C for one hour to from a tenacious greasy soil film. 2) The soiled slide is placed in the surfactant solution of interest and the mass of the soil is recorded over time to determine mass loss.

The tests described so far have been developed by scientists and engineers in academic research labs. In industry, however, companies either use the standard test method, such as an ASTM standard, or develop their own for specific purposes. A wet scrub abrasion test is one such industry standard used to test the effectiveness of hard surface cleaner formulations, figure 5.4. In the test, a mechanical arm passes a sponge soaked in the test solution over a soiled surface a pre-set number of times, determined by calibration with a standard reference cleaning solution. The surface is a ceramic tile coated in a model soil mixture which aims to mimic the dirt that may be found on a typical dirty kitchen surface. Carbon black aids quantification of the soil removed as the colour change caused by the cleaning process. Initially, the soiled tile is black. With the application of a cleaning solution, the soil, and therefore carbon black, is removed causing a decrease in the black colour until full soil removal, where the tile is white.

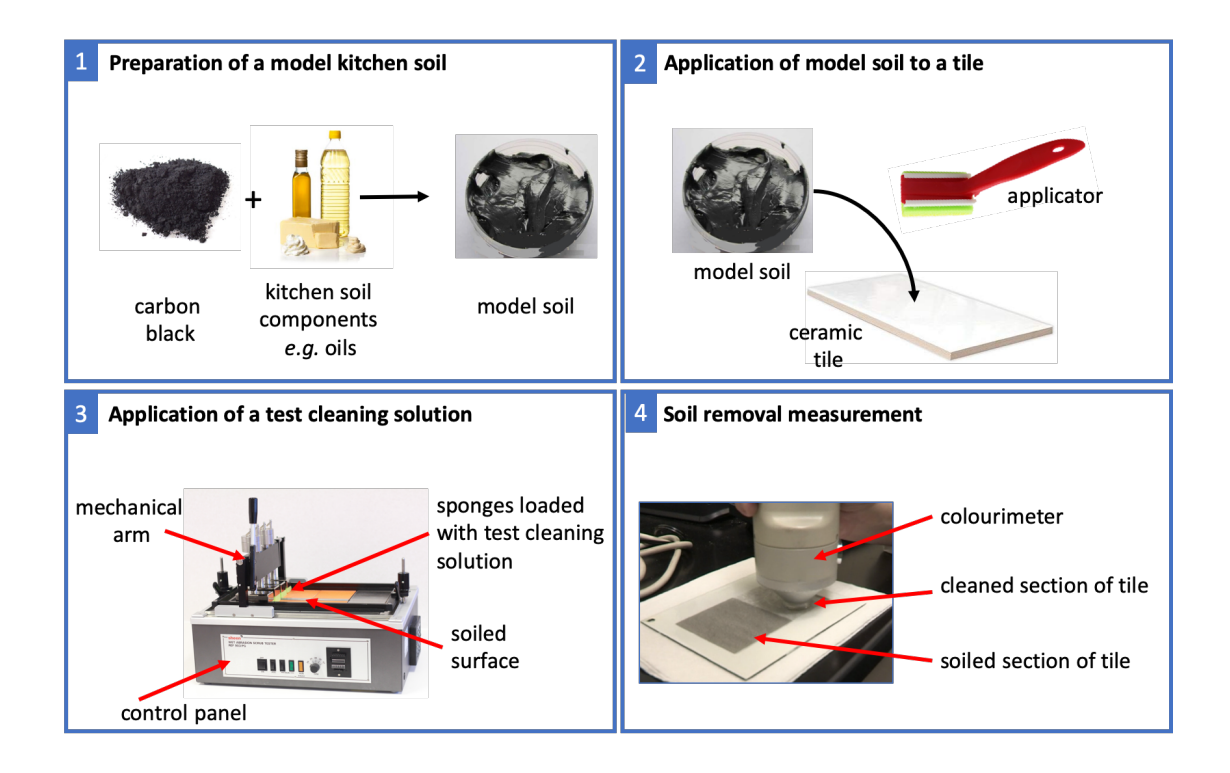


Figure 5.4: Schematic of the standard test method for measuring cleaning performance as detailed in ASTM.¹³

1) The preparation of a soil mixture mimicking that found in a kitchen, with addition of carbon black to aid measurement of soil loss by colour change. 2) The model soil is applied a ceramic tile in an even layer using an applicator. 3) The test solution is loaded onto a sponge which is moved across the surface of the soiled tile by a mechanical arm. 4) The soil removal is measured by a colourimeter to compare the colour of the "cleaned' vs 'soiled' sections. Image of the washability tester reproduced from https://www.enzymeinnovation.com/oils-fats/ and the model soil from https://www.indiamart.com/.

This test was reproduced in our lab to assess its feasibility for use in an optimisation experiment. Initially, 20 random solutions having different amounts of surfactant were selected to check whether the test was calibrated correctly, *i.e.* the solutions varied within the range 0 to 100% and did remove none or all of the soil. The same batch of 20 experiments was then repeated to check repetition accuracy.

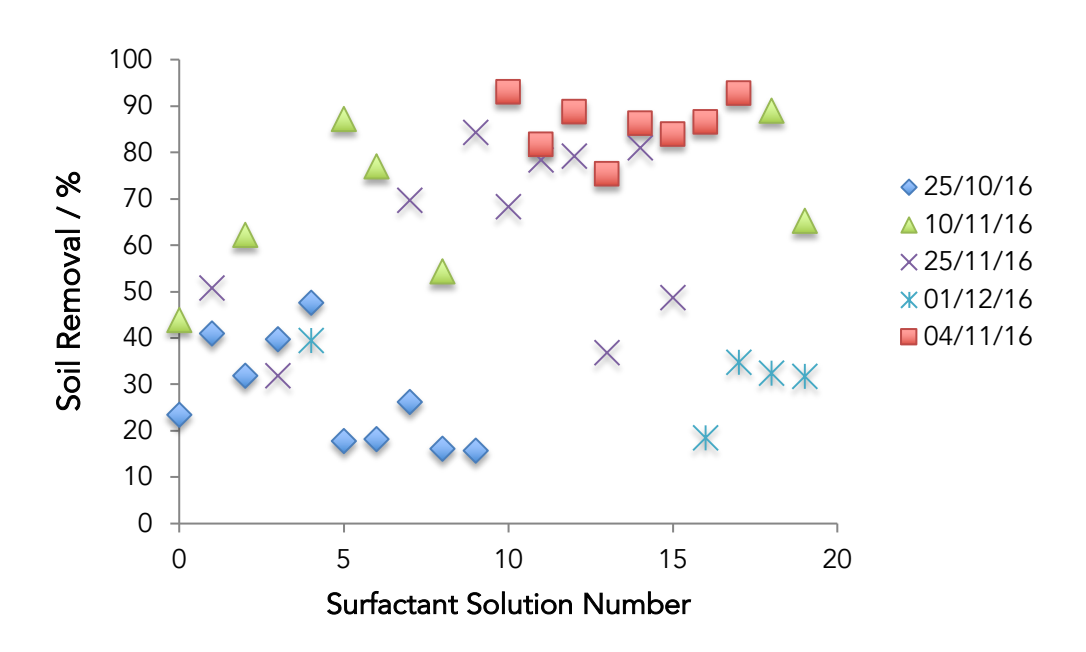


Figure 5.5: Mass of the model soil removed using the scrub abrasion test for 20 randomised test solutions showing the variation in the results obtained between batches on different dates (given in the key). Full removal is 100% and none removal is 0%.

The solution numbers are arbitrary, each is assigned to a combination of the surfactants LO and BC at a specified concentration and pH. Therefore, the soil removal for each numbered surfactant solution should be the same, within experimental error. Surprisingly, this is not the case; a high degree of variability is observed. For example, experiment 16 was measured on two occasions. Initially, it appeared to have excellent cleaning properties: 86.6% of the soil was removed. However, when the same (fresh) solution was measured a month later, the soil removal was much lower at 18.5%. The large differences in the results of this test are likely to be related to the response of the soil mixture to fluctuations in atmospheric humidity and temperature throughout the thermal treatment, storage and cleaning process. It is possible that the soil itself does not form a uniform film across the surface of the tile leading to the large standard deviation in the colour measurements measured across the area of the tile. An explanation for the irregularity in the film may be the soil mixture not being homogeneous as it is complex and contains multiple components, including some of which are mixtures themselves. For example, one of the components is egg albumin, which is made up of a variety of proteins and carbohydrates dissolved in water. Many months were spent trying to identify the reasons behind this variability but without success, so this industry test was abandoned.

To extend the Bayesian optimisation technique to optimize soil removal, a different test must be developed. Whilst industry require a test to assess the efficacy of formulations on a soil that closely mimics one seen by consumers, the priority in this study is a reproducible model soil.

5.2 Alternative Soil Removal Test

As the first soil removal test was not repeatable, the Fletcher and Dunstan method was tried. There are a number of differences in comparison to the industry standard method. First, the soil used was much simpler: a mix of lard, vegetable shortening or vegetable oil in equal quantities. Second, the surface to which to soil was applied is a glass slide rather than a ceramic tile. Third, the soil was removed from the surface by placing the soiled slide in a stirred surfactant solution rather than a surfactant loaded sponge on a mechanical arm. Finally, instead of measuring a colour change (as carbon black is not added to the soil), the soil removal was quantified using the change in mass of the soil on the slide after removal from the cleaning solution and drying in a vacuum desiccator.

The cleaning ability of an aqueous solution of 1% SDS was analysed using this method. In accordance with results reported previously, a lag time of approximately 30 minutes was observed before any mass was lost which was due to the time required for the surfactant to penetrate the surface of the TAG film. Following this delay, mass loss occurred as TAG was removed from the slides.

To test the repeatability of Fletcher and Dunstan's method, a preliminary test using 1% SDS solution as the cleaning bath was performed on three different days. From figure 5.6, it can be seen that the final values are comparable: mean mass loss over 24 hours was $11.20 \pm 0.95\%$. This is an improvement on variation in the industry standard test which was on average greater than 30%.

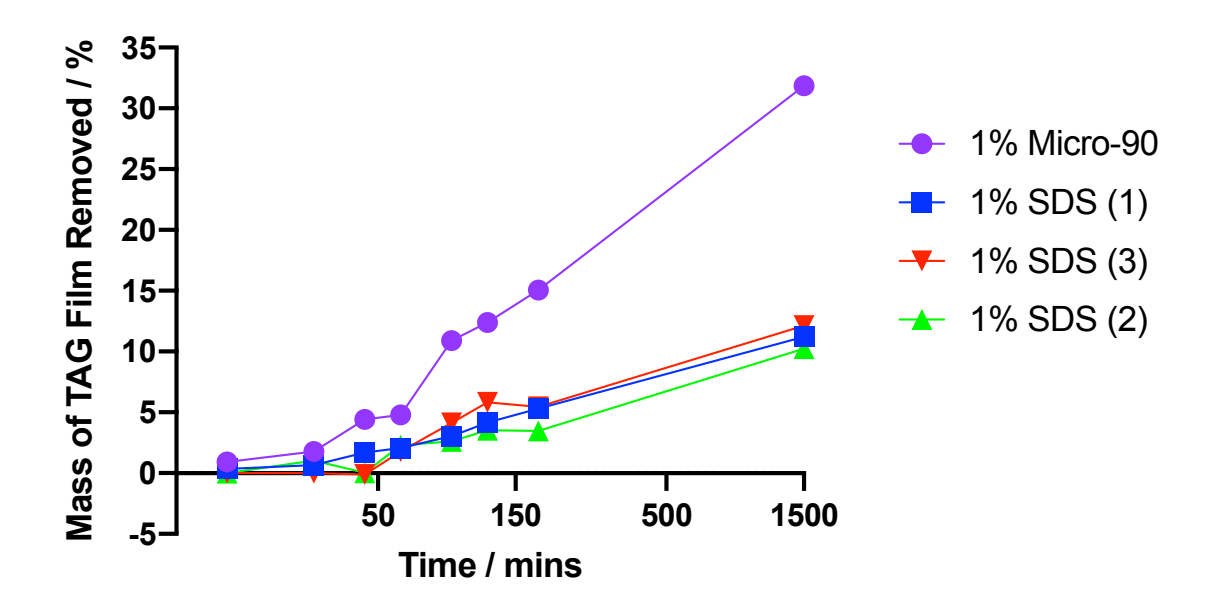


Figure 5.6: Mass of model soil (TAG film) removed from the surface of a glass slide, using the method detailed in Dunstan and Flectcher,¹¹ with time by an aqueous solution of SDS (1 w/w%) and a commercial cleaner,

Micro-90 (1 w/w%).

As this method is more reproducible, a commercially formulated cleaning product, Micro-90, was tested to see if the method could differentiate between cleaners having different soil removal powers. 31.9% of the film by mass was removed by the commercial cleaner over 24 hours. One source of error identified in the test was in the mass loss calculation due to the repetition of the slide removal and drying process. To minimise this, one time point was selected and therefore, subsequent tests were run for 24 hours and the soil removal only measured at that point.

In order to use the TAG removal test to optimise a mixture of surfactants, the measurements need to be both reproducible and repeatable. To obtain repeats of each experiment in the same conditions, the test was run in batches by increasing the number of slides placed in the surfactant solution. As the impact of altering the test in this way was unknown, an investigation into factors affecting the loss of film was performed.

5.3 Soil removal test development

To improve Dunstan and Fletcher's soil removal test for use in this project, the following factors were investigated: slide position, stirring rate, how the soil removal is quantified and the addition of drying oils and additives to the model soil mixture. The majority of the method was the same as described in Dunstan and Fletcher's paper, full details of the method are given in section 2.3.

The ternary solution of 0.012% LO, 0.003% BC and 0.103% DG, with a pH adjusted to 9, was selected for the test optimisation experiments due to its low surface tension of 28.08 mN m⁻¹. This solution was used as it was predicted to have good cleaning properties because low surface tension indicates high surface activity, aiding the removal of soil from a surface.

5.3.1 Slide Position

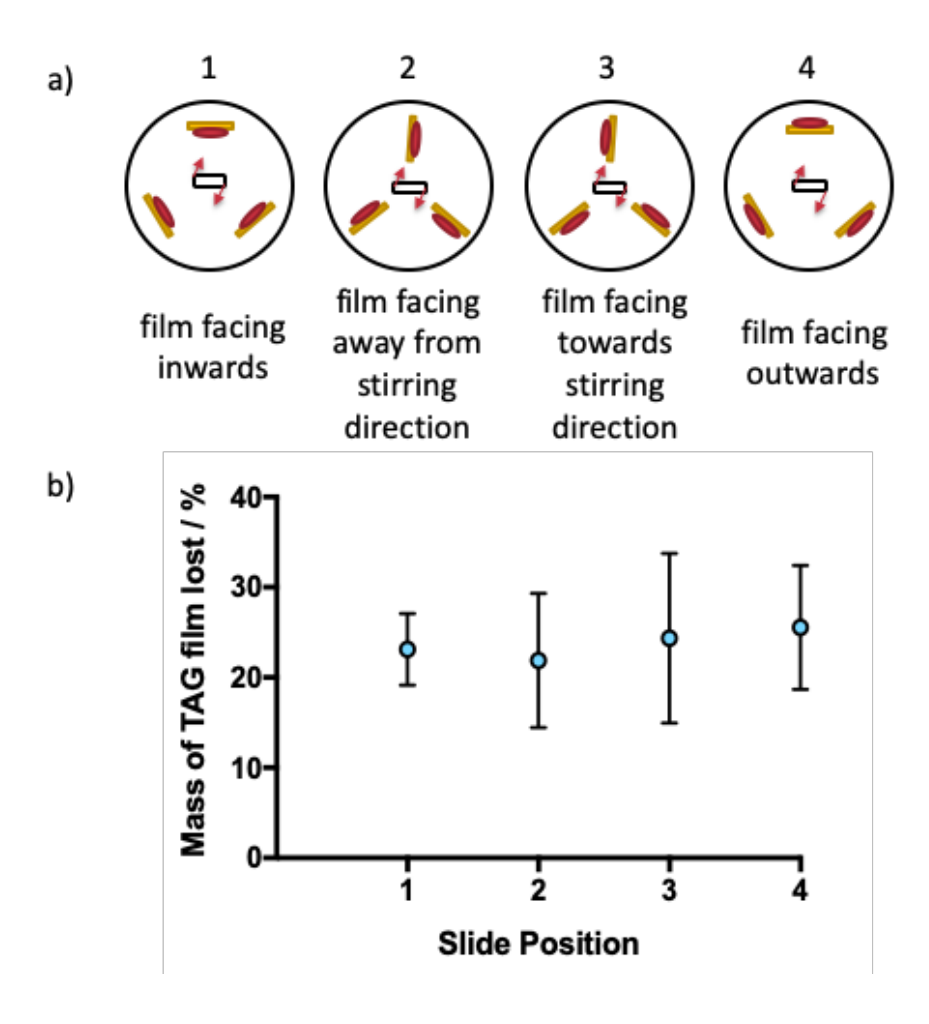


Figure 5.7: a) Four positions of model soil (TAG) coated glass slides in the solution with relation to the stirrer bar and b) is the mass of soil removed in each position: 1) TAG film facing towards the centre of the vessel 2)

TAG film facing away from the direction of stirring 3) TAG film facing towards the direction of stirring 4) TAG film facing outwards.

To discover whether the positioning of the soil on the 3 slides in the cleaning vessel has an impact on soil removal, four positions, where the slides are equidistant from each other, were examined. The direction of flow across the surface of the substrate is different in each position and therefore it was hypothesised that the mass of TAG film removal in each case could differ. Surprisingly, the difference in mean mass loss was actually very small: 3.7%. The lowest mass loss was seen in position 2, 22%, when the slides were facing away from the

direction of stirring whilst the highest mass loss was seen in position 4, 26%, where the films were facing towards the outside of the vessel. As observed in figure 5.7, the variability in the data shown by overlapping error bars indicates the difference in soil removal between all four positions is minimal, in fact within the limits of variability.

For all further tests, the slides were placed facing into the beaker, position 1. This choice was made for two reasons. Firstly, for practicality, there is less chance of damaging the films on the slides whilst placing the slides in this position as there is less chance of collision with the sides of the beaker or the other slides. Secondly, the standard deviation for this position is much lower which could indicate less variability.

5.3.2 Stirring Rate

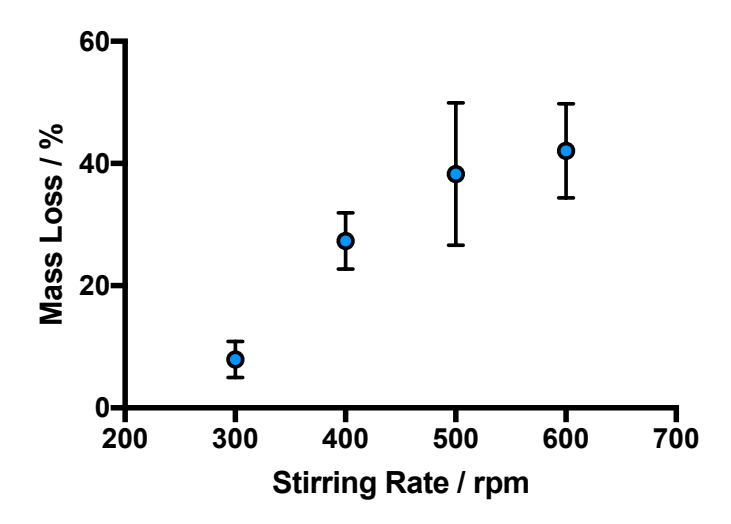


Figure 5.8: The mass loss of TAG from the surface of a glass slide immersed in an aqueous solution of 0.012% LO, 0.003% BC and 0.103% DG, with a pH was adjusted to 9, with increasing rate of rotation of the magnetic stirrer bar placed within the washing bath.

In the Fletcher and Dunstan test, the stirring rate is not specified. To determine whether the amount of agitation affects soil removal, four spin speeds were examined, from 300 rpm, the lowest speed required to get mixing of the full volume of solution to 600 rpm where a vortex is observed. Figure 5.8 clearly shows more TAG film is removed from the surface of the substrate as the stirring rate was increased. As the velocity of the liquid increases, the effective shear rate on the TAG film increases causing the TAG film to be more easily detached. For all experiments, a stirring rate of 500 rpm selected. Above this speed, there is no statistical increase in mass loss and a large vortex in the solution is observed at 600 rpm (which is not present at 500 rpm).

5.3.3 Measuring Film Area for Soil Removal

An alternative method to determine soil removal was considered by measuring the change in film area, rather than mass, was considered. The area of the film removed was calculated by taking photographs of the films before and after being placed in surfactant solution, Figure 2.12. The film removal from the two techniques was compared using solutions from across the surface tension range, figure 5.9.

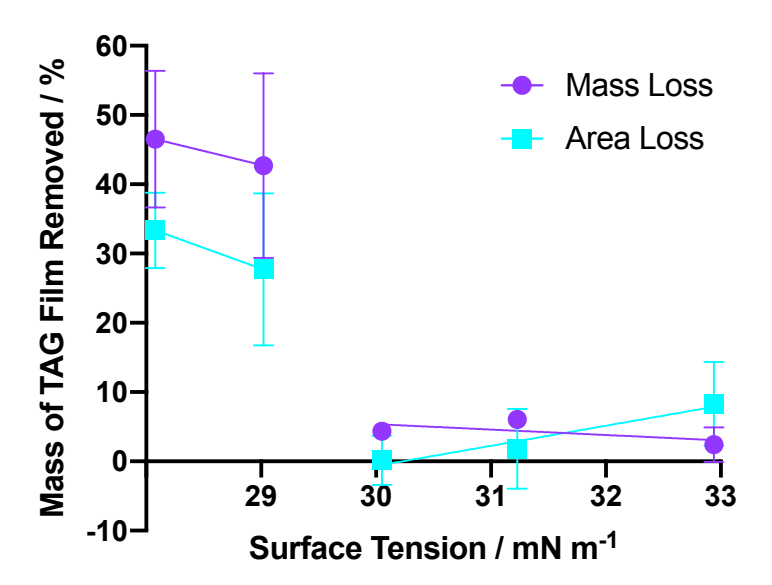


Figure 5.9: Comparison of the measurement of loss of TAG film applied to a glass slide for surfactant solutions with increasing surface tension as determined by mass loss (purple) versus area loss (blue).

As predicted, less film was removed from substrates placed in solutions with higher surface tension. There is much less variability in the results from tests with low film removal. For example, there is a large variability in the soil removal from the solution with a surface tension of 29 mN m $^{-1}$ which was 27.7 \pm 13.1% by area loss vs 42.7 \pm 10.1% by mass loss. As more film is removed, the solutions change colour from colourless to clear. In addition to TAG being solubilised, flakes of TAG film, large enough to be seen by the naked eye, were observed in the surfactant solutions of surface tension below 30 mN m $^{-1}$ corresponding with the greatest film removal ability, figure 5.10.

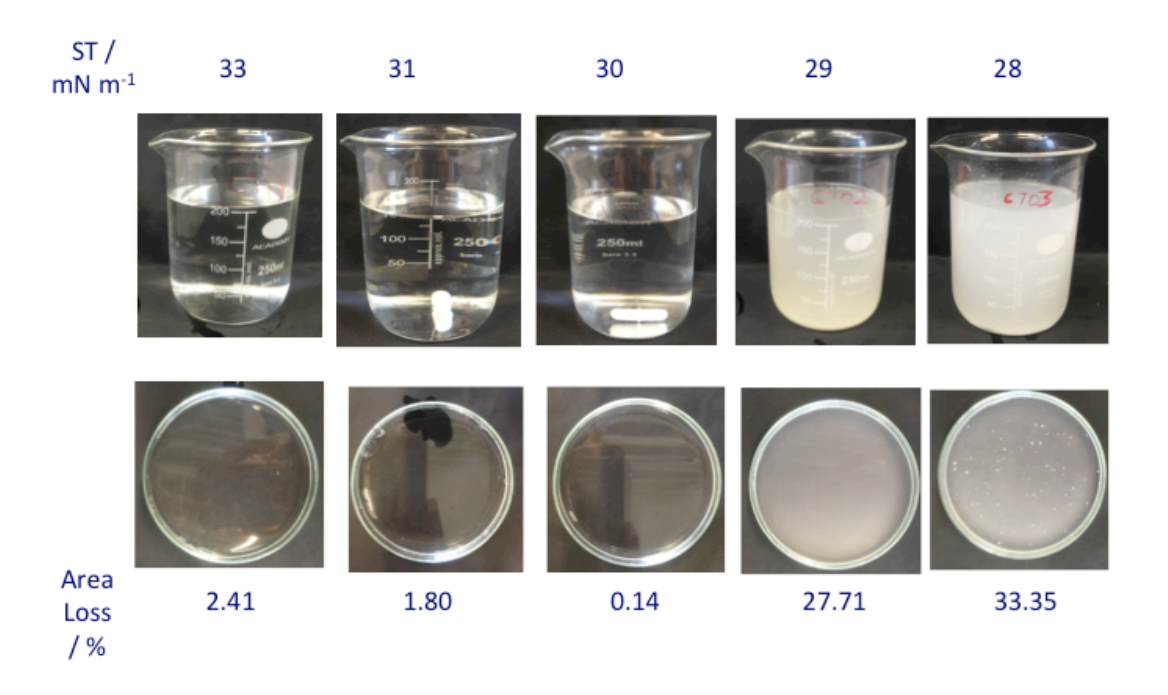


Figure 5.10: Area loss with decreasing surface tension with images taken by an iPhone. The top row of images show a side on view of beakers containing the supernatant from the washing of 3 TAG soiled slides placed in a beaker, stirred at 500 rpm. The bottom row of images show the top down view of a petri dish containing a small quantity of the supernatant. Note the flakes in the two solutions with greatest soil removal.

This study has been unable to demonstrate a clear benefit of using area change over mass loss to measure soil removal. However, it highlighted the drastic increase in soil removal occurring in some solutions where TAG flakes were observed indicating the film breaking off in fragments. To minimise this problem, an investigation of the components of the film to improve film properties was performed whilst collecting both mass and area change data for comparison.

5.3.4 Altering Film Components

As previously discussed, the removal of the TAG film in chunks increases the inconsistency of the test. One possible reason for removal of film flakes could be uneven auto-oxidative crosslinking of the unsaturated chains in the triglycerides. Auto-oxidative crosslinking occurs in unsaturated fatty acids when oxygen, from the air, reacts with the C-H next to a double bond to form a hydroperoxide group which can further react with other fatty acid chains to form crosslinks. If, during thermal treatment of the films, the crosslinking was uneven throughout the film, the result would be a final film with some areas more susceptible to detachment by surfactant penetration and solution flow than others.

Two methods commonly used in coatings and paint technologies to form uniform surfaces^{14–16} were considered to improve the homogeneity of the TAG films. First, the addition of a metal drier to the TAG mixture to provoke acceleration of reactions involved in oxidation.¹⁶ Secondly, replacing the vegetable oil, a semi-drying oil, with a drying oil. A drying oil contains a higher number of double bonds, which auto-oxidise in air causing film hardening.¹⁵

5.3.4.1 Driers

Driers are metal salts soluble in organic acids (i.e. fatty acids). The drier used was cobalt 2-ethylhexanoate, which is an active drier so can occur in multiple oxidation states and can undergo redox reactions and therefore, aid catalysis of reactions that occur in the autoxidation process, including peroxide decomposition.¹⁷ Cobalt driers have been shown to provoke the acceleration of all reactions involved in oxidation and the formation of a surface solid film.¹⁴ An additional benefit of cobalt driers is they can be used with both drying and semi - drying oils.

To dissolve the drier to the TAG mixture, it was first heated to its molten state and subsequently, a cobalt 2-ethylhexanoate drier, 0.1%, by mass, was added, as previous work by Mallégol *et al.* showed drier loadings of 0.1% were enough to catalyse the auto-oxidation reaction in air. Once dissolved, films of the mixture were prepared before thermal treatment at 200 °C. As can be seen in figure 5.11, with the addition of cobalt drier, the resulting film was brown whereas the original was yellow.



Figure 5.11: The TAG soils prepared under 3 different conditions: without drier and baked for 1 hour at 200 °C, with 0.1% cobalt 2-ethylhexanoate drier at 100 °C and 200 °C. The images on the left were taken after baking and before placing in the surfactant solution. The images on the right were taken after placing in a stirred surfactant solution (0.012% LO, 0.003% BC and 0.103% DG, with a pH was adjusted to 9) for 24 hours.

To investigate the effect of differing thermal treatment on the ease of film removal, films were prepared and subsequently heated for one hour at 100 and 200 °C, figure 5.11. Two problems were found with the resulting films. Firstly, at both temperature the films were not uniform. One possible explanation for this could be that the addition of the cobalt drier caused an increased speed of film drying leading to the dewetting from the surface. The second problem observed was the high resistance to removal of the film baked at 200 °C for 1 hour; only 20% was removed. In previous study by Dunstan and Fletcher, 11 with heating over longer timescales at lower temperatures, their TAG mixture (without drier) showed a reduction in unsaturation, indicating autoxidation had taken place. Therefore, to target slower film drying, another film was prepared with 0.1% drier and dried at 20 °C with a longer baking time of 2 hours. However, when drier was added to the TAG mixture, autoxidation did not take place at low temperatures, shown by a high level of soil removal, 57.05% by mass. Taken in combination, these results show that the addition of drier was not beneficial as the resulting films dry even less uniformly than without drier and are harder to remove.

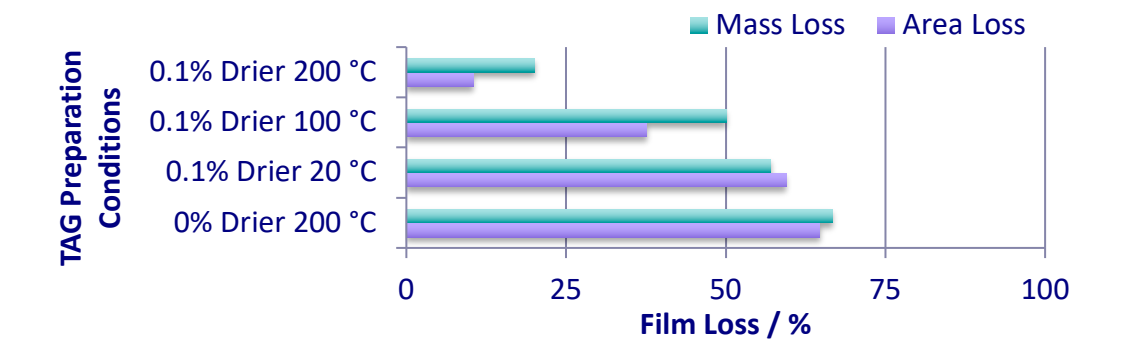


Figure 5.12: The mass and area loss of the TAG film, with addition of drier, baked at different temperatures in comparison with the TAG prepared without any drier and baked at 200 °C.

5.3.4.2 Drying Oils

The next section of the study concerns the use of drying oils to improve film uniformity. A drying oil contains a high proportion of double bonds which auto-oxidize in air causing film hardening. In the original TAG soil mixture, the oil used is rapeseed (canola) oil, labelled vegetable oil, which is a semi-drying oil. Semi-drying oils partially harden when exposed to air. A comparison between the chain lengths and unsaturation in the fatty acids of rapeseed oil and linseed oil, one commonly used example of a drying oil, is made in table 5.1. It can be seen that in linseed oil there is more unsaturation with the major fatty acids being linoleic and linolenic which have C18 chains with 2 or 3 double bonds, respectively. Contrastingly, in rapeseed oil the main component is oleic acid with only one double bond in the C18 chain.

Table 5.1: The difference in fatty composition between linseed oil and rapeseed oil, where C is the number is carbons in relation to D, the number of double bonds. 18

Acid Type	C:D	Linseed Oil Content/ %	Rapeseed Oil Content / %
Palmitic	16:0	5.1	4.3
Stearic	18:0	4.3	2.0
Arachidic	20:0	0.1	0.8
Behenic	22:0	-	0.4
Oleic	18:1	15.8	62.5
Linoleic	18:2	16.5	19.6
Linolenic	18:3	58.3	10

To see whether the increased unsaturation leading to film hardness will improve the homogeneity of the film, the vegetable oil (rapeseed) in the TAG mixture was replaced with linseed oil, at the same weight percent (33.3%). Figure 5.13 shows a number of differences in

images of the films after baking at a range of temperatures, room temperature, 100 and 200 °C. There is a difference in the yellow colour within the same sample and between samples due to differences in thickness of the film and the colour change to darker yellow that occurs during the autooxidation reaction. First, the film dried at room temperature for 72 hours (Figure 5.13 b)) did not show the colour change to a darker yellow indicative of the autoxidation reactions occurring upon drying and was gel-like in consistency. This indicated incomplete drying and hence, this sample was not used in the subsequent cleaning test. Secondly, the film dried at 100 °C appeared to dewet leading to reduction in film area and there was no darkening of the films which may suggest the double bonds in the film were unreacted. Finally, as observed in figure 5.13, the film dried at 200 °C did show the desired characteristic colour change without any apparent dewetting.

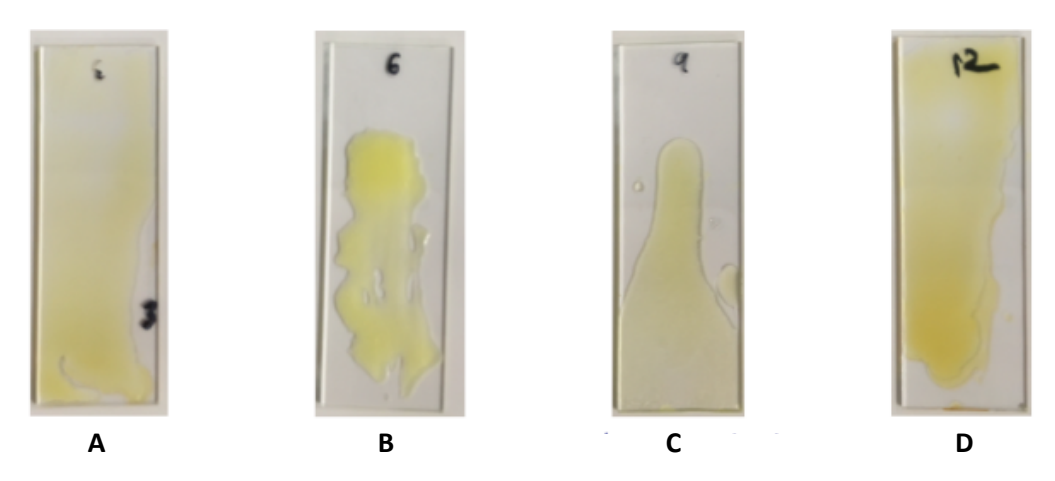


Figure 5.13: The effect of replacing vegetable oil with linseed oil, a drying oil, on the baking of the TAG soil, under different baking conditions. A) The control with a TAG soil of 33.3% vegetable oil, 33.3% vegetable shortening and 33.3% lard baked at 200 °C for 1 hour, B) the 33.3% vegetable oil was replaced with linseed oil and cured at room temperature for 72 hours, C) the 33.3% vegetable oil was replaced with linseed oil and baked at 100 °C for 1 hour, D) the 33.3% vegetable oil was replaced with linseed oil and baked at 200 °C for 1 hour. Images taken with an iPhone.

To compare the soil removal at the 100 °C and 200 °C, the thermally treated TAG films were analysed using the test described previously (using a surfactant mixture of: 0.012% LO, 0.003% BC and 0.103% DG adjusted to pH 9). As can be seen in the figure 5.14, the TAG film on the slide baked at 100 °C was almost entirely removed, 96.3% loss by mass, supporting the theory that the double bond in the chains were unreacted. In contrast, there was minimal film removal from the slide treated at 200 °C: 2.34% by mass and 3.72% by area.

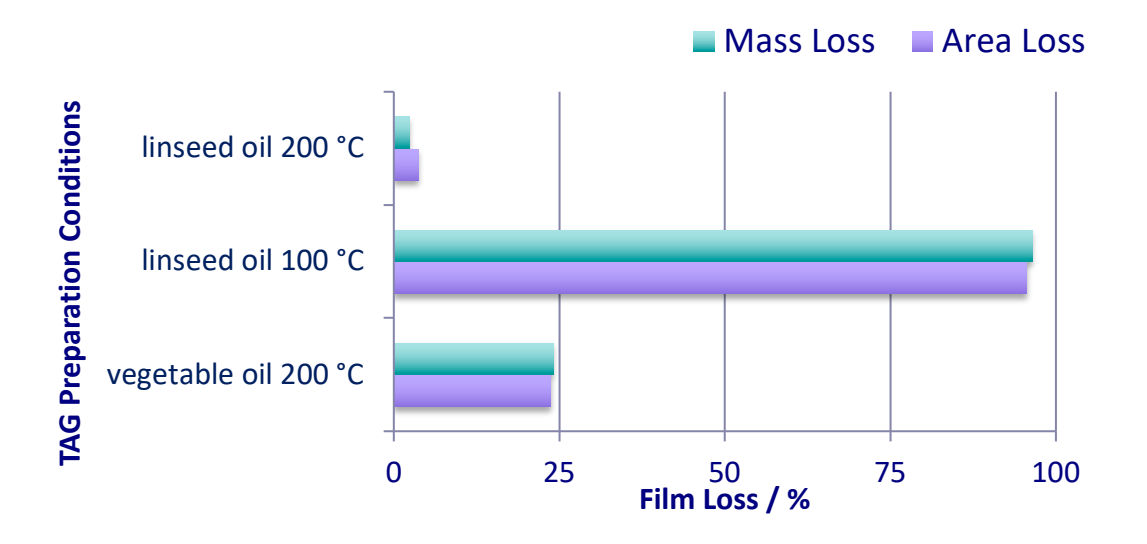


Figure 5.14: The mass and area loss of the TAG film, with replacement of vegetable oil with linseed oil, a drying oil, baked at 100 °C and 200 °C for 1 hour, in comparison with the original TAG film containing vegetable oil prepared and baked at 200 °C for 1 hour.

These results were supported by observations of the surfactant solutions (supernatant) after the 24-hour soil removal test had been performed and the slides were removed. In the sample treated at 100 °C, there were white particles and oil droplets observed in the solution highlighted in the magnified image in figure 5.15 D). The presence of non-dried oil in the washing solution may be due to skinning which is caused by the upper surface of a film drying without the drying extending through the film below. In comparison, the cleaning solution of the sample containing linseed oil baked at 200 °C, is colourless which further indicates that no film was removed.

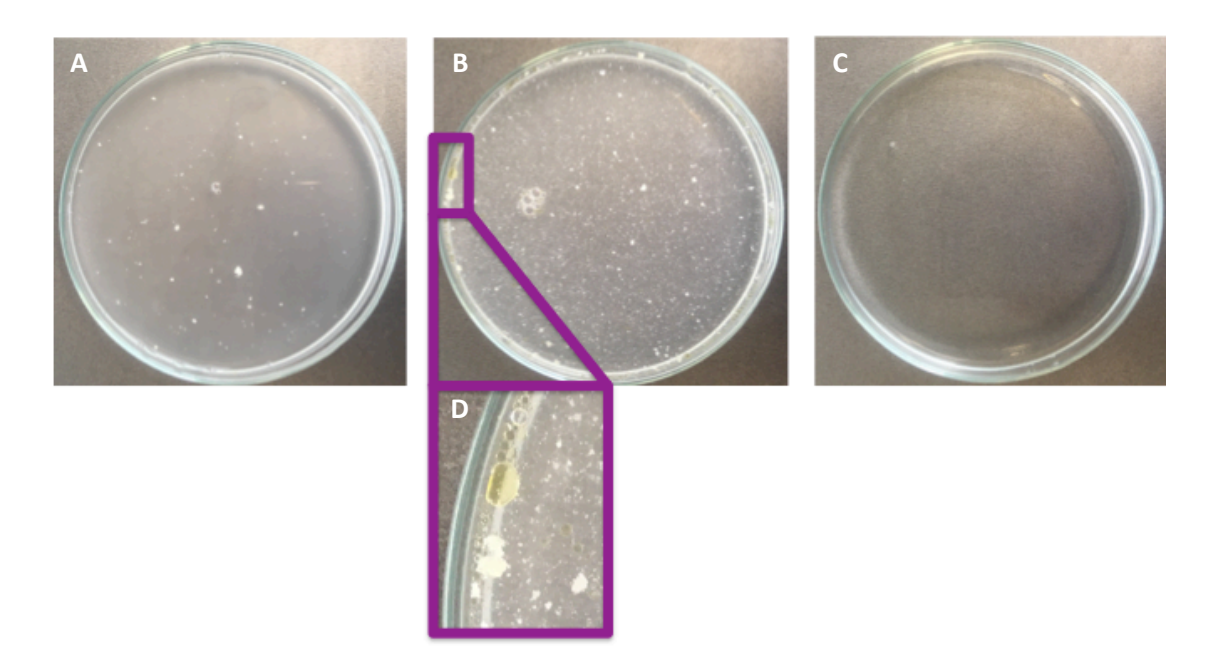


Figure 5.15: Final appearance of the surfactant solutions after they were used in the soil removal tests where A) was the original TAG mixture containing 33.3% vegetable oil, 33.3% vegetable shortening and 33.3% lard baked at 200 °C for 1 hour, B) was a TAG mixture where the 33.3% vegetable oil was replaced with linseed oil and baked at 100 °C for 1 hour, C) was a TAG mixture where the 33.3% vegetable oil was replaced with linseed oil and baked at 200 °C and D) is a magnified section of image B showing the presence of oil droplets and white particles.

To identify the optimal amount of linseed oil to add to the TAG mixture, the vegetable oil fraction of the soil, 33.3% of the mixture, was replaced with various ratios of linseed oil. The ratio of linseed to the total vegetable oil content was defined as ϕ_{lin} = [linseed oil]/([linseed oil] + [rapeseed oil]) and the ratios investigated were: ϕ_{lin} = 0, ϕ_{lin} = 0.25, and ϕ_{lin} = 0.5. Figure 5.16 compares the experimental data for the soil removal using soils prepared with addition of various proportions of linseed oil. As the quantity of rapeseed oil in the soil is increased, a greater mass of soil is removed during the cleaning test. Interestingly, there is little loss of area, in comparison to mass loss, in the samples with rapeseed oil added which suggests that the mass is lost from the full area of the film. In addition, the flakes of film seen previously were not observed in the surfactant solution post-test indicating homogeneous crosslinking across the film and a reduction in film lift-off by surfactant solution. ϕ_{lin} = 0.25 was chosen for subsequent experiments as it had the highest mass loss and lowest area loss, and there were no white flakes or oil droplets observed in the supernatant.

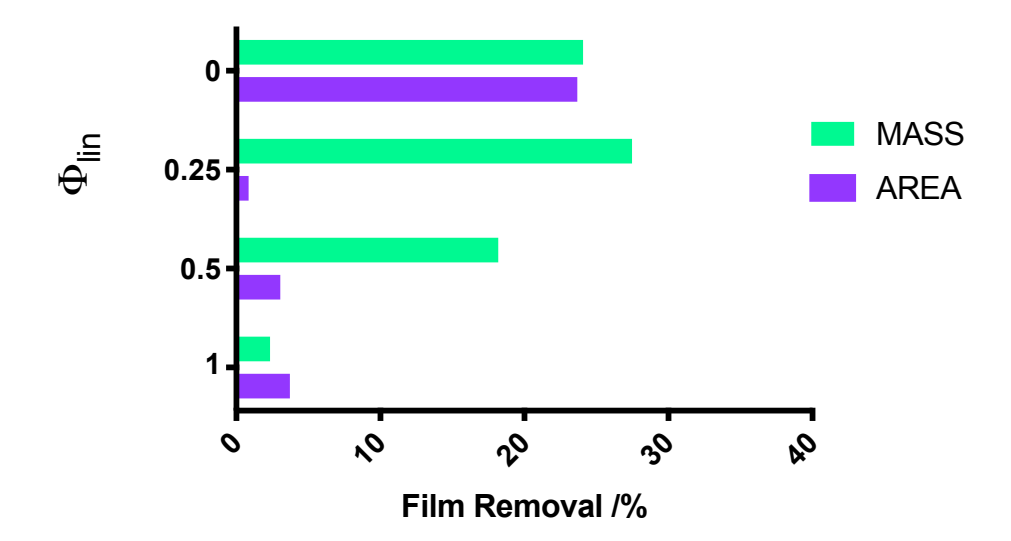


Figure 5.16: The removal of a TAG films, with varying amounts of linseed and rapeseed oil, in a surfactant solution (0.012% LO, 0.003% BC and 0.103% DG, with a pH was adjusted to 9) by mass and area.

To investigate whether the addition of linseed oil has slowed down the removal process, the removal of the TAG mixture of ϕ_{lin} = 0.25, was studied over time. The slides were placed in a surfactant solution and removed at regular intervals, subsequently dried in a desiccator, and the mass and area change measured. Figure 5.16 shows the loss of area was gradual showing an approximately linear trend: linear regression gave an R² value of 0.987. The rate of mass loss was greater over the first 24 - 48 hours, then became more gradual.

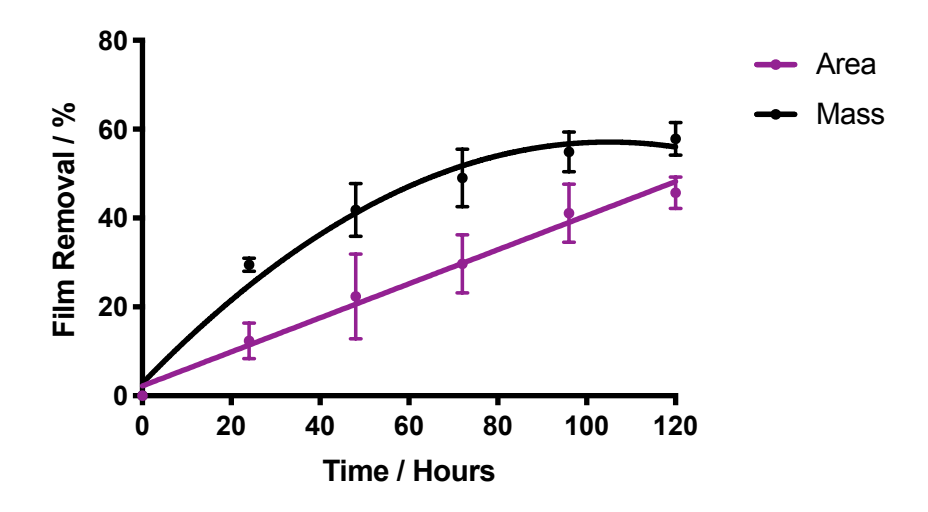


Figure 5.16: The removal of a TAG film of ϕ_{lin} = 0.25, in a surfactant solution (0.012% LO, 0.003% BC and 0.103% DG, with a pH was adjusted to 9) over 120 hours.

5.3.5 Control Experiment

The TAG removal by deionised water adjusted to various pH levels was studied as a control experiment. The unadjusted deionised water, used for previous studies, had a slightly acidic pH, 5.3, indicating absorption of atmospheric carbon dioxide and showed very low soil removal, 0.47%. Deionised water was adjusted to a range of pH's by addition of hydrochloric acid or sodium hydroxide and these solutions were used in the TAG removal test using the TAG soil with φ_{lin} = 0.25.

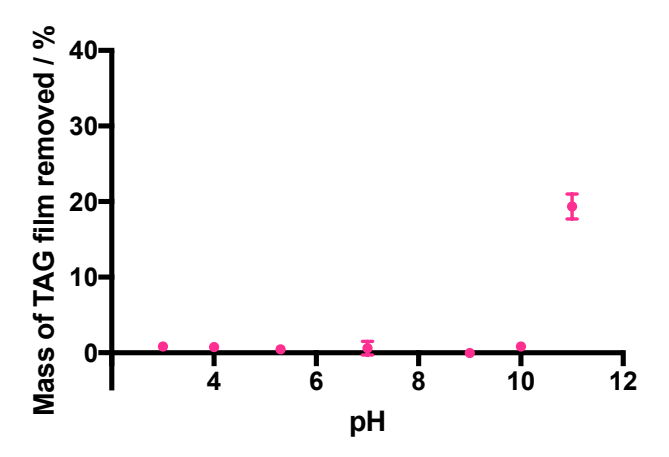


Figure 5.17: pH dependence of TAG film removal in deionised water

For the solutions up to pH 10, no or very little TAG film was removed. In contrast, 20% of the TAG film was removed in a 'cleaning solution' of deionised water pH adjusted to pH 11 with sodium hydroxide. Ali *et al.* observed fast soil removal for a baked lard soil with application of deionised water at pH 11 and suggested the cause may be the presence of hydroxyl ions weakening the electrostatic interactions between the soil and substrate. ^{19,20} An alternative explanation for this may be the triglyceride saponification. During the saponification of the triglycerides in the TAG soil, glycerol and fatty acid salts are formed in an autocatalysed reaction. The fatty acid salts can catalyse the reaction as well as creating a larger interfacial area between the TAG and the sodium hydroxide; initially, the TAG is not readily miscible with the alkaline water, however, as the fatty acids salt are formed, they can stabilise the formation of oil in water emulsions. There is further evidence of saponification from the observation of white solid flakes in the washing solution as the saponification of high oleic sunflower oil by sodium hydroxide has previously been shown to result in white solid soap formation.²¹

5.3.5 Summary of final method

In summary, the impact of four factors on the removal of soil were investigated: stirring speed, position of slides in the washing vessel, area loss calculations and alterations to the model TAG soil mixture. In order to create the most homogeneous, uniform TAG films, the following adaptations were made to the test detailed by Dunstan and Fletcher. In order to run in batches of three instead of one slide per stirring bath, slides were placed facing inwards, equidistant from each other, for ease of preparation as there was little difference in mass loss between the different slide positions investigated. The stirring rate was fixed at 500 rpm, as this ensured complete mixing of the solution without creation of a vortex. Although the area loss calculation investigated, it proved time-consuming without providing additional information and therefore, mass loss was used subsequently. Linseed oil was added to the triglyceride mixture in the ratio φ_{lin} = 0.25 so that final mixture was: 33.3% lard, 33.3% vegetable shortening, 25% vegetable oil and 8.3% linseed oil. This TAG mixture was pipetted onto glass slides and baked at 200 °C for 1 hour. The aim was to find a method to measure soil remove with a lower variability in the results than the industry standard test, which was greater than 30%. This was achieved, with the variability in the results of this test were all below 5%. For example, the surfactant solution used for method development, with 0.012% LO, 0.003% BC and 0.103% DG and pH adjusted to 9, had a mass loss of 12.39 ± 3.56 %.

5.4 Bayesian Optimisation with respect to soil removal

As the adapted test is repeatable with low variability, the Bayesian Optimisation method is now used to find the maximum mass removal for a ternary mixture of surfactants. The initial step in the process was to perform a random experimental design to generate 20 experiments, with boundary conditions of: total surfactant concentration limited to 5% and pH ranging between 2-11. The higher limit of surfactant concentration was raised, in relation to the surface tension optimisation, as surfactant concentration verses soil removal studies, discussed in section 6.3, showed that soil removal did not plateau before 2 w/w%. In figure 5.18, the experiments selected, and the soil removal results can be seen. There are clusters of experiments at pH 11 with high soil removal. In addition, high soil removal is observed with low concentrations of BC (green dots), this indicates that BC has no effect or a detrimental effect on soil removal. At pH 11, the cationic surfactant BC could be protonated,

decreasing the hydrophilicity of its headgroup, decreasing the likelihood of the surfactant positioning on the surface or the soil.

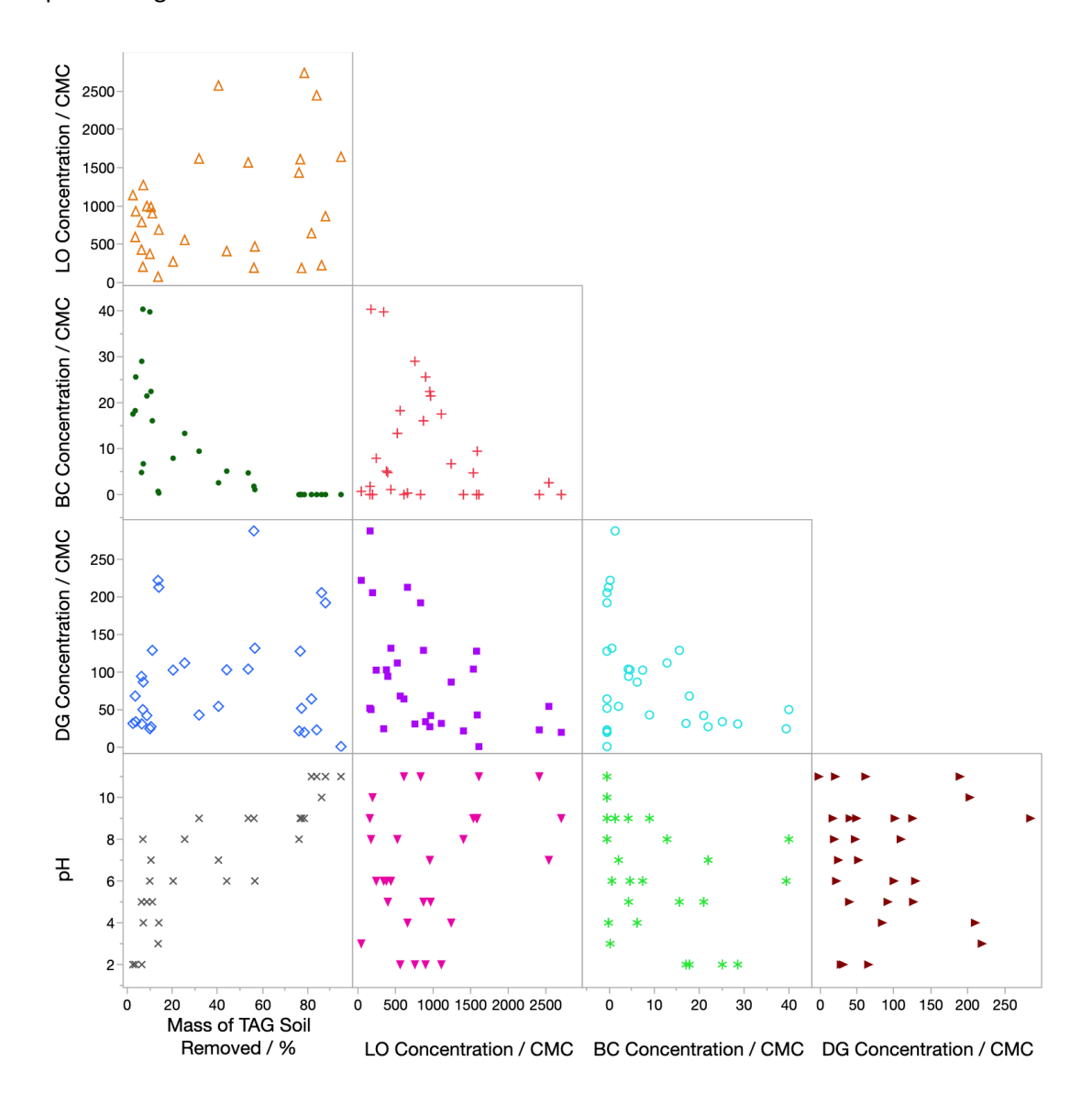


Figure 5.18: Experiments performed in a Bayesian optimisation of an aqueous ternary mixture of LO, BC and DG, with regards to mass of the TAG soil removed. The boundary conditions were: 0-5 w/w% of each surfactant, 95-100 w/w% water and pH 2-11. Each point represents a single experiment, of which there were 40. The concentration of the surfactants is given in units normalised to their CMC concentration, as an indication of surfactant synergism. In the graph of pH vs mass of TAG removed, there in trend of increasing mass loss with increasing (more alkaline) pH. concentration, there are points clustered at low concentration indicating convergence of the optimisation.

In contrast to the previous application of Bayesian optimisation in chapter 4, in which the surface tension was minimised, this application aims to identify the maximum value with regards to soil removal. The iterative process is the same. After the first batch of 20 experiments were measured, the algorithm suggested batches of 5 more experiments that

are either predicted to remove more soil than previously or are in regions of the formulation space where there is a lack of data points leading to higher uncertainty. The soil removal was measured for these 5 experiments and the process was repeated until the Bayesian Optimisation experiments were no longer predicted to be lower than those previously measured. Figure 5.19 shows that the soil removal by mass loss for each surfactant solution measured over the course of the optimisation, highlighting the highest mass loss at each iteration. It can be seen that the soil removal during the 32nd experiment was high, 95.7%, and the value could not be improved upon in the following experiments. The optimisation required fewer experiments than would be expected by other methods, such an experimental design for five parameters by full-factorial which would require 52 experiments or Box-Behnken which would require 46.²²

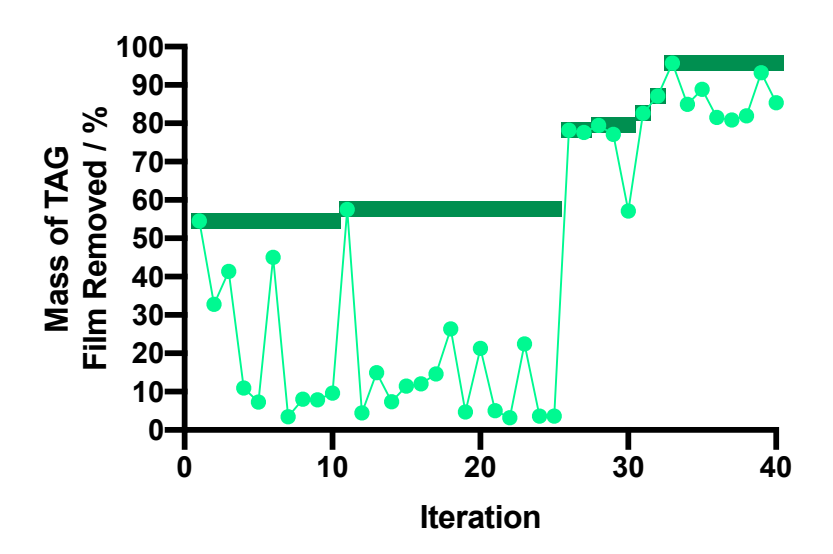


Figure 5.19: Improvements in mass of TAG film removed through the optimisation process of an aqueous ternary mixtures of LO, BC and DG, pH from 2 to 11. The highest TAG removal at each iteration is shown by the dark green line and the mass of TAG removed at that iteration is shown by a light green circle. No further improvement was seen after 32 experiments indicating the optimum had been identified.

By following the changes to the concentration of each surfactant in the selected mixtures, a number of interesting trends can be identified. After the initial batch of experiments, BC was either absent or included in very small amounts. This is an indication that BC does not have much effect in the soil removal process. The reason BC is added to cleaning formulations is because of its antimicrobial properties and not for its cleaning efficacy. Table 5.2 shows the surfactant compositions of the two best performing surfactant solutions. Both did not contain BC.

Table 5.2: The two best performing solutions, with regards to maximising the removal of TAG soil from a glass slide, as determined by a Bayesian Optimisation for a ternary mixture of 3 surfactants: LO, BC and DG within the pH range 2 to 11.

LO Concentration (/CMC)	BC Concentration (/CMC)	DG Concentration (/CMC)	Water Concentration (w/w%)	pН	Mean Mass Loss / %
973.6	0	45.07	97.91	11	93.23 ± 1.25
1638	0	1.518	97.52	11	95.73 ± 2.36

The two ternary mixtures in the above table contain LO and DG concentrations that are much higher than the CMCs of the individual surfactants. As the CMC is the concentration above which micelles occur, this indicates that, in addition to the presence of micelles, another factor must be important in soil removal. Additionally, there is a synergistic effect with regards to soil removal; it is beneficial to mix the two surfactants as they have a higher soil removing power than either alone (soil removal by each surfactant alone is discussed in section 6.3). These results are consistent with earlier studies of surfactant synergism in detergency. García Martín et al. observed the synergistic effect of adding alkylpolyglucosides to amine oxide surfactants resulted in improved the wetting properties towards hydrophobic surfaces, which would contribute to soil removal. This study found that in the top two optimised surfactant solutions of the ternary mixture, both have a pH of 11, which is consistent with the literature. At pH 11, the amine oxide group of the LO is likely to be negatively charged and could behave like an anionic surfactant.

There is evidence that surface tension may correlate with soil removal. In the previous chapter, CMC lowering was observed to be promoted in mixture of LO and DG at neutral to alkaline pH, and the same trend is observed for the optimisation with regards to soil removal. If the surfactant mixture behaves synergistically and reduces surface tension more effectively, there will be increased wetting of the soil and surface and potentially a greater reduction in interfacial tension. As surfactant adsorbs to the TAG soil and the surface, there is a reduction in the interfacial tension which aid any of the mechanisms of soil removal previously suggested i.e. roll-up, emulsification and solubilisation.

In this optimisation, the concentration of surfactant was limited to between 0 and 5% with the expectation that the optimum solution would have a surfactant concentration close to the upper limit (if more surfactant means greater surfactancy). However, there is an optimum in surfactant concentration. The two surfactant solutions which removed the

largest amounts of TAG contained 2.09% and 2.48% surfactant. This results implies that, in this system, higher surfactant concentrations above hinder soil removal which may be due to a phase change; to determine this, further work to obtain the phase diagram is required.

5.5 Conclusions

The main goal of this research was to apply the Bayesian Optimisation methodology to determine the optimal cleaning formulation, with regard to soil removal, from a ternary mixture of surfactants. In order to determine the optimal ternary system, a method of removing TAG was altered and optimized with respect to the soil composition, soil removal procedure, and soil removal analysis. From these changes, a repeatable method was developed that could then be used to optimize the system. Addition of linseed oil to the model soil mixture greatly improved the drying behaviour of the final film. The soil removal was measured by mass and area loss; area loss calculations proved too time-consuming without providing additional information and therefore, mass loss was used subsequently. Soil removal was measured in batches by increasing the number of slides in the cleaning vessels from 1 to 3.

Once a repeatable method had been developed, Bayesian optimisation was performed to find the ternary surfactant solution with the ability to remove the greatest mass of TAG soil. The optimisation found surfactant solutions with remarkable cleaning efficacy; they were able to remove >90% of the TAG film. This was an increase from 50% at the beginning of the experiment and much greater than alkaline water which removed 20%, in addition, a reduced number of experiments was required for the optimisation in comparison to DOE methods. One limitation of Bayesian Optimisation is, due to its inherent black-box nature, there is a lack of ability to provide insight into the mechanism of soil removal by the surfactant system. Hence, further study is required to investigate the behaviour of the surfactants causing this optimal solution.

5.6 References

- 1. Shaeiwitz, J. A., Chan, A. F. C., Cussler, E. L. & Evans, D. F. The mechanism of solubilization in detergent solutions. *J. Colloid Interface Sci.* **84**, 47–56 (1981).
- 2. Kabin, J. A., Sáez, A. E., Grant, C. S. & Carbonell, R. G. Removal rates of major and trace components of an organic film using aqueous nonionic surfactant solutions. *Ind. Eng. Chem. Res.* **38**, 683–691 (1999).
- 3. Jurado Alameda, E., Bravo Rodriguez, V., Bailón Moreno, R., Núñez Olea, J. & Vaz, D. A. Fatty soils removal from hard surfaces in a clean-in-place system. *J. Food Process Eng.* **34**, 1053–1070 (2011).
- 4. Beaudoin, S. P., Grant, C. S. & Carbonell, R. G. Removal of Organic Films from Solid Surfaces Using Aqueous Solutions of Nonionic Surfactants. 1. Experiments. *Ind. Eng. Chem. Res.* **34**, 3307–3317 (1995).
- 5. Detry, J. G., Rouxhet, P. G., Boulangé-Petermann, L., Deroanne, C. & Sindic, M. Cleanability assessment of model solid surfaces with a radial-flow cell. *Colloids Surfaces A Physicochem. Eng. Asp.* **302**, 540–548 (2007).
- 6. Boulange-Petermann, L., Debacq, C., Poiret, P. & Cromieres, B. *Effect of the physical chemistry of polymeric coating surfaces on fouling and cleanability with particular reference to the food industry. Contact Angle, Wettability and Adhesion, Vol 3* (2003).
- 7. Chan, A. F., Evans, D. F. & Cussler, E. L. Explaining solubilization kinetics. *AIChE J.* **22**, 1006–1012 (1976).
- 8. Kabin, J. A., Tolstedt, S. L., Sáez, A. E., Grant, C. S. & Carbonell, R. G. Removal of organic films from rotating disks using aqueous solutions of nonionic surfactants: Effect of surfactant molecular structure. *J. Colloid Interface Sci.* **206**, 102–111 (1998).
- 9. Prieto, N. E., Lilienthal, W. & Tortorici, P. L. Correlation between spray cleaning detergency and dynamic surface tension of nonionic surfactants. *JAOCS, J. Am. Oil Chem. Soc.* **73**, 9–13 (1996).
- Alameda, E. J., Bravo Rodríguez, V., Bailón Moreno, R., Núñez Olea, J. & Altmajer Vaz,
 D. Bath-substrate-flow method for evaluating the detersive and dispersant
 performance of hard-surface detergents. *Ind. Eng. Chem. Res.* 42, 4303–4310 (2003).
- 11. Dunstan, T. S. & Fletcher, P. D. I. The removal of thermally aged films of triacylglycerides by surfactant solutions. *J. Surfactants Deterg.* **17**, 899–910 (2014).
- 12. ASTM. Standard Guide for Evaluating Cleaning Performance of Ceramic Tile Cleaners. Astm i, (2015).
- 13. ASTM. ASTM D4488-95(2001)e1, Standard Guide for Testing Cleaning Performance of Products Intended for Use on Resilient Flooring and Washable Walls (Withdrawn 2009), ASTM International, West Conshohocken, PA, 1995, www.astm.org. *D4488-95* (2001).
- 14. Mallégol, J., Lemaire, J. & Gardette, J. L. Drier influence on the curing of linseed oil. *Prog. Org. Coatings* **39**, 107–113 (2000).
- 15. Lazzari, M. & Chiantore, O. Drying and oxidative degradation of linseed oil. *Polym. Degrad. Stab.* **65**, 303–313 (1999).
- 16. Tumosa, C. S. & Mecklenburg, M. F. The influence of lead ions on the drying of oils. *Stud. Conserv.* **50**, 39–47 (2014).

- 17. Soucek, M. D., Khattab, T. & Wu, J. Review of autoxidation and driers. *Prog. Org. Coatings* (2012).
- 18. Lewinska, A., Zebrowski, J., Duda, M., Gorka, A. & Wnuk, M. Fatty acid profile and biological activities of linseed and rapeseed oils. *Molecules* (2015).
- 19. Ali, A., Alam, Z., Ward, G. & Wilson, D. I. Using the Scanning Fluid Dynamic Gauging Device to Understand the Cleaning of Baked Lard Soiling Layers. *J. Surfactants Deterg.* **18**, 933–947 (2015).
- 20. Ali, A. *et al.* Development of a 'millimanipulation' device to study the removal of soft solid fouling layers from solid substrates and its application to cooked lard deposits. *Food Bioprod. Process.* **93**, 256–268 (2015).
- 21. Poulenat, G., Sentenac, S. & Mouloungui, Z. Fourier-Transform Infrared Spectra of Fatty Acid Salts Kinetics of High-Oleic Sunflower Oil Saponification. *J. Surfactants Deterg.* **6**, 305–310 (2003).
- 22. NIST/Sematech. e-Handbook of Statistical Methods. (2012).
- 23. Blagojević, S. N., Blagojević, S. M. & Pejić, N. Performance and Efficiency of Anionic Dishwashing Liquids with Amphoteric and Nonionic Surfactants. *J. Surfactants Deterg.* **19**, 363–372 (2016).
- 24. Blagojević, S. M., Pejić, N. D. & Blagojević, S. N. Synergism and Physicochemical Properties of Anionic/Amphoteric Surfactant Mixtures with Nonionic Surfactant of Amine Oxide Type. *Russ. J. Phys. Chem. A* **91**, 2690–2695 (2017).
- 25. García Martín, J. F., Herrera-Márquez, O., Vicaria, J. M. & Jurado, E. Synergistic effect on wettability of mixtures of amine oxides, alkylpolyglucosides, and ethoxylated fatty alcohols. *J. Surfactants Deterg.* **17**, 1035–1042 (2014).

6. Mechanism of Soil Removal

This chapter is concerned with methods used to gain some understanding about the mechanisms by which the triacyl glyceride (TAG) soil, discussed in chapter 5, is removed from hard surfaces, by the surfactants. The focus is on the surfactants and surfactant systems optimised in earlier chapters, namely, LO, BC, DG.

A number of analytical techniques have been used previously to study surfactant detergency of soiled surfaces.¹ The organization of surfactants on the surface or thin film of interest can be quantified by neutron reflectometry, ^{2,3} or ellipsometry^{4–7}. The topography of the soiled surface or the change in force in the presence of aqueous surfactant has been investigated by atomic force microscopy.^{8,9} Differential scanning calorimetry (DSC) provides information about the thermal properties of the residues that remain on surfaces after cleaning, indicating the occurrence of changes in composition.¹⁰ Analysis of the soil removed, present in the cleaning bath, has been studied by microscopy¹¹, HPLC¹² and UV-vis spectrometry.¹² Microfluidics has been used to study oil detachment by a surfactant solution, by imaging an oil droplet in a laminar flow cell.¹³ A quartz-crystal microbalance measures the changes in the mass on a surface in real time, which has been applied to study the surfactant-aided removal of oil from surfaces.^{14–16} The benefits of this method include the ability to study soil removal in real-time, the variety of choice in surface substrates, including the ability to coat the substrate with a film of interest.

For this project, the following techniques were used to study different parameters in the process of soil removal. The oil-surfactant-surface interface has been visualized using microscopy. The properties of the TAG soil before and after cleaning was analysed by DSC, where changes in the melting temperatures of the films would indicate the film composition has changed during cleaning . A comparison was made between each surfactant's efficiency, measured by surface tension, and soil removal efficacy determined by mass loss on the laboratory scale using the test adapted in chapter 5¹⁷. Real-time analysis of the soil removal process was investigated using a quartz crystal microbalance and dissonance (QCM-D) with analysis of the washing solution by dynamic light scattering (DLS).

6.1 Microscopy Investigation of Removal

With confocal microscopy, or laser scanning confocal microscopy (LCSM), it is possible to view processes occurring in samples in 3D, from combinations of a series of optical slices. In addition, higher resolution than wide-field microscopy is achieved due to the ability to remove out-of-focus light. A light beam fired at a pinhole, which blocks out-of-focus light, limiting the depth of focus, so imaging of layers of the sample can be performed. Confocal microscopy can be used to image the soil removal process directly, in real time.

Confocal microscopy has been used previously in the visualisation of detergency, specifically to investigate the mechanism of washing clothes. A procedure was developed whereby fibres were immersed in three model soils: oil, lard and a triglyceride (glyceryl tridecanoate) labelled with a fluorescent probe, Nile Red, and a mixture of surfactants and lipases were pumped over the fibres.¹⁹ The removal of the three soils was dependent on their melting points; olive oil is liquid at room temperature and was completely removed by a roll-up mechanism whereas only partial removal of the lard and triglyceride was observed so an emulsification-solubilisation mechanism was suggested.

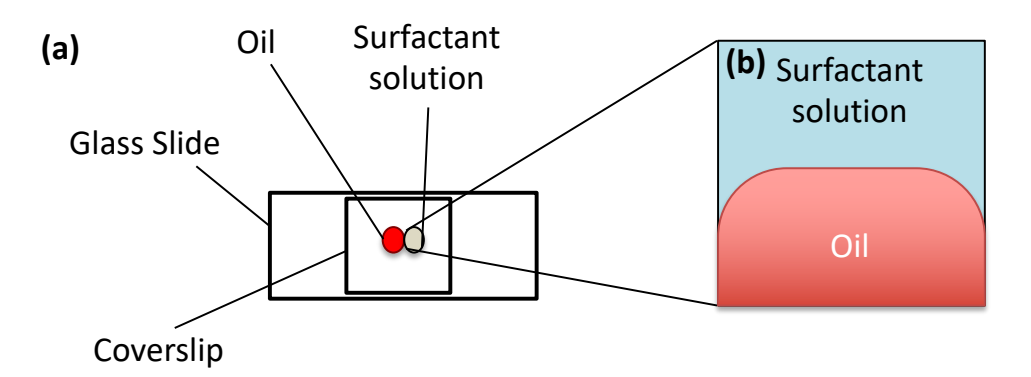


Figure 6.1: Schematic of the confocal microscopy experiment. a) a drop of oil labelled with nile red (red) and a surfactant solution (grey) are pipetted onto a glass slide. B) a diagram of the images taken by the confocal microsope of the interface where the oil(red) and the surfactant solution (blue).

In this project, LSCM was applied to study the removal of oil from a hard surface, shown schematically in figure 6.1. One of the components of the TAG soil was selected initially, rapeseed/canola oil, as it was liquid at room temperature, facilitating dye solubilisation. First, 100 μ L of the surfactant solution was pipetted onto a slide, followed by 100 μ L of oil containing 0.1 mg ml⁻¹ Nile Red dye, with a space between the two drops. A coverslip was then placed on top to force the two immiscible liquids to meet. Dental wax was used to seal

the coverslip, and a grid of images across the coverslip was taken every 5 minutes for 5 hours. The resulting images showed no movement at the interface, figure 6.2. Therefore, under these conditions and over a timescale of five hours, no vegetable oil is removed from the surface of the glass slide. For soil removal to occur some kind of mechanical action would be required to disrupt the surface due to the high viscosity of the oil, the lack of solubility of the rapeseed oil in the surfactant solution and the high interfacial tension between the oil and aqueous surfactant solution relative to that between the glass surface and the oil. However, there were some droplets formed from the action of applying the coverslip to the slide which were stable throughout the five hours. The stability of this droplet in an aqueous dispersion suggests the surfactant solution coated the surface of the oil and droplet. Therefore, the SDS has a role in the mechanism by preventing redeposition after the removal of a soil has taken place.

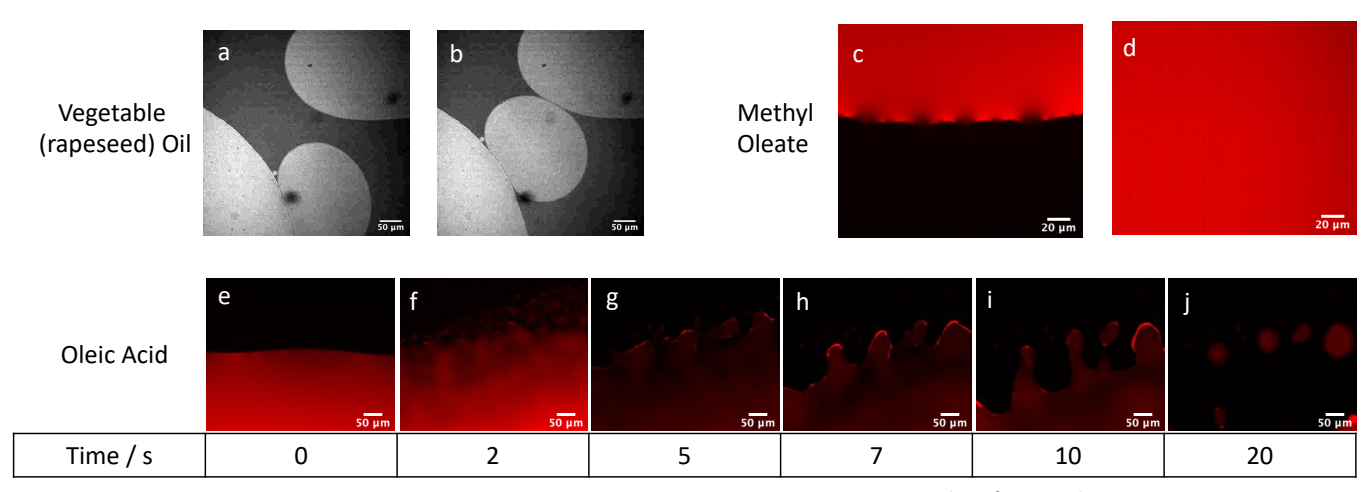


Figure 6.2: Confocal microscopy of the interface between an aqueous surfactant solution (1 w/w% SDS) and oils: vegetable oil, methyl oleate and oleic acid, dyed with 0.1 mg ml⁻¹ Nile Red. a-b) Vegetable oil is shown in white and the surfactant solution in dark grey. The droplets formed by external force (on application of a glass cover slip were shown to be stable over the imaging time (5 hours). c-d) Methyl oleate (red) at the start (c) and after contact (d) with a 1 w/w% SDS solution. The methyl oleate is spread over the surface of the glass. e-j) Images were selected at different time points (below each image) to show how the interfaces between the oleic acid/surfactant solution/slide changed. The contact line of the surfactant solution across the surface of the oil shows how the oleic acid (red) dewet from the surface of the glass slide.

This experiment was repeated with oleic acid which is a major constituent of vegetable oil (62.5%) but has a lower viscosity, 29.0 mPa·s at 23.9 °C (the viscosity of canola oil at 23.9 °C is 78.8 mPa·s). 20,21 Oleic acid appears to dewet from the surface of the slide when forced into contact with the 1 w/w% SDS solution. The dewetting may indicate an increase in the interfacial tension between the surface and the oil similar to the "roll up" mechanism.

Mixtures of SDS and oleic acid have been previously shown to undergo spontaneous emulsification. ²² In addition, oleic acid is itself surface active and its HLB is one, supporting the formation of water-in-oil emulsions rather than oil in water emulsions. Oleic acid may diffuse into the aqueous phase in a mixed SDS-oleic acid micelle. ²³ Alternatively, oleic acid in its ionised form can act as surfactant. Therefore, if the surfactant co-ions covert the outer layer of the oleic acid to a charged acid group which repels the surface facilitating its removal. To investigate this theory, methyl oleate was used in the same experiment as it cannot form the ionised form. Methyl oleate was not removed from the surface as shown in table 6.1. Instead, the surfactant solution spread the oil over the surface of the glass slide confirming the ionisation hypothesis above. In this case, the surfactant does not cause any change in the interfacial tension between the oil and surface. As the oil does not appear to be change visually, during the timescale of the experiment, this indicates that the methyl oleate is not solubilised. This is similar to visualization of vegetable oil; therefore, their mechanisms of removal may be the comparable.

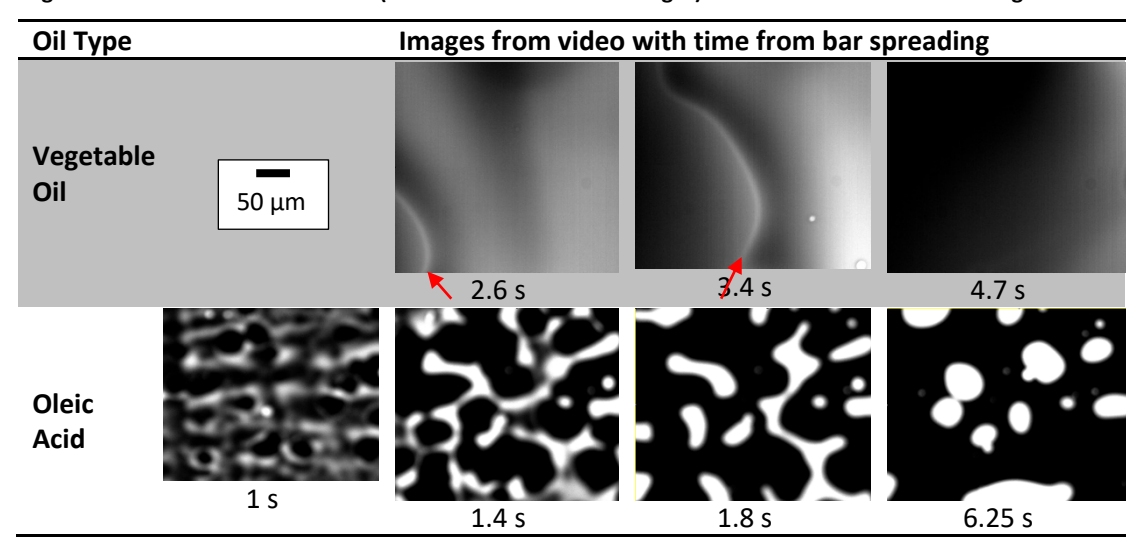
Table 6.1: Summary of oils studied by confocal microscopy and the imaging result for the interface between an aqueous surfactant solution and oils: vegetable oil, oleic acid and methyl oleate.²⁰

Oil Type	Chemical Composition	Molecular Weight / g mol ⁻¹	Imaging Result
Rapeseed	Mixture of fatty acids:	-	Interface unchanged
Oil	mostly oleic (62.5%) and linoleic		Particles stabilised
	(19.6%)		
Oleic	.	282.5	Fast dewetting from
Acid	OH		the surface
	j.,		Speed of leading edge:
	C ₈ H ₁₇		3.58 ms ⁻¹
Methyl	• 	296.5	Surfactant solution
Oleate	C ₈ H ₁₇		passes over oil layer

The combination of these results suggests that mechanical action is required in addition to detergency to remove these oils and fatty acids from surfaces (within the 5 hour timescale of study). To investigate the addition of mechanical action to the application of a surfactant solution to an oily soil, the use of bar spreader microscopy was attempted.²⁴ The passing of a bar over the surface of the surfactant-oil solution is an analogy, if oversimplified, to the abrasive force of cleaning a substrate. The "bar" was a razor blade, which has a lower surface roughness than typical cleaning implements, *e.g.* paper, sponges or scourers, and therefore, applied a lower abrasive force on the soil's surface.

The bar-coater was positioned within a microscope equipped with a $10\times$ objective (as shown in figure 2.9 in section 2.2.7.2). Vegetable oil and oleic acid, dyed with 0.1 mg ml⁻¹ Nile Red, were drawn across the surface using a blade 50 μ m above the surface to create a film. Image acquisition by a microscope positioned above the slide was started prior to a 1 w/w% SDS solution being pulled across the surface using the bar-coater. Images were collected for 30 seconds with a frame rate of 20 frames per second (fps).

Figure 6.3: Bar-spreader microscopy of the interface between an aqueous surfactant solution (1 w/w% SDS) and oils: vegetable oil and oleic acid, dyed with 0.1 mg ml⁻¹ Nile Red. The bar moved the surfactant solution from left to right in each image. Images were selected at different time points (below each image) to show how the interfaces between the oil/surfactant solution/slide changed. The contact line of the surfactant solution across the surface of the oil (red arrow) shows how the SDS solution moved across the surface of vegetable oil whereas the oleic acid (white in bottom row of images) dewet from the surface of the glass slide.



The bar-spreader microscopy images in figure 6.3 show a vast contrast between the oleic acid and vegetable oil. In the vegetable oil sample, the bar spreader moves the surfactant solution across the surface of the oil and the contact line (highlighted by the red arrow) was observed to move across the length of the surface (from left to right). However, visual observation of the slide at the end of the experiment showed no removal of the oil. The fluorescence intensity is decreased throughout the frames due to the spreading of the oil across the surface. Even with the addition of the force from the movement of the blade, oil is not removed from the surface. In the oleic acid sample, the fatty acid dewets from the surface within a second of contact with the SDS solution. The end result being droplets on the surface of the slide which would be caused by a reduction in interfacial tension due to the behaviour of oleic acid mentioned previously. Although the final images shown in table

6.2 were taken 6 seconds after movement of the surfactant solution, images were collected for 2 minutes and no further changes were observed after that time, figure 6.3.

Both microscopy methods, LCSM and bar spreader, were unable to visualize the removal process of vegetable oil from a surface in real-time. The reason for this may be the high interfacial tension between the oil and our glass substrates. However, it was observed by LCSM that once oil droplets are formed by external forces, they were stabilized by the presence of surfactant, which prevents their redeposition on the surface of the remaining oil or the substrate, figure 6.2.

Figure 6.4 suggests how the process of the removal of vegetable oil with the addition of surfactant and a method of abrasion may occur. These avenues of investigation using microscopy with and without "scrubbing" were subsequently abandoned as it seemed unlikely to be able to deal with the tenacious soils that were of primary interest. The TAG soil contains a mixture of fats which are chemically crosslinked during the baking process, making them adhere even more strongly to the glass surface.

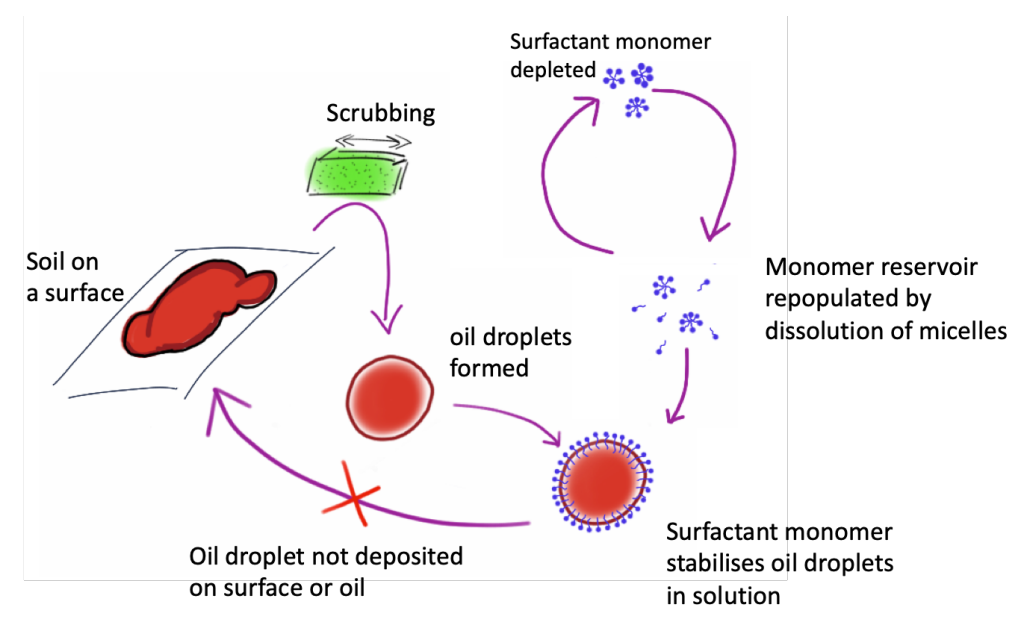
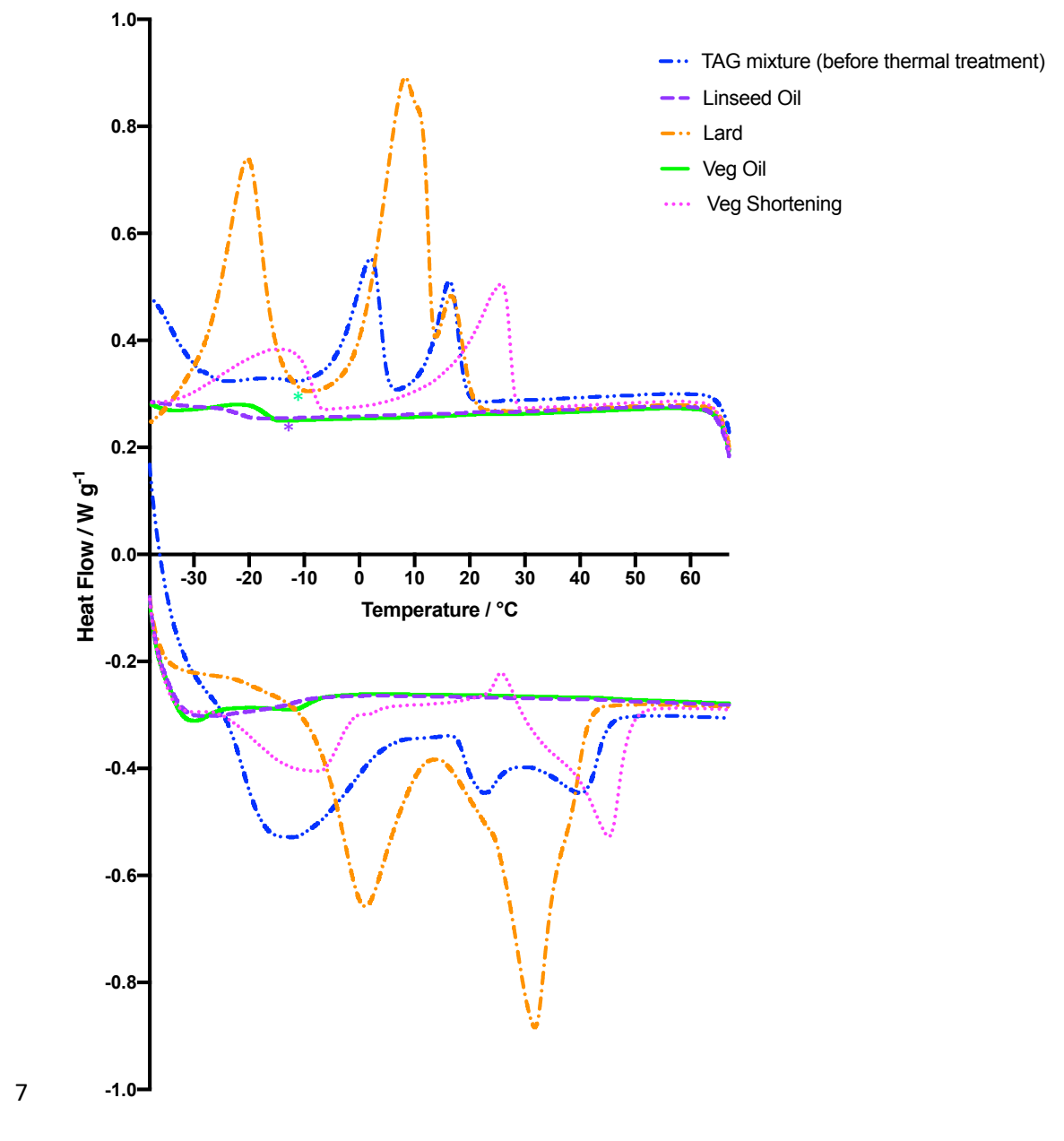


Figure 6.4: The removal of a viscous soil, e.g. vegetable oil, from the surface of a glass slide requires mechanical action to disrupt the surface of the soil and form droplets of oil. The oil droplets are stabilized by surfactant monomer present in the cleaning solution which prevents redeposition of the oil on the soil surface.

The surfactant from the monomer reservoir is repopulated from dissolution of micelles.

6.2 Analysis of the model soil



8 Figure 6.5: DSC heating (top) and cooling (bottom) curves for a sample of the TAG mixture (without thermal treatment) and its components: vegetable (rapeseed) oil, vegetable shortening, lard and vegetable shortening. The graph shows data from the second cycle of heating to 70 °C, holding at 70 °C for 5 min and cooling to -40 °C with a heating/cooling rate of 10 °C/min.

A simple, repeatable, cleaning test was developed in chapter 5 which used a difficult-to-remove greasy soil consisting of: 33.3 % lard, 33.3% vegetable shortening, 25% vegetable oil and 8.3% linseed oil. DSC was used to compare the melting/crystallisation temperatures of the TAG mixture and its components as shown in figure 6.5. The DSC curve from heating linseed oil and vegetable oil, at a rate of 10 °C/min, shows they both have glass transition

temperatures at approximately -20 °C (both highlighted by *). Lard shows the largest endotherms presumably due to a high level of crystallization. Both lard and vegetable shortening have more than one endotherm which suggests they contain multiple fractions, triglycerides, fatty acids and with each component having a different melting/crystallization temperature. This observation is in agreement with previous DSC studies of solid fats.²⁵ The sample of vegetable shortening contains a higher melting component than lard, with melting complete at 60 °C rather than 50 °C. The heating curve of the TAG mixture shows melting peaks at approximately 1 and 16 °C, which are intermediate between the peaks for lard (-20, 10 and 15 °C) and vegetable shortening (-10 and 27 °C).

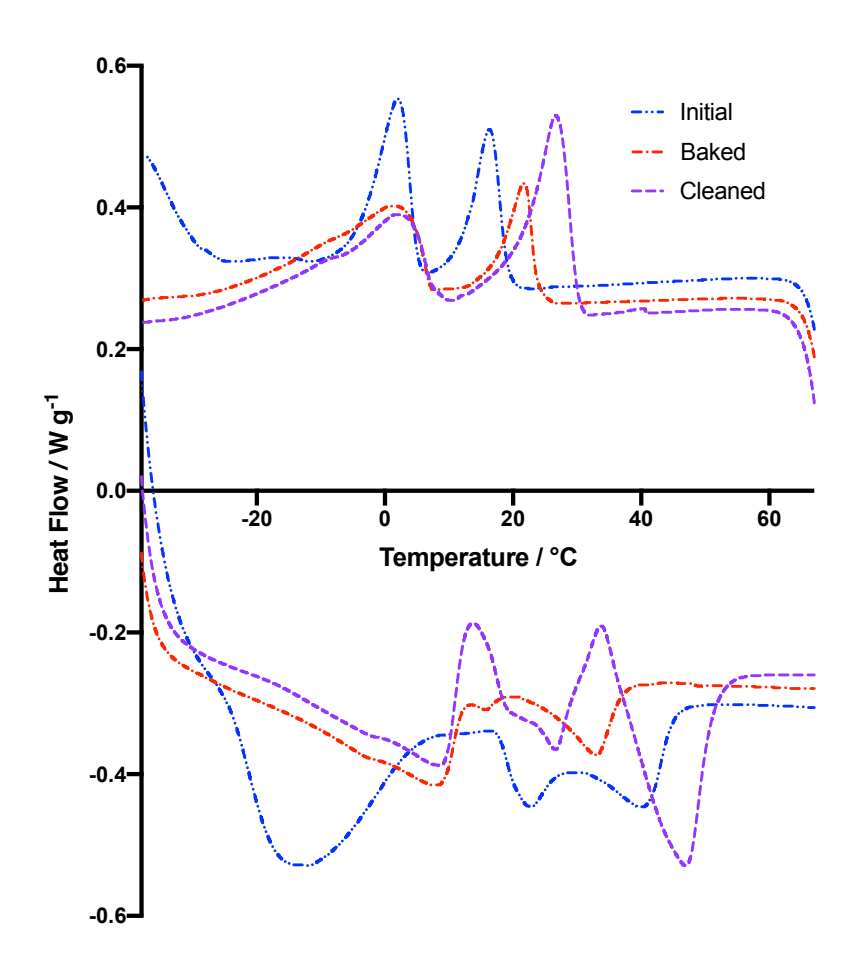


Figure 6.6: DSC heating (top) and cooling (bottom) curves for a sample of the TAG mixture with and without thermal treatment (baked on a glass slide at 200 °C for 1 hour) and the residue from cleaning the slide in a solution of 1 w/w% LO. The graph shows data from the second cycle of heating to 70 °C, holding at 70 °C for 5 min and cooling to -40 °C with a heating/cooling rate of 10 °C/min.

DSC of the TAG mixture initially (initial), after thermal treatment at 200 $^{\circ}$ C for 1 hour (baked) and the TAG remaining on the slide at the end of the soil removal test using a solution of 1 w/w% LO (cleaned) is shown in figure 6.6. The unbaked TAG shows sharp crystallisation

peaks at -13, 20 and 42 °C. The melting peak at 15 °C was shifted to 24 °C in the thermally treated TAG.

The residue from cleaning shows a melting peak at a higher temperature than either of the other samples. A possible explanation for this observation is the selective removal of a fraction within the TAG mixture with a lower melting temperature.

To investigate whether the change in the melting temperatures of the TAG film during the cleaning process, SAXS of a sample of the TAG prepared by the method outlined in chapter 5, with one difference: the substrate was a 15 mm mica disk of 25-micron thickness rather than a glass slide. The prepared TAG was analysed by SAXS before and after the TAG soil removal test had been performed (using a 1 w/w% LO solution). In figure 6.7 a), the differences in the two patterns at low q, $0.01-0.08~\text{Å}^{-1}$ show there is a change in the morphology of the film during cleaning. This suggests that the components removed during cleaning leave pores or voids behind, creating structure in the TAG film. This void scattering is the extra intensity seen at low q. As the interfaces become rougher, the slope of the curve changes from ~4, indicating a solid, sharp interface, to 3.4 indicative of fractal voids with rough interfaces.

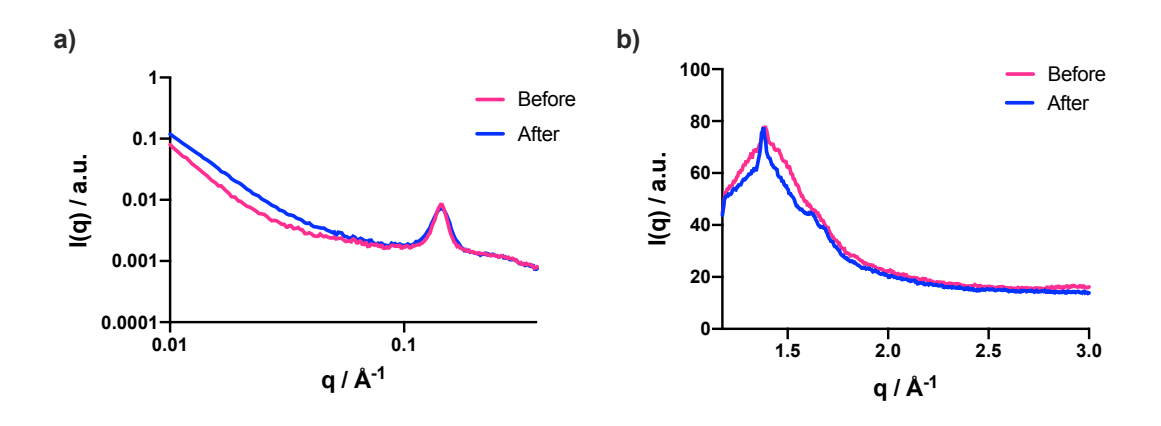


Figure 6.7: X-ray scattering patterns for a film of TAG removed from the surface of a glass slide used in the bulk laboratory soil removal test, after baking at a 200 °C and before "cleaning" (pink) and after removal from the cleaning test and drying in a vacuum dessicator for 12 hours (blue). a) SAXS where the peak at 0.3 Å-1 is the same in both patterns indicating the crystal structure of the fat is unchanged during the cleaning process. However, the differences in the two patterns at low q show there is a change in the composition of the film during cleaning. b) WAXS where the presence of crystallinity in the TAG, for both samples, is observed by peak at 1.5 Å-1.

The peak at 0.3 Å⁻¹ in the SAXS pattern and at 1.5 Å⁻¹ in the WAXS pattern (figure 6.7 b)) is observed in both patterns. Therefore, there is crystallinity in the TAG, which is not removed during the bulk TAG test, *i.e.* the "after" sample is more crystalline and there are higher order peaks from the crystalline material that are consistent with the increase in melting temperature as the sample is more crystalline. This indicates that the components of the TAG mixture that are harder to remove by surfactant solution contain these crystalline regions.

6.3 Comparison of Surface Tension and Soil Removal

In chapter 5, a simple, repeatable, cleaning test was developed and used to optimize a mixture of commercial surfactants. The optimal mixture as determined by the optimization favoured high proportions of LO to DG and exclusion of BC, in addition to high pH. To investigate these observations further and to gain insight into the mechanism of soil removal, the TAG removal test was used to investigate the dependence of cleaning efficacy on surfactant type and concentration, pH and its relationship to surface tension.

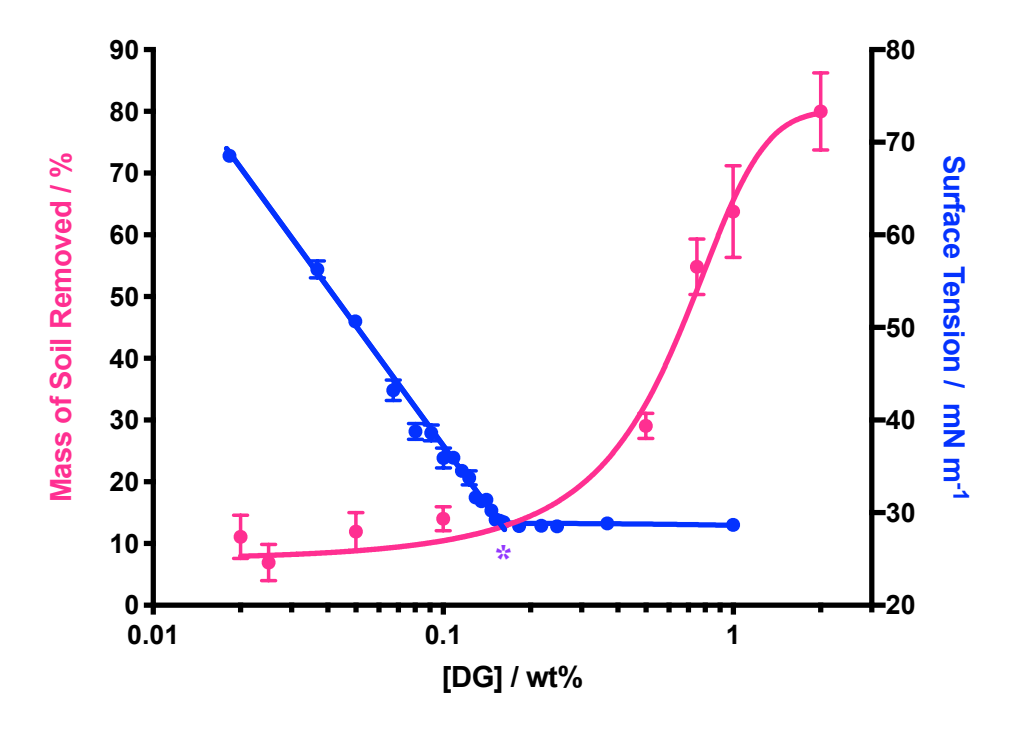


Figure 6.8: Relationship between TAG soil removal and surface tension for various aqueous DG concentrations at unadjusted pH (11). The surface tension decreases with concentration until the point of inflection at the CMC where the surface tension plateaus. The soil removal begins to increase around the DG concentration of the CMC (*).

To gain an understanding of the contribution of each surfactant, in the binary/ternary mixtures discussed in previous chapters, to the removal of the soil from a surface, the TAG removal test was performed at various concentrations for each individual surfactant species. Figure 6.8 compares the DG solution surface tension and soil removal with increasing surfactant concentration. The most remarkable result to emerge from the data is that the concentration of DG at which the surface tension becomes constant, indicating the CMC (*), is the same as the concentration above which an appreciable amount of soil begins to be removed. Above the critical micelle concentration (CMC), micellular aggregates form in dynamic equilibrium with the 'free' surfactant in the solution, i.e. surfactant monomers that are not at the interface or in micelles, therefore, this finding suggests that the presence of aggregated surfactant provides a reservoir of surfactant which aids soil removal.

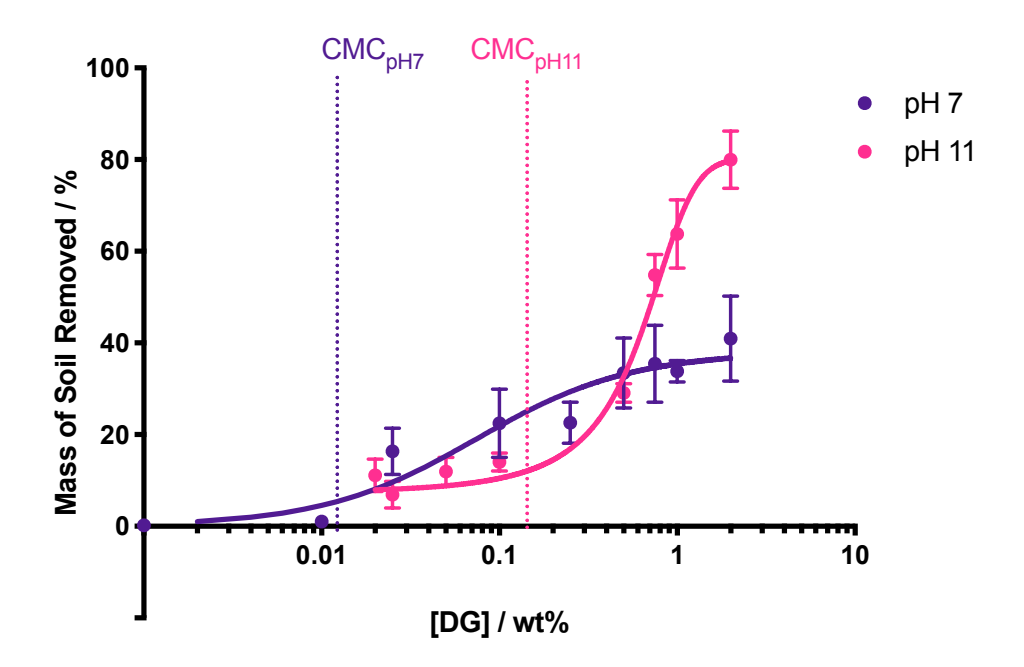


Figure 6.9: pH dependence of TAG soil removal with surfactant concentration for DG. Arrows indicate position of the CMC

From figure 6.9, it can be seen that the minimum concentration of DG at which soil removal occurs is comparable to the CMC, and a lower concentration of DG is required at pH 7 than pH 11. The CMC of DG changes from 0.011 w/w% at pH 7 to 0.1 w/w% at pH 11. Jin *et al.* previously observed an increase in CMC with pH has been observed previously for alkylpolyglucosides. This effect was caused by the hydrotropic effect whereby the deprotonation of headgroup with addition of sodium hydroxide causes the surfactant molecules to behave like anionic surfactants with increased repulsive interactions between their headgroups. ²⁶

At pH 7, the increase in soil removal with concentration plateaus above 0.9 w/w% whereas at pH 11 the soil removal continues to increase beyond 1 w/w%. In addition, at pH 11 and concentrations of DG below 0.1 w/w%, there is ~ 9% of the TAG soil. Both of these observations could be due to saponification occurring increasing the amount of TAG solubilized. In chapter 5, ~5 % of the TAG was removed by deionised water at pH 11 so there is a pronounced synergistic effect of DG in alkaline conditions.

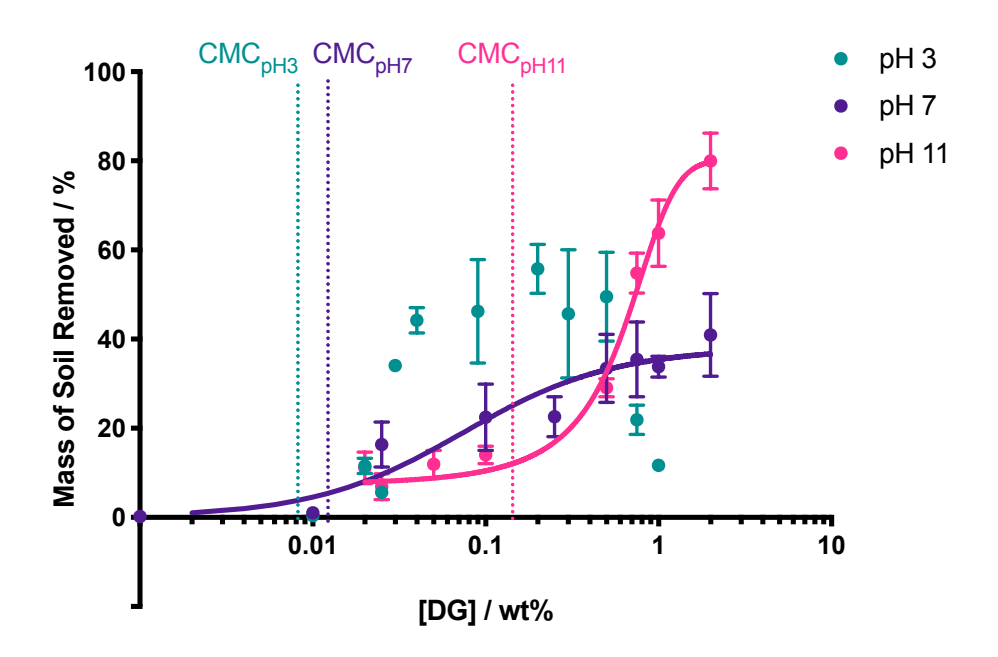


Figure 6.10: pH dependence of TAG soil removal with surfactant concentration for DG. The dotted vertical lines indicate position of the CMC at each pH.

The cleaning behaviour of DG at pH 3 differs significantly from pH 7 and 11. At pH 3, there is a decrease in removal of the TAG soil above 0.2 w/w% of DG, from 55.7% to 11.7% at 1 w/w%, figure 6.10. It may be that a change in micelle shape could change the amount of soil removal and therefore, analysis of DG at pH 3 and 11 by SAXS was performed. However, there is no difference in the shape of the micelles at pH 3 and pH 11, shown in figure 6.11. Therefore, further investigation would be required to determine the reason for this observation as the reason for this is unclear.

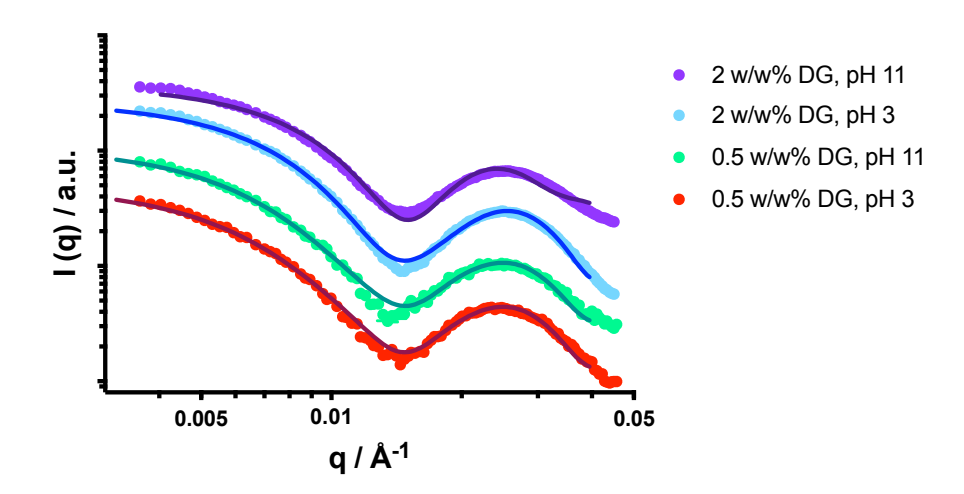


Figure 6.11: Offset SAXS patterns for 0.5 and 2 w/w% DG, at pH 3 and pH 11, indicating that the micelles are the same shape in all cases from the good fit of a core-shell ellipsoid model.

Although the CMC correlates well with the onset of soil removal for DG, the same cannot be said for the cationic surfactant, BC. The soil removal of BC at two different pH's was performed: pH 7, for comparison with the other two surfactants, and pH 11, which is the pH at which many household cleaning formulations are prepared.²⁷

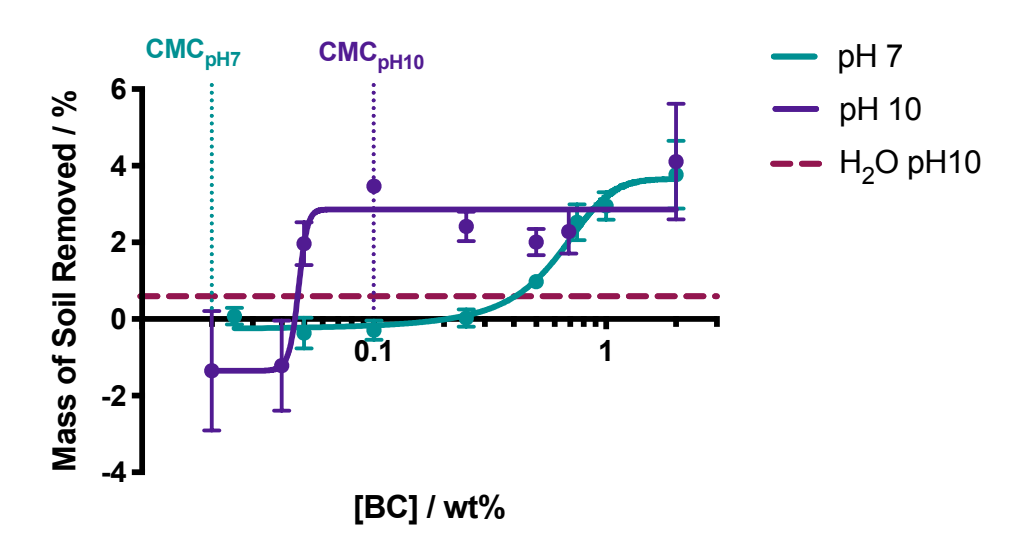


Figure 6.12: pH dependence of TAG soil removal with BC concentration at pH 10 (purple) and pH 7 (green). The dotted vertical lines indicate position of the CMC at each pH. The CMC of BC, at both pH, is lower than the point at which soil begins to be removed. However, relative to other surfactants studied, the overall soil removed at the highest concentration is low (4.1% at pH 10).

As figure 6.12 shows, the total TAG film removed over the time of the experiment was low for all concentrations of BC at both pHs, having a maximum removal of 4.1% at 2 w/w% of BC at pH 10. At low BC concentration, there is "negative" soil removal, due to an increase in

mass of the TAG film. The mass of the soil increases over 24 hours, which is not observed for deionised water alone, and therefore, this indicates swelling by absorption of aqueous surfactant. The amount of TAG removed by the 2 w/w% of BC at pH 10 was higher than that removed than in the pH 10 water alone, 3% versus 0.5%. This result indicates the surfactant is removing some of the TAG in the soil removal. At both pH 7 and 10, the concentration above which soil removal begins to occur is well above the CMC, which indicates that a large excess of surfactant is required to remove TAG from the glass surface.

In addition, BC is again ineffective at removing soil from the surface: the concentration of surfactant required to remove 5% of the TAG over 24 hours is over 100 times higher than the CMC. As discussed previously, this result is to be expected as BC is added to cleaning formulations as a biocide rather than to play a role in soil removal and in this context, BC is essentially not an active surfactant.

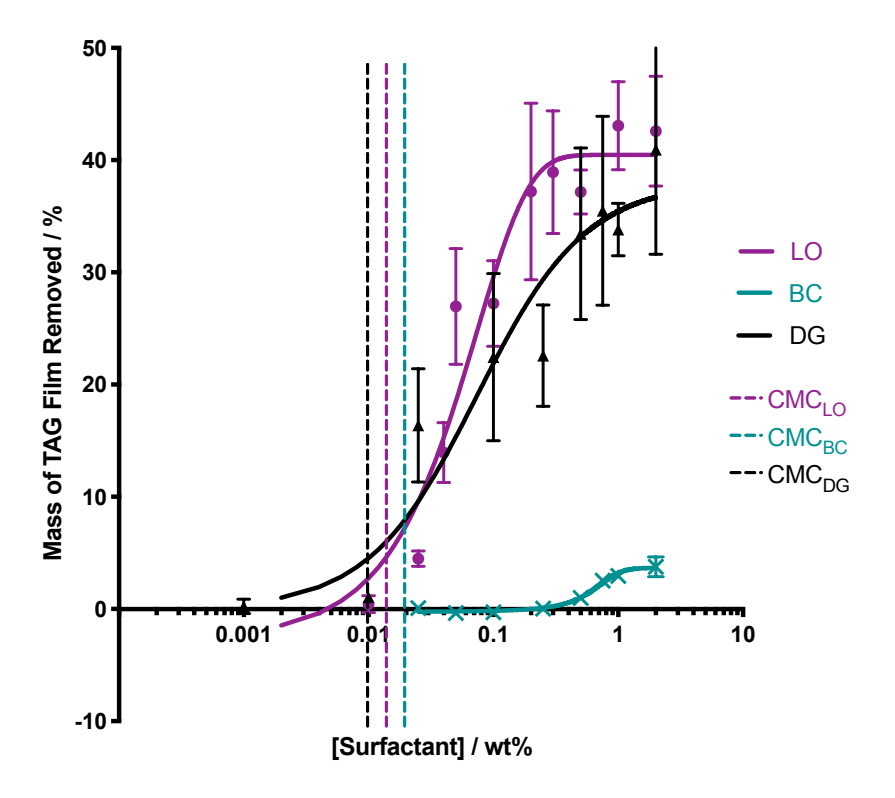


Figure 6.13: TAG soil removal with surfactant concentration for LO, BC and DG at pH 7. The dotted vertical lines indicate position of the CMC at each pH.

The soil removal for LO with increasing concentration can be seen in purple in figure 6.13. The shape of the curve is similar to DG indicating the mechanism of soil removal may be the same. The CMC of LO relates to the concentration at which the removal of TAG begins to

occur. The amount of soil removed increases at a constant rate with concentration of LO between 0.02 and 0.2 w/w% and then plateaus.

The next study compared the three surfactants at pH 7. The coloured dotted lines in figure 6.13, indicate the CMCs for LO, DG, and BC at pH 7, which are all between 0.01-0.02 w/w%. At this point, the LO and DG begin to significantly decrease. The comparison of the three surfactants clearly shows that the CMCs of LO and DG are related to their soil removal whereas BC does not remove any TAG until concentrations greater than ten times its CMC. LO and DG also remove a much greater mass than BC. The maximum soil removal observed for each surfactant was: 43.1% for LO, 40.9% for DG and 3.7% for BC.

6.4 Oil in Micelles

One potential mechanism of TAG removal is that all or part of the TAG soil is solubilised within surfactant micelles. To investigate whether the oily TAG soil could be solubilised within the surfactant micelles, resulting in an increase in micelle size, the addition of increasing volumes of hexane to LO micelles was studied by SAXS. Hexane was chosen as an initial test as it is analogous to the alkyl chains in the fatty acids and is a liquid at room temperature. The concentration of the LO was kept constant, 2w/w%, whilst the amount of hexane was increased. In the following discussion, Φ_{LO} is the ratio of LO to hexane. Each mixture was prepared, sonicated and stirred overnight before SAXS analysis. The shift in minima around 0.1 Å to lower q with increasing volume of hexane addition, indicates an increase in micelle size.

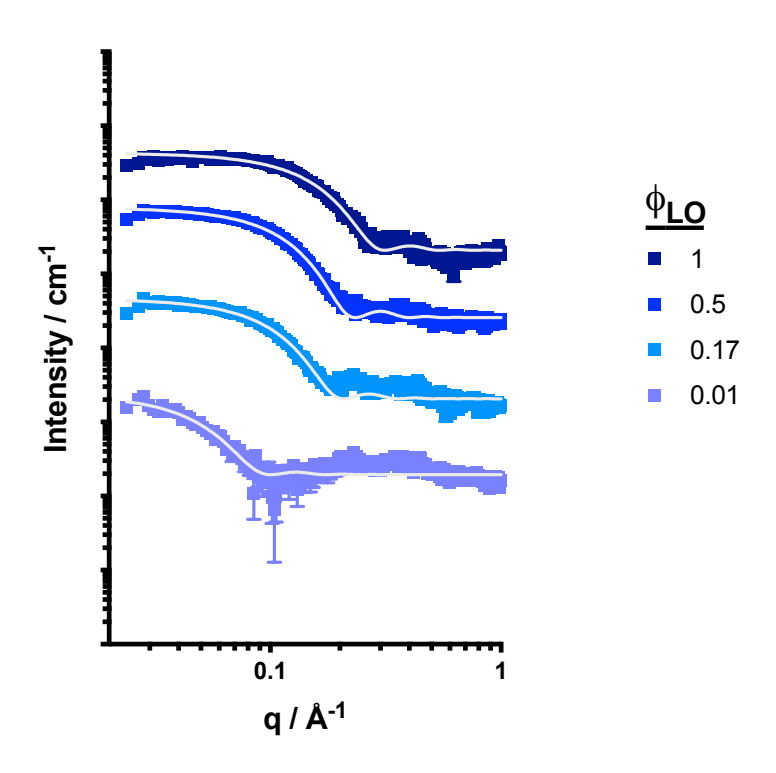


Figure 6.14: q dependence of the normalised scattering intensity for the mixing of hexane with 2 w/w% LO, for Φ_{LO} = 1, 0.5, 0.17, 0.01. Lines indicate fit with a model describing spheres.

Table 6.2 shows the radii of the micelles in each case was obtained from a spherical model. The increase in micelle radius appears is directly related to the increase in hexane concentration.

Table 6.2: Increasing micelle radius of the LO micelles with addition of hexane, as determined by SAXS. Hexane was mixed with 2 w/w% LO, a model describing spheres was used.

Ratio of LO to hexane	Radius / Å
1:0	14.3 ± 0.0
1:1	19.2 ± 0.0
1:5	21.6 ± 0.1
1:100	44.7 ± 0.8

These results show that LO micelles can be swollen by oil with the addition of force (in this case, stirring and sonication) and a long equilibration time (24 hours). Therefore, it is possible for LO to remove oil from a surface by solubilization-emulsification mechanism with sufficient mechanical action.

6.5 QCM-D

QCM-D measures frequency and dissipation of an oscillating sensor enabling the calculation of the change in mass and viscoelasticity of thin films on the surface of the sensor, both with addition and subtraction of a film. Previously, QCM has be used to study soil removal and detergency. There are a number of advantages over other techniques, including high sensitivity, large choice is surface and soil type and time-resolved experiments.

The first example of using QCM to investigate detergency of hard surfaces was by Weerawardena in 1998.²⁹ A solid organic soil, tripalmitin, was applied to the surface of a sensor by vacuum sublimation. The rate and amount of soil removal was calculated by the frequency changes and used to rank surfactant efficiency of two nonionic surfactants: pentaethylene glycol mono-n-dodecyl ether and octaethylene glycol mono-n-dodecyl ether. In 2003, a similar QCM experiment was performed to study removal of 3 lipids: tripalmitin, trimystirin and cetyl alcohol, using two other surfactants: anionics, sodium dodecylbenzensulfonate and SDS, nonionics, dodecyl heptaethyleneoxide and hexadecyl heptaethyleneoxide.³⁰ For all surfactants, there was lipid swelling but no soil removal at concentrations below their CMC. At higher concentrations, the lipid is removed once the swelling stage is complete.

More recent QCM studies have followed the rate of removal of stearic acid. The detergent formulations studied have a range of applications; from cleaning surfaces for vacuum deposition, ¹⁵ biomedical implant cleaning ¹⁵ to washing synthetic textiles. ^{14,31} QCM determined the loss of the fatty acid film occurred in two stages. First, the water and detergent adsorbed or was absorbed by the stearic acid layer, followed by detachment of the stearic acid layer.

QCM has been suggested for ranking of cleaning formulations by their performance in the product development process. ¹⁶ Eight, undisclosed, formulations were flowed over the surface of a QCM sensor coated in a film of used cooking oil. QCM was used to compare the cleaning formulations by metrics that evaluate a formula's ability to get rid of a soil such as: rate of soil swelling, which is indicative of penetration by surfactant and water, the rate of mass loss, and total mass loss. Two typical QCM-D cleaning profiles showing soil swelling by surfactant and water and subsequent soil loss are shown in figure 6.15.

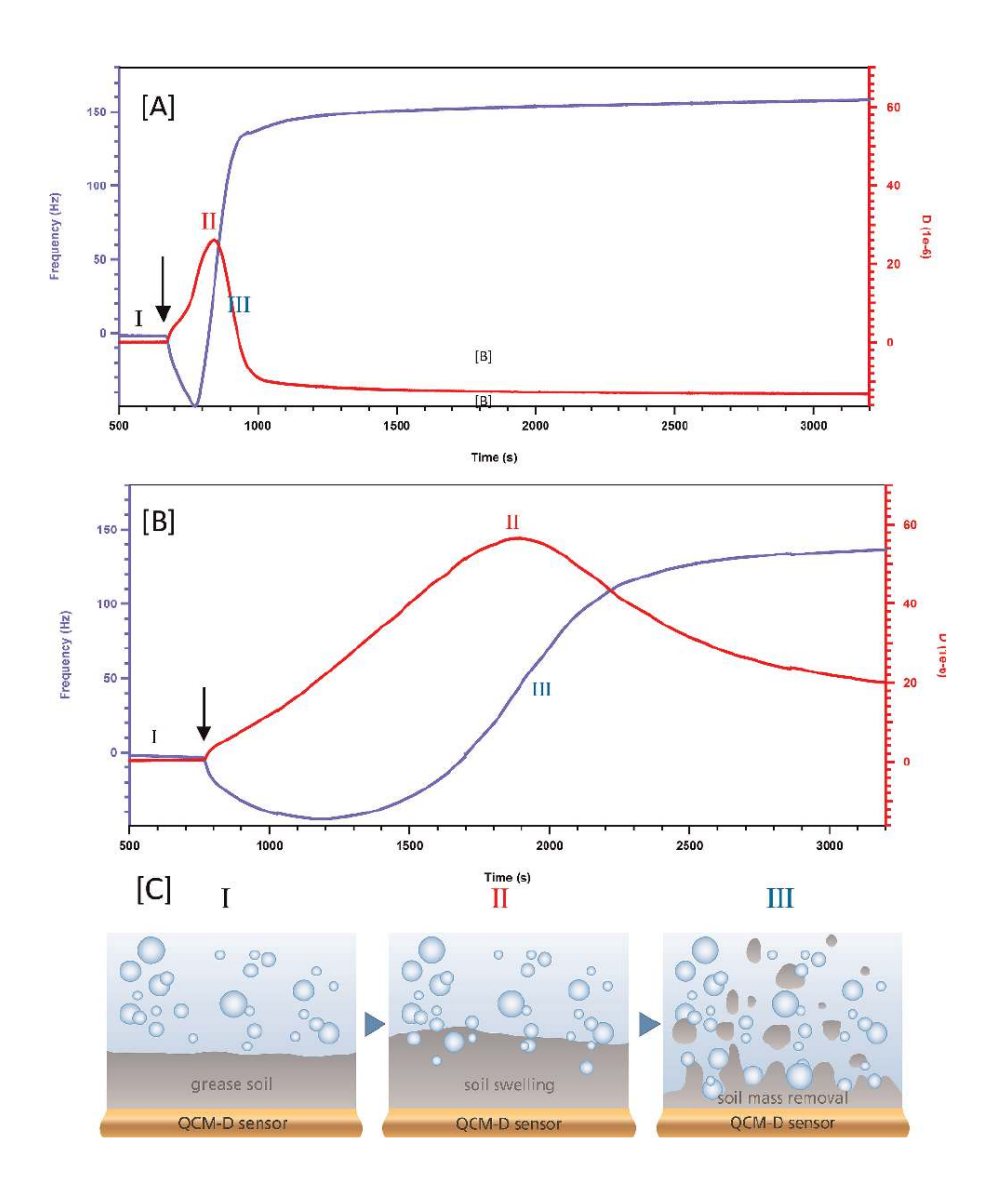


Figure 6.15: Two cleaning profiles for application of a surfactant solution to a grease soil attached to a QCM-D sensor. The black arrows show the time of surfactant solution injection. [A] is the QCM-D data for a surfactant solution with a short swelling time, the time taken for surfactant and water penetration into the grease, this is indicated by the increase in dissipation and decrease in dissipation after solution injection. The soil removal time is also short, shown by the increase in frequency and decrease in dissipation between 800 and 100 seconds. [B] is the QCM-D data for a surfactant solution with a slower soil swelling time, shown by a more gradual increase in dissipation and decrease in frequency. The soil removal begins around 1900 seconds with the decrease in dissipation and increase in frequency. This diagram was taken from K. Olesen *et. al.* ¹⁶

In previous chapters, a mixture of surfactants was optimised for maximum soil removal of TAG. However, it would be difficult to monitor the changes in mass, using the bulk TAG test, at short timescales and over time, due to the requirement to remove and vacuum dessicate the films before mass determination. The advantage of QCM-D is the ability to monitor changes in mass in real time. Hence, to further study the mechanism of how the surfactants are removing the soil, QCM-D is used to look at the rate of soil removal and soil swelling.

6.5.1 Spin coating TAG on a QCM-D Sensor

To study the mechanism of removal of the TAG film by surfactant using QCM-D, application of a thin homogenous coating of TAG to a quartz sensor is required. SiO_2 coated quartz sensors were selected as the most comparable to the glass surface used in the large-scale cleaning test.

Thin films can be produced uniformly by spin coating from solution.³² In order to spin-coat TAG onto a sensor, a suitable solvent for TAG is required to obtain films thin enough to not excessively damped the sensor in the QCM. Previous solubility studies have shown some fatty acids (oleic and linoleic) and tristearin, a triglyceride, are soluble in ethyl acetate, acetone, hexane and toluene.^{33–35} As the TAG mixture is a mixture of triglycerides from different fatty acids including oleic, linoleic and stearic, the solubility of the TAG mixture in these four solvents was investigated. Toluene was the only solvent that dissolved the TAG at room temperature although only at concentrations below 20 w/w%, indicating the limit in solubility.

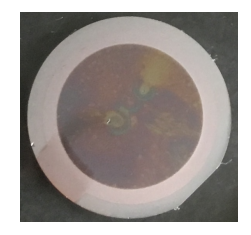
The first experiments focused on spin coating the SiO₂ sensor with TAG which had not been baked previously. Films that were initially uniform, by visual inspection, were produced by spin coating 10 microlitres of 20 w/w% TAG in toluene. However, the film dewets and forms a large droplet on the surface of the sensor caused by the extreme temperatures of the baking at 200°C. This droplet required multiple cycles of immersion in toluene and cleaning in an ultrasonicator to remove. Therefore, this preparation procedure could not be used for QCMD as the soil was too difficult over shorter timescales for the surfactant solution to remove without abrasion and the film was of uniform thickness. Therefore, an alternative method of film preparation, with lower temperature baking, that produces uniform films was required.

Xue and Han previously studied how to prevent dewetting of thin films. 36 There are four methods: changing the surface energy of the substrate, maintaining the temperature of the film below its glass transition temperature (Tg), increasing the thickness of the film and use of a higher molecular weight polymer. 36 All four methods will be discussed in relation to coating of TAG on SiO₂ sensors below.

The surface energy of the substrate could be changed to encourage uniform film formation. In this case, SiO_2 coated sensors are the closest in surface properties to the glass slides used in the laboratory TAG loss test. In addition, the process to clean the slides was matched to the laboratory TAG test: sonication in a detergent solution, micro-90, followed by sonication in deionised water. Thus, the surface energy of the sensor was set and therefore, the most favourable way to prevent dewetting was to either increase the thickness of the film applied to the surface of the QCM sensor or lowering temperature the temperature of baking. Increasing the thickness of the film can be acheived by lower spin speeds on the spin-coater or increased mass of the TAG toluene solution. Therefore, three methods to generate films of greater thickness were examined: using lower spin speeds, more concentrated TAG in toluene solutions and application of larger volumes of the solution when spin coating. In addition, thermally treating the TAG films at lower temperatures was used.

The following conditions were identified to form a uniform film: spin coating 40 μ L of 20 w/w% TAG at 1000 RPM for 20 s and subsequently baking at 70 °C for 1 hour. Although, this method produced uniform films, the films were too thick, > 2 μ m. Due to the film thickness, the oscillations of the sensor in the QCM were dampened to the extent that the resonant frequencies could not be found. Therefore, this film preparation method was not able to be used to study the film removal by surfactant solutions.

Another method to prevent dewetting is using a higher molecular weight polymer; however, altering the soil was not within the remit of this study. The aim was to study the 'model soil' developed previously which contained: 33.3% lard, 33.3% vegetable shortening, 0.25% vegetable oil and 0.083% linseed oil. During the process of baking, an increase in the molecular weight of the triacylglyceride molecules was previously observed by Dunstan and Fletcher, due to autoxidative crosslinking. Therefore, in order to use thinner films, the TAG mixture was baked prior to spin coating (to form a high molecular weight polymer). Rather than baking the film on the SiO_2 sensor, the TAG was prepared by the same method as the TAG removal test (pipetting molten TAG solution on glass slides and then baking at 200 °C for 1 hour) and then scrapped off the slides and dissolved in toluene. This TAG toluene solution was then used to spin coat the sensors at 2000 RPM for 20 seconds, using 20 μ L of 5 w/w% TAG in toluene, figure 6.16. A final step was to place the coated sensors in an oven at 50 °C to ensure evaporation of toluene.



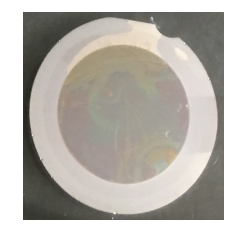


Figure 6.16: SiO₂ sensors coated with TAG prepared by thermally treating TAG, dissolution in toluene at 5w/w%, spin coating onto SiO₂ QCM sensors and baking at 50 °C.

The average thickness of the final film was 1.1 μ m, determined from the mass and density of the TAG applied, assuming uniform film thickness. To determine whether the final film was stable to soil removal; the coated chip was analysed in deionized water. When a coated sensor was submerged in a container of deionised water for 24 hours, no visible changes in the film or immersion solution are observed. In addition, there was no change in the frequency observed over several hours when deionized water was flowed over the coated chip in the QCM.

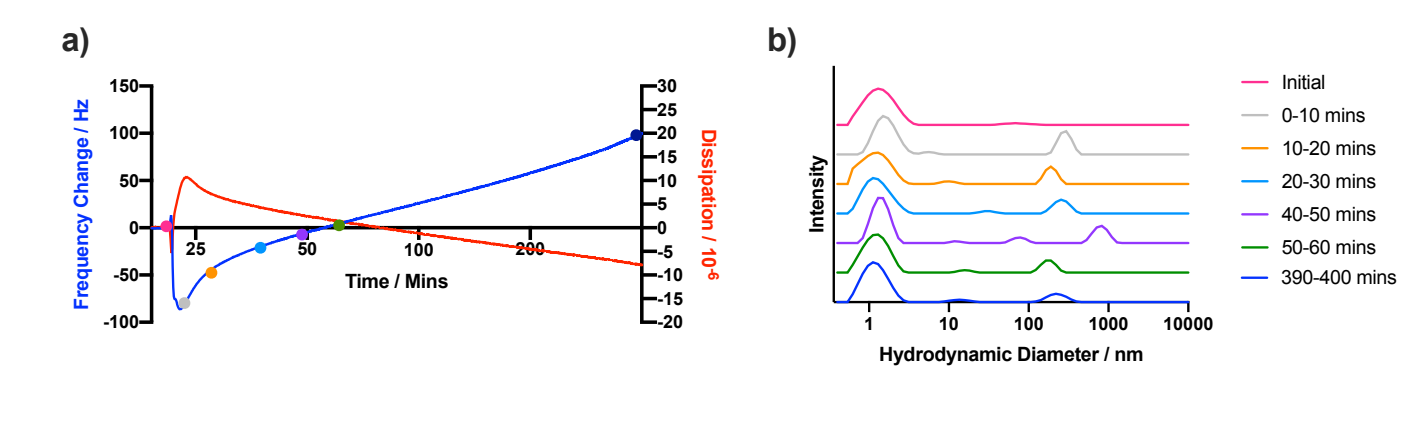
6.5.2 Kinetics of surfactant-aided TAG film removal

To gain understanding of the kinetics of the removal of the previously developed model TAG soil, the method to coat a SiO₂ coated quartz crystal QCM sensor with TAG was used to study the behaviour of three surfactants: LO, DG and BC and the mixture optimised by BO. For all experiments, the resonances were found in deionised water and the measurements were begun as the surfactant solution flowed into the measurement cell. In each case, the surfactant solutions were studied at concentrations well above their CMC, 10 times the CMC, and below the CMC, 0.5 times the CMC. DLS was used to monitor the size distribution of the TAG particles removed from the surface of the sensor. The surfactant solution exiting the QCM was collected over intervals of ten minutes, in order to collect a sufficient volume for analysis (1 ml). Previously, it has been shown that solid organic soils initially take up water until a saturation point is reached.²⁹ This was also observed in this experiment; there was a decrease in frequency (indicative of mass increase) of about 50 hertz over 60 minutes, followed by a plateau.

The change in oscillation frequency of the QCM is related to the change in mass on the sensor by the Sauerbrey equation, defined in section 2.2.6.1. However, the Sauerbrey equation is not valid in the following examples because the TAG film is not rigid, which is one of the required assumptions. There are models to relate frequency change to mass change, such as the Voinova-Voigt model, however, these cannot be applied here because the density of the film is required for the calculation which cannot be determined because

of changes during the cleaning process. As previously discussed in section 6.2, DSC and SAXS suggested the removal of TAG is selective for different components in the TAG mixture, potentially causing voids or porosity in the film. Hence, the following discussion of the QCM results are qualitative.

In the bulk TAG removal test on glass slides used previously, aqueous BC was shown to be ineffective at removing TAG. The thought was the cationic surfactant initially penetrated the soil with water, causing swelling, followed by a slow and minimal soil removal step. To investigate this, a comparative experiment using TAG coated sensors placed in a QCM cell under flow of 1 w/w% BC solution, with an unadjusted pH of 7.3, was performed. A 1 w/w% solution is a concentration of 10 times the CMC of BC (figure 6.17).



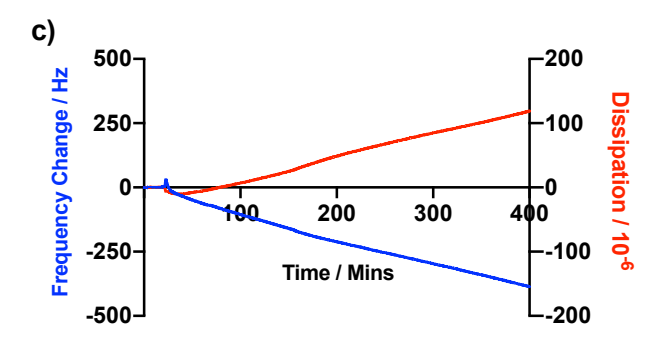


Figure 6.17: Cleaning of a TAG soil using a 1 w/w% BC solution, which is 10X CMC, monitored by: a) QCM and b) DLS of the supernatant. The colours of the dots in a) indicate the times the supernatant was sampled and analysed by DLS, which match the colours of the lines in b). The peak at ~ 300 nm (not observed in the intial solution) indicates the size of the TAG particles, removed from the QCM sensor surface, in the supernatant. c) QCM data for the cleaning of a TAG soil using 0.05 w/w% BC solution, half the CMC, which shows a decrease in frequency, indicative of mass uptake, and an increase in dissipation, indicative of softening of the TAG film.

The frequency decreased over the first 10 minutes, indicative of mass uptake of surfactant and water, and subsequently increased gradually over the next 4 hours. The experiment

could not be continued due to time constraints however, it may be expected that the frequency would continue to increase, due to mass loss continuing until the upper limit of soil removal, followed by a plateau. The slow and small mass of TAG removal (relative to LO and DG discussed later) is in agreement with the results of the the "bulk" TAG test where the soil removed was low over 24 hours, <4%. In addition, the dissipation increased over the first 20 minutes. This dissipation increase indicates the softening of the film by the BC surfactant. The peaks in the dissipation occurs at the same time as the frequency, followed by a decrease. This suggests that the softening of the TAG aids its removal from the sensor surface by BC as the loss of TAG from the surface means the remaining mass is less viscoelastic.

Figure 6.16 b) shows the size distributions of any scattering objects in the supernatant: the BC solution collected after flowing through the QCM. The top pink trace, the 'initial' solution of 1 w/w% BC, has only one peak at \sim 1 nm in diameter which is the size of the BC micelles. DLS was used to follow the size distribution over the time of the QCM experiment. At all times where supernatant was collected, a peak is observed indicating surfactant stabilises particles of diameter \sim 300 nm. As the intensity of the scattering is lower than that of the surfactant, the concentration of the particles is low which is in agreement with the small mass loss seen by QCM-D. In comparison to the soil removal of LO and DG (shown subsequently), the rate of mass loss is slow.

Figure 6.16 c) shows the frequency and dissipation changes, monitored by QCM-D, for an aqueous solution of BC at half its CMC, 0.05 w/w%. In this case, there was no increase in frequency which signifies the soil was not removed, or a greater mass was absorbed than removed. The slow decrease in frequency and increase in dissipation indicates soil softening by surfactant and water and there were no changes seen during DLS of the initial surfactant and the supernatant. Both of these observations indicate that no soil was removed; which may be because the time required for soil removal is longer than the duration of the experiment. An alternative explanation is that the surfactant (and water) adsorbs on the surface of the TAG and softens it, but BC does not readily desorb from the surface leading to

the lack of removal of the soil. To develop a better idea of the adsorption and desorption kinetics, techniques such as ellipsometry, neutron reflectometry or AFM could be used.⁶

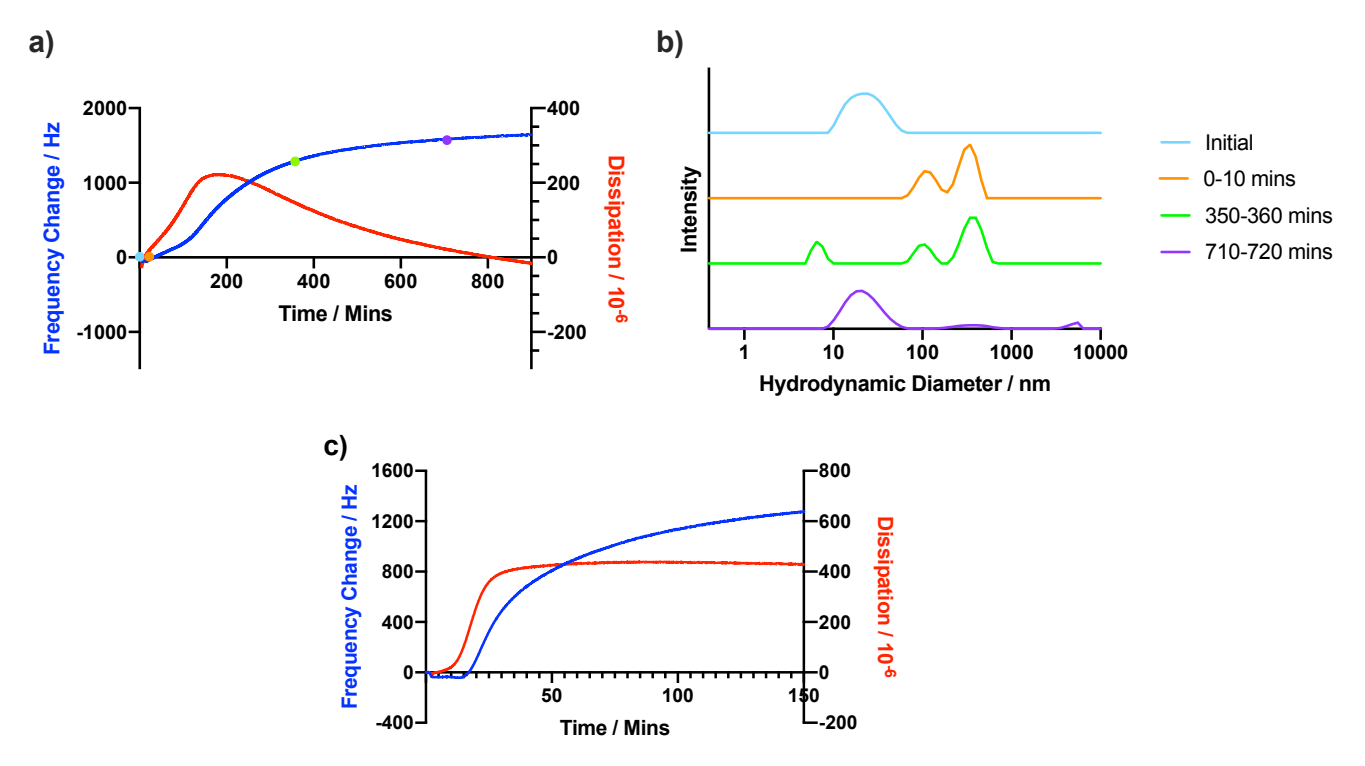


Figure 6.17: Cleaning of a TAG soil using DG solution of 10X CMC a) monitored by QCM b) supernatant monitored by DLS. c) Cleaning of a TAG soil using DG solution of 0.5X CMC monitored by QCM.

The second surfactant studied was DG. At 2 w/w%, the DG solution was shown in the previous bulk lab test on glass slides to remove 80% of the model TAG soil. Solutions of DG in deionised water, with a native pH of 10.5, were prepared at concentrations ten times the CMC and half the CMC to study the soil removal with and without the presence of surfactant micelles. These solutions were flowed over the TAG coated sensor in the QCM-D, the results of which are shown in figure 6.17 a). In agreement with the earlier observation, the solution at ten times the CMC was effective at removing the TAG films. In figure 6.17 a) there is a change in frequency as the soil is removed and interestingly there are two stages in the frequency increase. The increase in frequency in the first stage is of a smaller gradient indicating mass loss for the first 120 minutes was slower. The subsequent increase in gradient indicates a faster rate of soil removal until a plateau at ~400 minutes with the end of soil removal. In this comparison to BC, there was no initial decrease in frequency suggesting that the soil is removed by a different mechanism which does not require soil penetration by water and surfactant to soften the soil. After the initial increase in dissipation associated with soil softening, the dissipation decreased to its initial baseline which may be due to the high mass loss from the surface leaving a hard surface at the end.

Figure 6.17 b) shows DLS of the supernatant collected after being flowed through the QCM. The top blue data is for an aqueous solution of DG at a concentration of 10 times the CMC which has one broad peak at ~ 30 nm in diameter for DG micelles. This broad peak may be a combination of the two peaks at ~ 8 and 100 nm as in the supernatant collected there are 3 peaks rather than two. Over the first 10 minutes (orange in figure 6.17 b)), during the first stage, and in the second stage, 350 to 360 minutes (green in figure 6.17 b)) showed the size of particles stabilised by the surfactant were the same, 450 nm. The final sample of supernatant was collected from 710 to 720 minutes and contains very little of the 450 nm particles. These large particles may have been caught on the surface of the QCM suggesting TAG is not being removed at this time. This is in agreement with the frequency plateau and dissipation decrease suggesting no further mass loss.

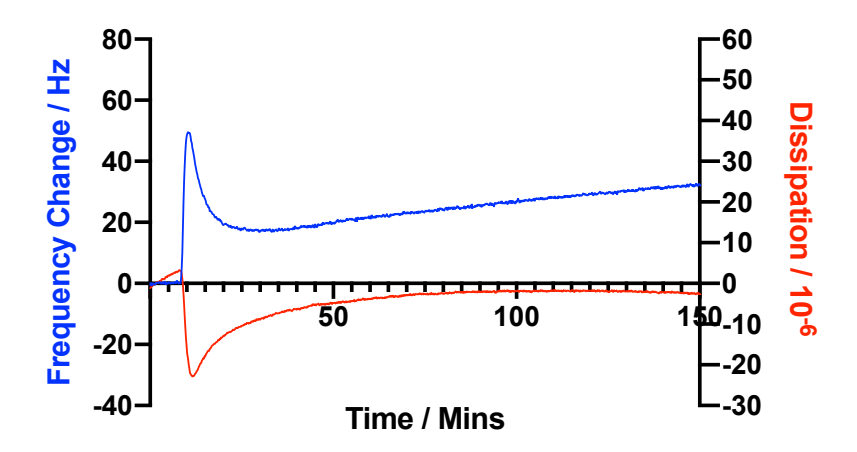


Figure 6.18: Cleaning of a TAG soil using water adjusted to pH 11 with sodium hydroxide monitored by QCM

In the next experiment, water with pH adjusted to 11 was studied using QCM-D to make comparisons with the studies of DG. DG is naturally basic, pH 10.5, and the previous experiments studying water at high pH using the bulk TAG soil removal test showed a small amount of soil removal. Figure 6.18 shows an increase in frequency and decrease in dissipation, due to mass loss, until a peak at 10 minutes. This peak is followed by a decrease in frequency and decrease in dissipation and subsequently, a small increase in frequency. By 150 minutes, the change in dissipation is small and the frequency change is ~20 Hz, indicating small amount of soil removal. Most of the mass loss occurs over 30 minutes which is similar to the rate of saponification of oil, which has been studied previously and shown to occur in less than 20 minutes.³⁷

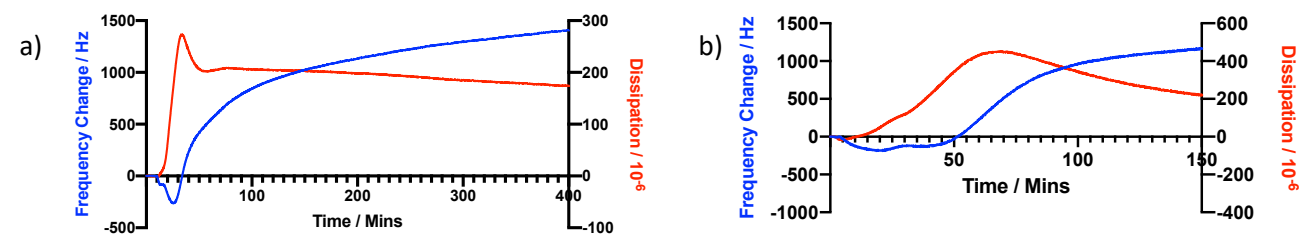


Figure 6.19: Cleaning of a TAG soil monitored by QCM using LO solution of concentration a) 10X CMC and b) 0.5X CMC

The final surfactant studied was LO which was effective at removing TAG in the laboratory removal test discussed in Chapter 5: 40% of the TAG film was removed using a 1 w/w% solution. For the QCM-D experiment, a solution of 10 times the CMC of LO was used, to study soil removal in the presence of micelles, which had a pH of 8.0. During the first 50 minutes of the experiment, there were two events. First, over the initial 20 minutes, there is a rapid increase in dissipation accompanied by a small decrease in frequency. As the change in dissipation is large, relative to the changes seen for DG and BC, LO softens the TAG film to a greater extent before mass loss occurs. In the subsequent, 30 minutes there was a small decrease in dissipation and increase in frequency due to mass loss. After 100 minutes, the rate of mass loss decreases towards a plateau.

Figure 6.19 b) shows the change in frequency and dissipation of TAG films subjected to an LO solutions at concentration of half its CMC. A small amount of mass loss is observed (relative to the mass loss/frequency increase observed for the same surfactant solution at concentrations 10x CMC) which suggests that micelles are not required for soil removal and there was a delay of 50 minutes, before the frequency began to increase which is much greater than at concentrations 10 times the CMC of LO. An explanation for this might be that with less surfactant, there is an increase in the time required for surfactant to penetrate the soil on the sensor surface which aids removal.

In Chapter 5, the soil removal efficacy of a mixture of the three previously discussed surfactants, BC, DG and LO, was optimised using a Bayesian Optimisation method. One of the best performing solutions was selected, 1.46 w/w% LO (973.6 X CMC), 0.631 w/w% DG (45.1X CMC) at pH 11, and the QCM-D method was used to study its soil removal behaviour with time.

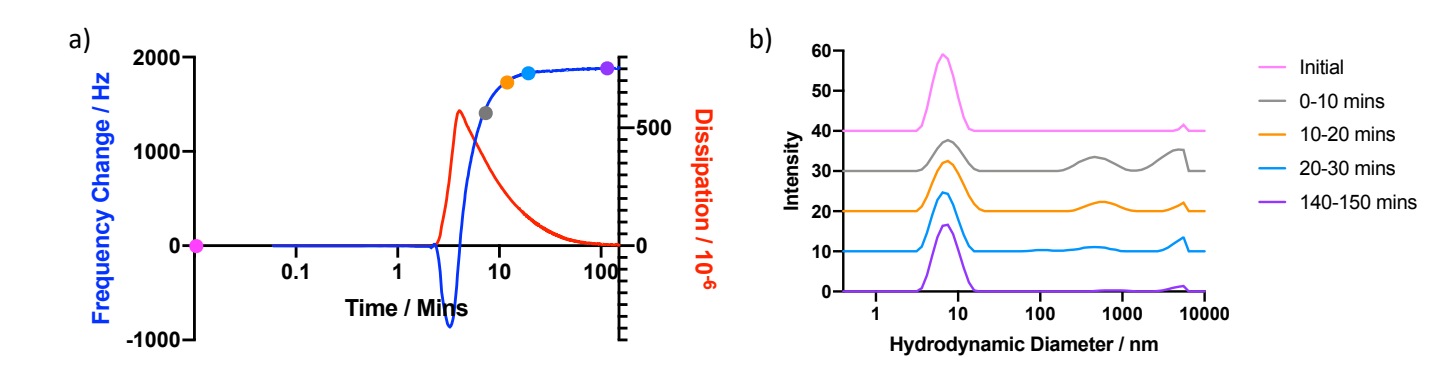


Figure 6.20: Removal of a TAG soil using surfactant mixture optimised using a Bayesian Optimisation a) monitored by QCM b) supernatant monitored by DLS

This optimised solution showed the highest change in frequency of the surfactant solutions tested which suggests the most mass loss. In addition, the mass loss occurred at the fastest rate: figure 6.20 a) shows a plateau in frequency change after 20 minutes. In figure 6.20 b), the final sample of supernatant taken between 140 and 150 minutes, there are no particles observed by DLS which is another indicator that the removal of soil had completed by this time. The DLS of the supernatant in the samples at 0-10, 10-20 and 20-30 minutes show the soil particles are approximately 700 and >10000 nm.

Table 6.4: Removal of a TAG soil, monitored by QCM, for LO, BC and DG solutions at concentrations of 10 times the CMC and a surfactant mixture optimised using BO, 1.46 w/w% LO (973.6 X CMC), 0.631 w/w% DG (45.1X CMC) at pH 11.

Surfactant	Time to maximum swelling / mins	Rate of Soil Removal / Hz min ⁻¹
Lauramine Oxide	23	39.8
Decyl Glucoside	150	5.32
Benzalkonium Chloride	21	0.539
Optimised Mixture	1.9	1170

Table 6.4 compares the kinetics of soil removal of the surfactants alone and the surfactant mixture optimized by the Bayesian optimization. The swelling time was calculated by the time from the introduction of surfactant to maximum in dissipation and the rate of removal was calculated from the steepest slope of the change in frequency. This highlights how effective the optimized mixture is at soil removal with an increase of 40 times the rate of soil removal and a 10 times shorter time to maximum swelling relative to the best performing surfactant. In addition, the correlation between short times to maximum swelling to the highest rates of soil removal shows the importance of swelling and softening of the TAG for its removal and the truly synergistic effect of mixed surfactants.

6.6 Conclusions

This chapter attempted to investigate the mechanisms and kinetics by which the TAG soil is removed from hard surfaces, by the surfactants: LO, BC, DG. A number of techniques were used including microscopy, characterisation of the TAG soil, comparison of the CMC of the surfactants and their soil removal using the bulk TAG test and QCM-D.

Confocal microscopy was used to study observe the oil-aqueous surfactant interface. However, with no external force applied, the surfactant had no effect on both oils, rapeseed oil and methyl oleate, over 5 hours. Imaging of a droplet formed prior to imaging showed the surfactant, SDS, was able to prevent redeposition of the droplet into the oil and stabilizes the oil droplets formed. Bar spreader microscopy, which images application of a surfactant solution using a bar spreader to impart some additional force, showed no changes at the oil-surfactant interface, and therefore, no removal of the oil from the glass slide. Therefore, a larger force is required to emulsify the vegetable oil within the timescale of study. As the soil of interest, TAG, is a more viscous, crosslinked film than vegetable oil, it would be more difficult to remove from the glass slide. Therefore, information about the mechanism of soil removal could not be obtained using these methods could. Further investigation into the visualisation of the removal of TAG would require a method to apply a greater force to the surface of the TAG film to promote soil removal.

DSC and SAXS was used to study the model soil before and after cleaning. DSC showed changes in the melting and glass transition temperatures of the TAG film during the cleaning process. SAXS analysis indicated some large structure in the film after cleaning, which could be due to porosity or voids in the film. The crystalline structure present in the initial film is still present after cleaning which indicates the crystalline fat is the harder to remove

constituent; this may require mechanical force. These observations suggest the TAG is not removed in layers; some of the components in the TAG mixture were readily removed by surfactant whereas the harder to remove, more tenacious, oils and fats left were on the surface.

The comparison of the CMC of DG and LO with the relationship between concentration and soil removal shows a correlation between the onset of soil removal and the formation of micelles, which suggests that surfactant micelles are required for the removal of soil. In contrast, for BC, the soil removal required concentrations of surfactant well above the CMC and even in that case, there was only a small amount of soil removal, <4%. This indicates a higher amount of surfactant and/or micelles needed than for LO and DG and highlighted the fact that BC is poor at soil removal, with its primary role as an antimicrobial agent. The study has also shown that a high pH causes soil removal, due to saponification of the surfactant.

LO micelles were shown by SAXS to increase in size with the addition of hexane indicating the swelling of micelles with the addition of force, by stirring and sonication, over a long time, 24 hours. The results suggest LO to removes oil from a surface by solubilization-emulsification mechanism with sufficient mechanical action.

A method was developed to convert the in-lab soil removal test to an analogous QCM-D test by spin coating the previously developed TAG soil onto a QCM-D sensor. The soil removal by each surfactant in real time was subsequently studied for each surfactant. There was good agreement between the in-lab test and the QCM-D studies: BC was much poorer at soil removal than LO and DG and the surfactant mixture optimized by the Bayesian optimization showed the highest rate of soil removal and shortest time to maximum swelling. The improved soil removal of the mixed surfactants is compelling evidence that there are synergistic effects in the cleaning efficacy of surfactant mixtures, and, that Bayesian optimization is an efficient way of finding the mixture with the greatest synergy. Further investigation of the behaviour of mixed surfactant solutions is required to understand how the surfactants are behaving in the final formulation to get such superior soil-removing properties.

6.7 References

- 1. Chateau, M. E., Galet, L., Soudais, Y. & Fages, J. A new test for cleaning efficiency assessment of cleaners for hard surfaces. *J. Surfactants Deterg.* (2004).
- 2. Briddick, A. *et al.* Blooming of Smectic Surfactant/Plasticizer Layers on Spin-Cast Poly(vinyl alcohol) Films. *Langmuir* (2018).
- 3. Campana, M. et al. Surfactant adsorption at the metal-oil interface. Langmuir (2011).
- 4. Bäckström, K. & Engström, S. Removal of triglycerides from hard surfaces by surfactants: An ellipsometry study. *J. Am. Oil Chem. Soc.* (1988).
- 5. Malmsten, M. & Lindman, B. Ellipsometry Studies of Cleaning of Hard Surfaces. Relation to the Spontaneous Curvature of the Surfactant Monolayer. *Langmuir* (1989).
- 6. Atkin, R., Craig, V. S. J., Wanless, E. J. & Biggs, S. Mechanism of cationic surfactant adsorption at the solid-aqueous interface. *Advances in Colloid and Interface Science* (2003).
- 7. Engström, S. & Backstrom, K. Ellipsometry as a Tool To Study Detergency at Hard Surfaces. *Langmuir* (1987).
- 8. Zbik, M. S. & Frost, R. L. AFM study of forces between silicon oil and hydrophobic-hydrophilic surfaces in aqueous solutions. *J. Colloid Interface Sci.* (2010).
- 9. Sigua, G., Adhikari, S., Frankel, G. S. & Pascall, M. A. The use of atomic force microscopy to measure the efficacies of various chemical sanitizers in removing organic matter from glass surfaces. *J. Food Eng.* (2010).
- 10. Komaki, M., Kim, S. K. & Hashimoto, T. Fatty acid soil detergency performance of poly(sodium α-hydroxyacrylate). *J. Surfactants Deterg.* (2002).
- 11. Obendorf, S. K., Mejldal, R., Varanasi, A. & Thellersen, M. Kinetic study of lipid distribution after washing with lipases: Microscopy analysis. *J. Surfactants Deterg.* (2001).
- 12. Ramcharan, T. & Bissessur, A. Analysis of Linear Alkylbenzene Sulfonate in Laundry Wastewater by HPLC-UV and UV-Vis Spectrophotometry. *J. Surfactants Deterg.* (2016).
- 13. Fréville, V., van Hecke, E., Ernenwein, C., Salsac, A.-V. & Pezron, I. Effect of Surfactants on the Deformation and Detachment of Oil Droplets in a Model Laminar Flow Cell. *Oil Gas Sci. Technol. Rev. d'IFP Energies Nouv.* (2014).
- 14. Kanasaki, Y., Kobayashi, Y. & Gotoh, K. Dynamic Analysis of the Removal of Fatty Acid from a Pet Surface Using a Quartz Crystal Microbalance. *J. Surfactants Deterg.* **19**, 627–636 (2016).
- 15. Favrat, O., Gavoille, J., Aleya, L. & Monteil, G. Real time study of detergent concentration influence on solid fatty acid film removal processes. *J. Surfactants Deterg.* **16**, 213–219 (2013).
- 16. Olesen, K., Van Leeuwen, C. & Andersson, F. I. Revealing detergent efficiency and mechanism by real-time measurement using a novel and tailored QCM-D methodology. *Tenside, Surfactants, Deterg.* **53**, 488–494 (2016).
- 17. Dunstan, T. S. & Fletcher, P. D. I. The removal of thermally aged films of triacylglycerides by surfactant solutions. *J. Surfactants Deterg.* **17**, 899–910 (2014).

- 18. Pawley, J. B. Confocal and two-photon microscopy: Foundations, applications and advances. *Microsc. Res. Tech.* **59**, 148–149 (2002).
- 19. Sonesson, A. W., Callisen, T. H., Elofsson, U. M. & Brismar, H. Imaging the detergency of single cotton fibers with confocal microscopy: The effect of surfactants and lipases. *J. Surfactants Deterg.* **10**, 211–218 (2007).
- 20. Lewinska, A., Zebrowski, J., Duda, M., Gorka, A. & Wnuk, M. Fatty acid profile and biological activities of linseed and rapeseed oils. *Molecules* (2015).
- 21. Noureddini, H., Teoh, B. C. & Davis Clements, L. Viscosities of vegetable oils and fatty acids. *J. Am. Oil Chem. Soc.* **69**, 1189–1191 (1992).
- 22. Kotidou, A. & Shaeiwitz, J. A. Periodic concentration phenomena during spontaneous emulsification in the oleic acid-sodium dodecyl sulfate-water system. *J. Colloid Interface Sci.* **92**, 265–268 (1983).
- 23. Rudin, J. & Wasan, D. T. Mechanisms for Lowering of Interfacial Tension in Alkali/Acidic Oil Systems: Effect of Added Surfactant. *Ind. Eng. Chem. Res.* **31**, 1899–1906 (1992).
- 24. Haq, E. U. *et al.* Real time laser interference microscopy for bar-spread polystyrene/poly(methyl methacrylate) blends. *J. Polym. Sci. Part B Polym. Phys.* **52**, 985–992 (2014).
- 25. Huyghebaert, A., Kiekens, L. & Hendrickx, H. Differentiation of lard and tallow by differential scanning calorimetry. *Z. Lebensm. Unters. Forsch.* (1972).
- 26. Jin, X., Zhang, S., Yang, J. & Lv, R. Surface tension and micellization of aqueous alkyl polyglucosides solutions: Influence of the molecular structure and the addition of electrolyte. *Tenside, Surfactants, Deterg.* (2004).
- 27. Flick, E. W. *Advanced Cleaning Product Formulations: Volume 3.* (Noyes Publications, 1996).
- 28. Shaeiwitz, J. A., Chan, A. F. C., Cussler, E. L. & Evans, D. F. The mechanism of solubilization in detergent solutions. *J. Colloid Interface Sci.* **84**, 47–56 (1981).
- 29. Weerawardena, A., Drummond, C. J., Caruso, F. & McCormick, M. Real time monitoring of the detergency process by using a quartz crystal microbalance. *Langmuir* **14**, 575–577 (1998).
- 30. Shimomura, K., Onozawa, H., Komiyama, J. & Sehata, A. Lipid Detergency as Observed by the Quartz Microbalance Method. *Text. Res. J.* **73**, 509–514 (2003).
- 31. Yada, S., Matsuoka, K., Nagai Kanasaki, Y., Gotoh, K. & Yoshimura, T. Emulsification, solubilization, and detergency behaviors of homogeneous polyoxypropylene-polyoxyethylene alkyl ether type nonionic surfactants. *Colloids Surfaces A Physicochem. Eng. Asp.* **564**, 51–58 (2019).
- 32. Hall, D. B., Underhill, P. & Torkelson, J. M. Spin coating of thin and ultrathin polymer films. *Polym. Eng. Sci.* **38**, 2039–2045 (1998).
- 33. Hoerr, C. W. & Harwood, H. J. The solubility of tristearin in organic solvents. *J. Phys. Chem.* **60**, 1265–1269 (1956).
- 34. Hoerr, C. W. & Harwood, H. J. The Solubilities of Oleic and Linoeic Acids in Common Organic Solvents. *J. Phys. Chem.* **56**, 1068–1073 (2005).
- 35. Eggenberger, D. N., Broome, F. K., Ralston, A. W. & Harwood, H. J. The solubilities of the normal saturated fatty acids in water. *J. Org. Chem.* **14**, 1108–1110 (1949).

- 36. Xue, L. & Han, Y. Inhibition of dewetting of thin polymer films. *Progress in Materials Science* **57**, 947–979 (2012).
- 37. Norris, M. H. & McBain, J. W. CLXII. A study of the rate of saponification of oils and fats by aqueous alkali under various conditions. *J. Chem. Soc. Trans.* **121**, 1362–1375 (1922).

7 Conclusions

The initial aim of this study was to use a machine learning methodology to optimize a cleaning formulation. The first optimisation experiments were conducted with respect to surface tension because it is a relatively simple, and easily accessible method of quantifying surfactant behaviour. A Bayesian optimisation methodology was used to optimise binary and ternary mixtures of surfactants, targeting the minimum in surface tension. For the binary mixtures, the minimum in surface tensions found were 29.89 ± 0.07 mN m⁻¹ for LO and BC and 29.54 ± 0.03 mN m⁻¹ for LO and DG and for the ternary mixtures, the minimum found was 28.04 ± 0.20 mN m⁻¹. The concentration of surfactants was lower than their individual CMCs for the mixture of LO and BC and in the ternary mixture of LO, BC and DG, not only was the concentration of the individual surfactants in the binary mixture lower than their individual CMC's but also the total surfactant loading was lower. The number of experiments required to reach to optimum was reduced compared to other design-ofexperiment methods. Subsequently, the Bayesian optimisation was performed on a parameter with a greater indication of cleaning formulation performance (i.e. soil removal). The Bayesian optimisation with respect to cleaning efficacy was performed using an adapted TAG removal test to obtain an optimal solution with high soil removal effectiveness, >95%, with a relatively small number of measurements. In addition, the total concentration of surfactants in the optimal mixture identified is less that 2.5 w/w%, which is comparable to the amount used in industrial hard surface cleaning formulations (~2-5 w/w%). In summary, Bayesian Optimisation has been shown to identify an aqueous surfactant mixture using relatively small surfactant concentrations with a minimal number of experiments. This could be a useful tool to formulators as the experiments to characterise soil removal of a cleaning formulation can be time-consuming, so by reducing the number of experiments required and potentially identifying solutions with less surfactant, these products could be formulator more quickly with a reduction in cost.

To advance the Bayesian Optimisation studies, more cleaning components could be added to the model, *e.g.* co-solvents, fragrances, rheology modifiers and chelators, in addition to supplementary inputs or outputs, *e.g.* cost, antimicrobial efficiency and foaming ability. However, currently there are computational challenges restricting the capability to deal with the number of input and output variables being greater than 10 which would require solving first.¹ An alternative area of research could be the correlation between the two output variables with regards to the optimisation. Previously, it has been shown that if the outputs of a multi-output process can be correlated, it is possible to model the relationship in order for an output that is simple, fast or inexpensive to obtain to be used to optimise a formulation with regards to a more time-consuming or expensive to obtain

output.^{2,3} Future work could determine whether this would apply for an optimisation with regards to cleaning efficacy (a time-consuming test) using surface tension (a fast measurement).

One drawback of the Bayesian optimisation is that the information it provides is specific to the given system. The black-box nature of the optimisation means the physicochemical reasons that cause the conditions of the optimum formulation to perform best are not known and predictions about systems beyond the initial system selected cannot be made. Hence, the second aim of this study was to gain an understanding of the mechanism that underpins the surfactant-aided removal of an oily soil from a hard surface. With relation to this aim, the key findings are discussed below.

First, DG was effective at soil removal. DG was found to be a major component in the optimised mixture with respect to both surface tension and soil removal efficacy. This is in agreement with the finding in chapter 6 that the concentration of DG at which surface tension becomes constant (indicative of the CMC), is the same concentration above which an appreciable amount of soil begins to be removed. QCM-D of DG at concentrations above and below the CMC, indicated that there is no soil swelling step, due to surfactant and water penetration, but soil was removed at a fast rate (relative to LO and BC).

Second, the removal of the TAG soil is aided by high pH. For the ternary mixture of surfactants, the optimised mixture with regards to soil removal was at pH 11. The cleaning test was performed on water with increasing pH and it was found that at every pH except 11, there was little to no soil removal. At pH 11, 20% of the soil was removed indicating that it is not only the changes to the surfactant that occur at high pH which encourages soil removal. This suggests that saponification of the TAG, which occurs with addition of sodium hydroxide, is plays a role in the soil removal mechanism.

Third, BC is a poor choice of a surfactant for removing soils. In both ternary mixture optimisations (for surfactancy and cleaning), BC was not required for the optimal formulation. By both the laboratory soil removal test and QCM-D, it was observed that at very low surfactant concentration there was an increase in mass of the soil due to swelling by water and surfactant. In addition, the concentration at which a small amount of soil is removed is much 100 times greater than the CMC. BC as is not an active surfactant in this system; the reason for BC's inclusion in 'real' formulations is for an alternative function: its role as an antimicrobial.

Finally, there is evidence that surface tension is a good proxy when investigating soil removal. For example, the concentration of surfactant above which an appreciable amount of soil begins to be removed was the CMC for both LO and DG. BC was shown to be poor at lowering surface tension

and soil removal by being excluded from the surfactant mixtures optimised using the Bayesian method. However, optimizing the surface tension and formulations with respect to soils on a given substrate does not give you the whole picture of cleaning. There are many more factors and substrates to consider. Therefore, further study is required to gain an understanding of the mechanism of soil removal adopted by the surfactants of interest, including developing a method to study the action of surfactant with to help understand the reasons, and the mechanism, behind why both surfactant and mechanical action are required to achieve excellent cleaning.

References

- 1. Li, C. *et al.* Rapid Bayesian optimisation for synthesis of short polymer fiber materials. *Sci. Rep.* **7**, 5683 (2017).
- 2. Alvarez, M. & Lawrence, N. D. Sparse convolved Gaussian processes for multi-output regression. *Adv. Neural Inf. Process. Syst.* 57–64 (2009).
- 3. Alvarez, M. A. & Lawrence, N. D. Computationally efficient convolved multiple output gaussian processes. *J. Mach. Learn. Res.* **12**, 1459–1500 (2011).